A Study of the Reactions Involved in the Surface Treatment of Wool Fibre by Glow Discharge Plasmas

by

Xiu Juan DAI

September 1995

A thesis submitted for the degree of
Doctor of Philosophy
of the Australian National University

This thesis is entirely my own work,

except where explicitly indicated.

Xiu Juan DAI

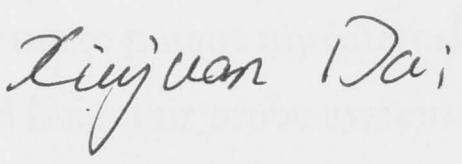

Plasma Research Laboratory

Research School of Physical Sciences and Engineering

The Australian National University

Canberra, ACT 0200 Australia

Acknowledgements

It is firstly a pleasure to thank my supervisors, Professor Sydney Hamberger, Dr.Andrew Perry, and Dr.Rod Boswell. This new project would have never been carried out without Professor Hamberger's effort and foresight. It was he who gave me the opportunity to come to Australia to start this significant new epoch in wool pre-treatment industry. His suggestions have on many occasions given me valuable insights and I have benefited from his great enthusiasm, his sparkling ideas, and help with written English through my all research and this thesis. Dr.Andrew Perry has always encouraged and supported me to pursue my interests and has given me much guidance on plasma sources and langmuir probe systems, and made many valuable comments and suggestions for this thesis. His guidance and suggestions through my all Ph.D study have benefited me greatly. Dr.Rod Boswell has given me great encouragement and understanding during my Ph.D study, and very valuable comments on Chapter 3.

I wish particularly to thank Dr.Boyd Blackwell and Mr.John Wach. Dr.Boyd Blackwell has been very helpful in establishing the control system and the data acquisition system and providing the box-car integration program for vuv spectroscopy, and in discussions of plasma physics. I have benefited from his strong ability to find the solution to every problem. Mr.John Wach has been of great assistance in establishing this new laboratory with his expert technique which included the mechanical design of the apparatus. I wish to thank Professor Bob Dewar for his encouragement and understanding through my Ph.D study. I would like to thank Dr.Deming Wang not only for his expertise on EPR for measurements of free radicals on wool surface, but also for his very helpful discussions

and valuable suggestions for this thesis; and to Dr.Simon Hewlett and Dr.Yi Mu for their enthusiastic help in computer programs.

Among the many other people who deserve thanks, Dr.Robert Porteous, Dr.Chris Charles, and Dr.Gerard Borg have been of great assistance, particularly in discussion of plasma experiments; and Dr.Harold Persing for very valuable comments in Chapter 3 and very helpful discussions for plasma diagnostics; and Dr.A.Durandent for very valuable suggestions in Chapter 6; and Dr.I.J.Donnelly of Australian Nuclear Science and Technology Organisation for the valuable discussions about particle confinement time; and Dr.B.R.Lewis for the loan of the monochromator and his valuable advice on vuv spectroscopy; and Dr.P.Turner and Dr.B.Holcombe of CSIRO, D.W.T. for their expert advice on wool; and Professor G.A.George of Queensland University of Technology for his encouragement and interest in this new research area; and Dr. Kim Wells for his enthusiastic help in correcting English in this thesis. There are also those who have given me much by way of advice and encouragement: Dr.Henry Gardner, Dr.Les Sharp, Dr.John Howard, Dr.Mikael Persson, Dr.M.Shats, and Dr.Helen Smith. I also wish to thank Helen Hawes for her help and encouragement.

I wish to thank my fellow students of PRL, particularly Beichao Zhang, Darryn Schneider, Bert Ellingboe and Mark Jarnyk for discussing plasma physics and experimental problems, and Jerome Lewandowski and Sean Depprick for discussing computer programs. Stuart Hudson deserve my special thanks for his great enthusiasm as my English teacher.

I wish to thank the technical staff of PRL and vuv group, particularly Clint Davies, Ray Davies, Steve Hyde, Peter Alexander, Eddie Wedhorn, Colin Dedman, and Kevin Lonsdale for the enthusiastic help they have given me. I also wish to thank the staff of the School, stores, electronics, computer unit, and workshops for their friendliness and help.

There are many friends who have helped me in many other aspects over the years. I thank particularly Xuehuan and Dinhuan, Cristina and Vittorio, Rajumati and Dugald, Ann, Baiming, Shu, and Fangxin for their kindness, understanding, and support which have always warmed my heart, especially in my hard time.

I acknowledge financial support for this research from the Australian Wool Research and Promotion Organization and for my scholarships from the Australian National University.

This thesis is dedicated to

my daughter and my parents

Their loving support

throughout my whole life

has made this work possible.

Note

This plasma-wool processing project began in 1991 with the financial support from the Australian Wool Research and Promotion Organization. The whole laboratory scale plasma equipment and diagnostic systems have been developed since late 1991 at the Plasma Research Laboratory of the Australian National University under the supervision of Professor Sydney Hamberger. The surface property measurements were provided by the CSIRO Division of Wool Technology as part of the collaboration (details see section 2.4).

Abstract

The modification of the properties of wool fibre surface by contact with an RF produced plasma and the reaction mechanism between the wool and the plasma have been extensively studied. The wettability, dyeability, printing, and shrink-proofing of wool are greatly improved after plasma treatment without any changes to the bulk of the fibre being caused.

Many experiments have been carried out in oxygen plasma to investigate thoroughly the electron energy distribution functions, the plasma potential, and the various plasma components (the charged particles, the neutral reactive particles, and uv radiation) as well as their effects on the wool surface properties, and to find the most efficient treatment levels required to achieve a specific level of change through the control of the experimental parameters.

The use of different plasma gases and various selective baffles to separate the plasma source from the reaction chamber help to identify the main reactive species responsible for this modification of wool surface properties and for determing the actual physical and chemical processes which takes place between the plasma and the wool fibre surface. It has been found that the atomic oxygen is the most important reactive species (with some acceleration by ultraviolet) in this modification.

A theoretical model has been successfully developed for the chemical reaction kinetics for this plasma processing, and an overall reaction model proposed for the interaction between the plasma and the wool surface to explain the experimental results.

CONTENTS

1

INTRODUCTION

1.1 BACKGROUND AND MOTIVATION

Wool has become more and more important in daily life as a primary source of high quality fibre. Since its surface properties are important determinants of its usefulness, most commercially important wool used requires the surface of the fibre to be first modified to obtain good surface properties.

The intricate structure of the wool fibre surface acts almost as a challenge to its modification. Traditionally, the only process that has been used on a production scale for doing this is chlorination (a wet chemical method). This oxidation process, in which chlorine compounds are used as the oxygen source, is carried out in a strong acid solution with high consumption of both chemicals and energy. For example, to pretreat one tonne of fabric, the following is typically needed: 387kg sodium hypochlorite (with varying Cl_2 content); 93kg sulphuric acid; 143 kg sodium bisulphite, and 235 m^3 water. The total energy required to produce these chemicals as well as for the chlorination process itself has been estimated to be 7MWh per tonne of fabric [1]. Besides the pollution resulting from the disposal of the strong acid solution and the high energy consumption involved in supplying water and drying the materials, the wet chemical treatment has other problems which are difficult to overcome, including some obvious side effects (yellowing, loss of mass, damage to the bulk, change in handling characteristics etc.) to the

wool after the treatment, reduced workplace safety, and limited reproducibility of treatment results. Therefore, an alternative pre-treatment of wool surfaces using other technologies has become increasingly important.

Today, plasma processing of various materials is being actively researched and is already in industrial use for many applications. Low temperature plasma technology is widely applied to the manufacture of semiconductor and optical devices [2, 3] and is extensively used as a means for altering the surface properties of synthetic polymers [4, 5]. Plasmas are gaseous mixtures of neutral species (including free radicals), charged particles, photons etc. and are usually produced by electrical gas discharges. Plasma processing has special advantages for surface modification of materials as it is a dry process, requires only short treatment times, as well as being easily controlled by various independent parameters such as gas pressure, discharge power and exposure time and generally presents safer working conditions. Most importantly, the effects of the plasma do not penetrate below about 10nm from the polymer surface [6]. Ward *et al* [7] have found that wool is almost completely covered by a layer of saturated hydrocarbon (i.e. polymer) as in a lipid layer. In view of this, we can safely expect that the plasma treatment of wool would only affect a small portion of the fibre. Thus, if we consider even the finest wool fibre (diameter 10μm), 99.8% of its bulk should remain unchanged after treatment. With such minor changes the treated wool should retain its strength and its highly desirable natural appearance.

Early interest in wool treatment by plasma was aimed at improving shrink-resistance: in 1966 Thorse [8, 9, 10] used a corona discharge, and found that by increasing the corona cell temperature (up to 100°C) by using a high voltage he could make the treatment effective. However, small holes were burned in the samples: this could be prevented by using a corona cell with dielectric material at both electrodes. He also used different gases (O_2, N_2, air and chlorine) to

compare the effectiveness of the treatment. During the 1970's, Pavlath [11, 12] made many measurements on resistance to shrinking and on yarn strength which were both substantially improved by various plasma gases, using radio-frequency excitation through both capacitive and inductive coupling. Both these studies were performed under laboratory conditions.

The plasma treatment of wool has not been considered as a serious alternative to the wet chemical method until recently. The first plasma processing for wool under industrial conditions was reported in 1989 by Rakowski [1] who built a prototype chamber for wool treatment by plasma to improve spinning, printing, and anti-felting. The results showed quite marked changes in fibre-fibre friction, increased cohesion, colourfastness ratings of prints, better abrasion resistance and tensile strength, and much less yellowing and greying compared with chlorinated fabrics. Shortly after this (1991), the Deutsches Wollforschungsinstitut in Germany installed a plasma chamber and started to treat wool. This was in response to pressure from the German government which forced the textile industry to develop new more environmentally friendly processes as an alternative to wet chlorination because the AOX (Absorbable Organo-halogens) discharges in the industrial waste water for most German textile companies exceeded the maximum limits (0.5mg/l) [13]. They demonstrated the improved dyeing properties of wool after microwave plasma treatment in laboratory conditions, showing an increased rate of dye absorption and bath exhaustion, a high degree of uniformity and fastness, and a considerable reduction of dyeing time. Although plasma treatment of wool has attained a certain level of interest and is slowly finding its way as an industrial process, very little effort has been devoted elsewhere to understanding the actual physical and chemical processes which take place between the plasma and the wool fibre surface, nor to quantify the treatment levels required to achieve a specific level of change. This seems to have slowed down the progress of further research and the development of an industrially viable process.

The aim of the research described in this thesis is to study the actual physical and chemical processes involved in the plasma and in the wool-plasma reactions, and to relate the characteristics of the plasma to the chemical and physical changes which it produces. It is hoped that the outcome of this research will lead to an improved commercial process for the treatment of wool fibres that results in: higher quality fibres; reduced environmental impact; reduced energy consumption; and reduced labour cost compared to present commercial wool treatment processes.

1.2 WOOL STRUCTURE AND PLASMA TREATMENT

1.2.1 General Description of Wool Fibre

In order to understand the chemical and physical changes on the surface of wool fibre by plasma, the structure of the untreated fibre is briefly described.

Wool fibres consist mainly of keratin, a type of protein. The fibres are made up of two types of cells, the long spindle-shaped cortical cells in the inner cortex section and the flattened cuticle cells which surround this, shown in Fig.1.1 [14]. A cell membrane complex known as "intercellular cement" occurs between each cell. The exposed scale edges point towards the tip of the fibre which results in a higher coefficient of friction in the tip to root direction than from root to tip.

As the plasma treatment does not affect the bulk properties of the wool fibre, we shall focus on the cuticle cells, i.e. the surface properties of the wool fibre. The cells in the cuticle overlap like roof tiles to form a protective outer layer for the fibre. The layered structure within each cuticle cell can be seen using

transmission electron microscopy [15] and is diagrammatically shown in Fig.1.2 [16].

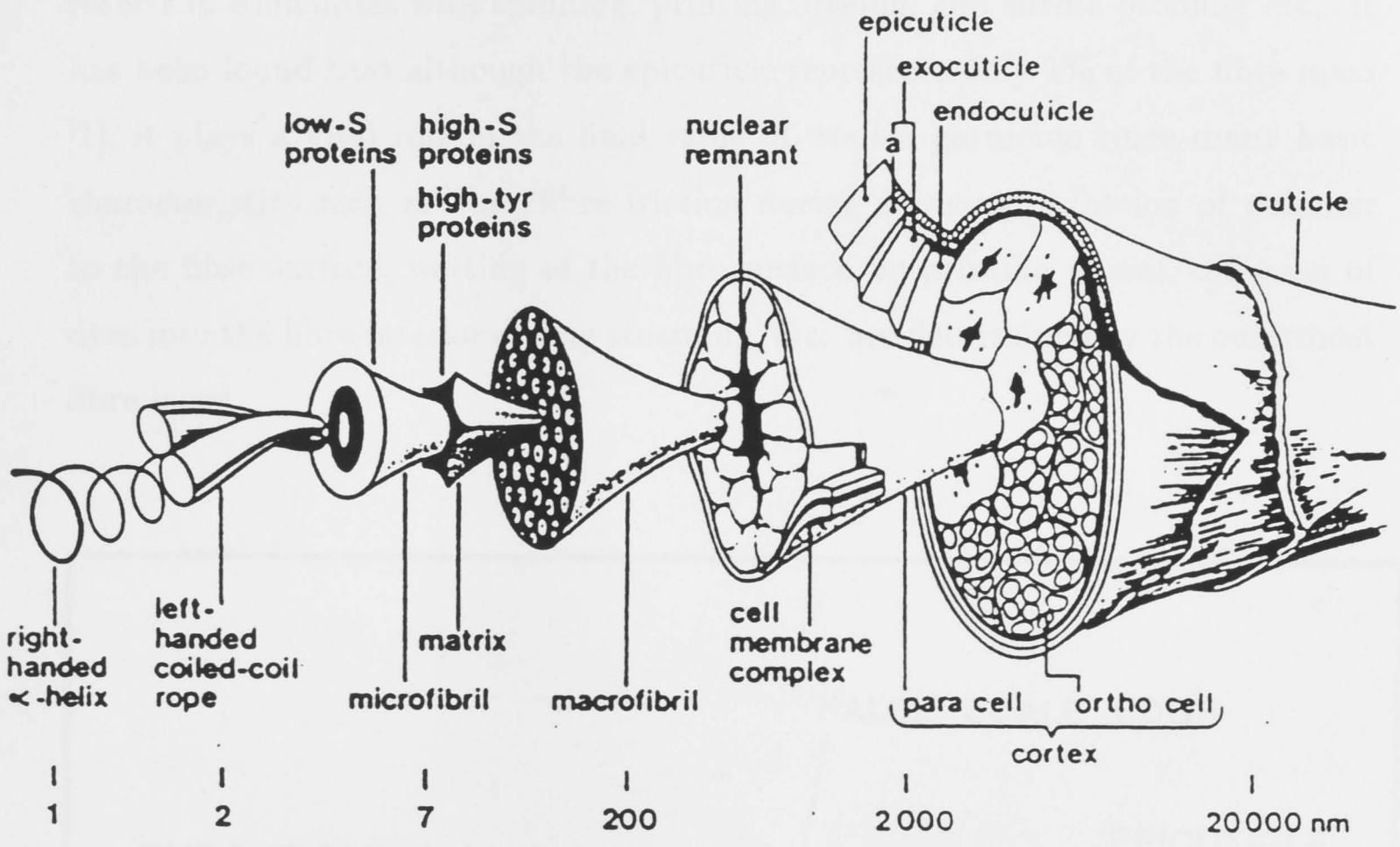

Fig.1.1 Schematic diagram of the structure of a fine wool fibre

The outer region of the cells is termed the *exocuticle* which is a tough and resilient layer resulting from the high concentration of disulphide cross-links [17]. Beneath the exocuticle is the *endocuticle* which consists of soft non-keratinous protein [18]. There is believed to be a thin chemically-resistant outer membrane about 5 nanometer thick, termed the *epicuticle*, on the surface of the fibre though it can not be clearly seen by electron microscopy [19]. The outermost layer of the epicuticle is composed predominantly of lipids, and resembles a saturated

hydrocarbon-like polymer (denoted by RH in Chapter 6), as consistent with the hydrophobic character of wool [20, 21]. It is known that this hydrophobic character corresponds to low surface energy. Low surface energy of the wool surface results in difficulties with spinning, printing, dyeing, and shrink-proofing etc.. It has been found that although the epicuticle represents only 1% of the fibre mass [1], it plays a vital role in the final value of woolen garments since many basic characteristics such as fibre/fibre friction during spinning, adhesion of polymer to the fibre surface, wetting of the fibre surface by printing pastes, diffusion of dyes into the fibre interior during steaming, etc. are determined by the outermost fibre layer.

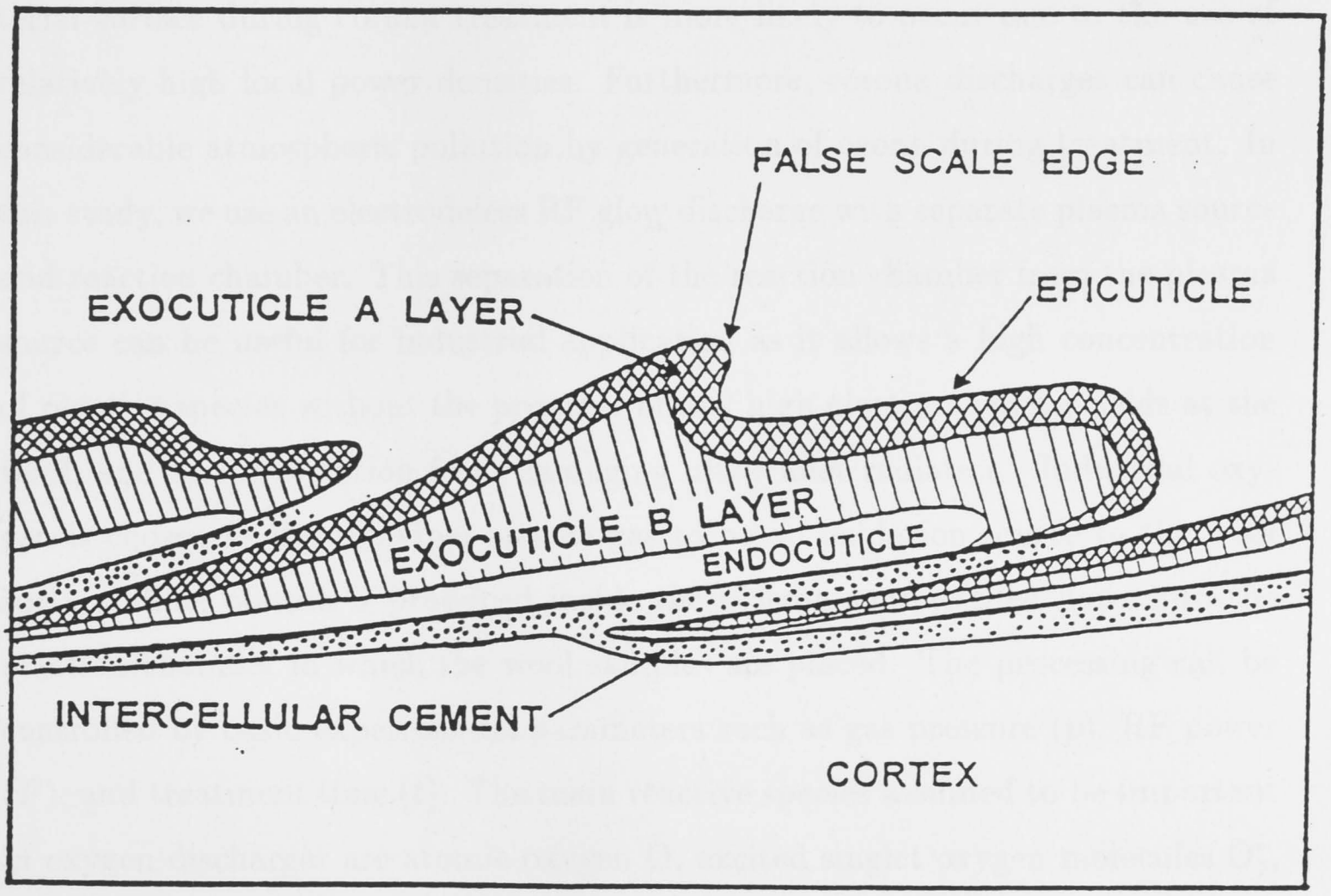

Fig1.2 Schematic diagram of the structure of a cuticle cell

1.2.2 Plasma Treatment

As stated, plasma treatment has special advantages for surface modification of materials. Generally, industrial plasma treatment falls into two categories: by corona produced by an a.c. electric discharge at atmospheric pressure, and by glow discharges produced at low pressure by d.c., radio-frequency (capacitively or inductively coupled), or by microwave power. These plasmas, which generally have high electron temperatures (between 10,000 and 50,000 K), but gas temperature near ambient, are very well suited for the chemical treatment of materials sensitive to high temperatures. In many cases, it is found that the corona treatment is less effective than that using glow discharges as the residence time of the reactants is very short at atmospheric pressure. Also, damage to the material surface during corona treatment is more likely to occur due to the use of relatively high local power densities. Furthermore, corona discharges can cause considerable atmospheric pollution by generation of ozone during treatment. In this study, we use an electrodeless RF glow discharge with separate plasma source and reaction chamber. This separation of the reaction chamber from the plasma source can be useful for industrial application as it allows a high concentration of reactive species without the presence of any high electromagnetic fields at the wool, and allows isolation from damaging ultraviolet radiation. Industrial oxygen is chosen as the principal plasma gas to be an oxidation source to the wool surface. The plasma is produced inside the plasma source, then flows into the reaction chamber in which the wool samples are placed. The processing can be controlled by basic experimental parameters such as gas pressure (p), RF power (P), and treatment time (t). The main reactive species assumed to be important in oxygen discharges are atomic oxygen O, excited singlet oxygen molecules O_2^*, positive ions N_i, and electrons. Therefore, in this study the plasma is characterised by its properties such as neutral particle density ($N[O]$, $N[O_2^*]$), charged particle density N_i and N_e, and electron energy distribution function ($f(E)$).

In contrast to earlier studies, the increase in wool surface energy is taken as the quantitative measure of the improvement of wool surface properties in this study. To this end, many experiments using different plasma gases and different plasma conditions have been conducted to find out which active species in plasma corresponsible for the observed surface energy increase, and to find the optimum experimental parameters for achieving the most effective surface change. The effectiveness of the plasma treatment can be illustrated by comparing it with wet chemical treatment which produces a maximum surface energy of around 50 mJ/m^2 (NB: the surface energy of untreated wool fibre is $\sim$ –4 mJ/m^2 with respect to water) taken after a 60 minute treatment in 0.1 Mol methanolic KOH [22]. Our results show that surface energy increases rapidly and reaches values $\sim$ 60 mJ/m^2 after treatment by oxygen plasma for only a very short time (< 1sec), using low RF power, and a carefully chosen gas pressure. In addition, the properties of wool such as shrink-proofing, printing and dyeing have also been studied after treatment. The results show that all the commercially important properties of wool are considerably improved, e.g. shrinkage is greatly reduced, colour depth is effectively increased, and dyeing is not only deeper but also much more even and more rapid than for untreated fibre.

1.3 OUTLINE OF THE THESIS

The interaction of a plasma with wool is a very complicated process, both because of the intricate chemical and physical structure of the wool fibre surface and the complex composition of the plasma which consists of a mixture of ions, electrons, neutral particles, free radicals, and photons. An investigation of the modification of the wool surface by a plasma should attempt to answer the following questions: Why can plasma modify the wool surface so dramatically and successfully? What reactive species in the plasma actually play the most important role in the mod-

ification of wool surface? How are the reactive species produced in the plasma? and How do they react with the wool surface?

The main attention is first focused on a detailed experimental investigation of the behaviour of various plasma components and their effects on wool surface properties. As the production of the reactive species is dominated by the electrons, the electron energy distribution function has been study so that the measured values can be included in a theoretical model of the kinetics of chemical reactions occurring in the plasma. Finally a qualitative reaction model between wool and plasma is proposed based on the whole study from the experiments and the theoretical model.

The apparatus consists essentially of a plasma source mounted above a reaction chamber in which the wool samples to be treated are placed. The experimental apparatus and the relevant measurement techniques used in this study are described in Chapter 2.

Chapter 3 presents the measurement results of charged particle density and plasma potential, as well as electron energy distribution functions both in the plasma source and in the reaction chamber. This chapter also includes the effect of introducing various baffles between the source and the chamber to allow us to study separately the effects of different particles and radiation on the wool.

Chapter 4 is concerned with the measurement of the concentrations neutral reactive species in oxygen discharges and the investigation of their concentration in the reaction chamber using a vacuum ultra-violet absorption measurement method. This chapter also describes a useful improvement in exciting a vuv continuum radiation source which greatly improves the absorption measurements.

A theoretical model for the kinetics of the chemical reactions occurring in the plasma is developed in Chapter 5. Included in this chapter are a discussion of the

fundamental production and loss processes of the main reactive species, development of the most important reaction equations, theoretical calculations of the concentration of the reactive species, and some comparison with the experimental results.

The overall mechanism of the wool surface modification by plasma is discussed in Chapter 6. For completeness, besides including the changes of surface energy as well as the chemical and physical changes on the wool fibre surface after plasma treatment, some brief discussion on the changes of other surface properties, e.g. the effects on shrink-proofing, printing and dyeing etc. is included. After discussing the effect of using different plasma gases and using different baffles, the relationship between the surface properties of wool and the reactive species in the plasma is discussed, and a possible reaction model between the wool surface and the reactive species is proposed.

The final chapter summarises the main results and suggests possible further research.

2

EXPERIMENTAL EQUIPMENT AND DIAGNOSTICS

The wool-processing experiments and plasma measurements referred to in this thesis have been carried out with the experimental equipment described in section 2.1. Sections 2.2 and 2.3 respectively describe the Langmuir probe system used to measure the plasma parameters and the vacuum ultra-violet (vuv) spectroscopy system used to study the neutral particles. The analytical techniques used for studying the wool surface is briefly described in section 2.4.

2.1 EXPERIMENTAL APPARATUS

A schematic diagram and a photograph of the apparatus are shown in Fig.2.1 and Fig.2.2 respectively.

The plasma source consists of a glass cylinder, 150mm dia and 300mm long, mounted vertically above a continuously pumped metal reaction chamber. As mentioned in Chapter 1, this separation of the reaction chamber from the plasma source has significance for industrial applications as it allows high concentrations of reactive species without the presence of any high electro-magnetic fields [23, 24] at the wool, and allows isolation of damaging ultraviolet radiation if necessary. The working gas (either industrial oxygen (purity 99.5%), dry air, industrial

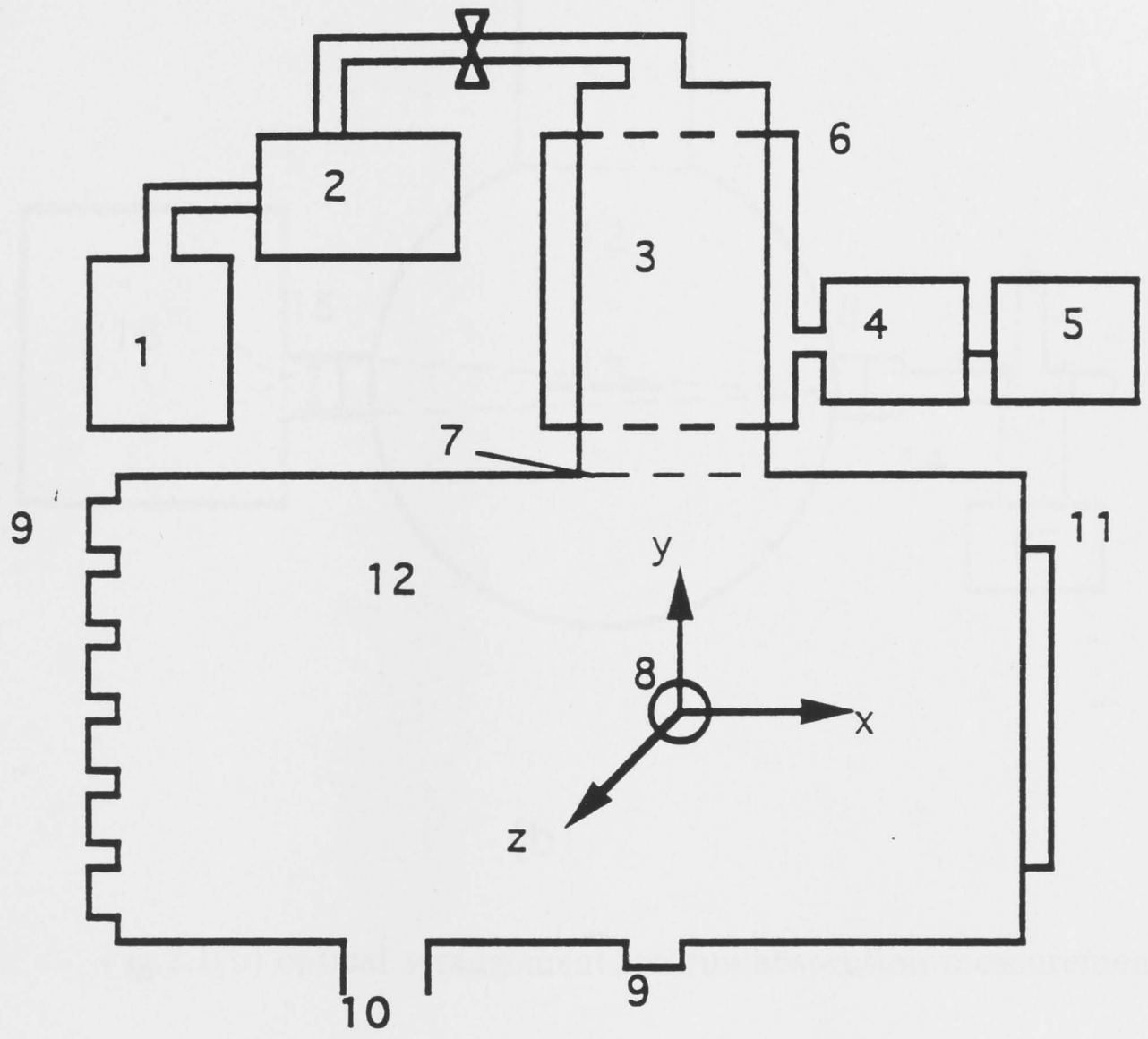

(a)

Fig.2.1(a) Schematic diagram of the experimental apparatus: 1 working gas; 2 flow controller; 3 plasma source; 4 RF matching box; 5 RF generator; 6 RF antenna; 7 baffle position; 8 MgF_2 window; 9 access ports for Langmuir probes; 10 vacuum system; 11 viewing window and sample access; 12 reaction chamber; 13 sample location; 14 vuv light source; 15 MgF_2 lens; 16 vuv monochromator and its detection system;

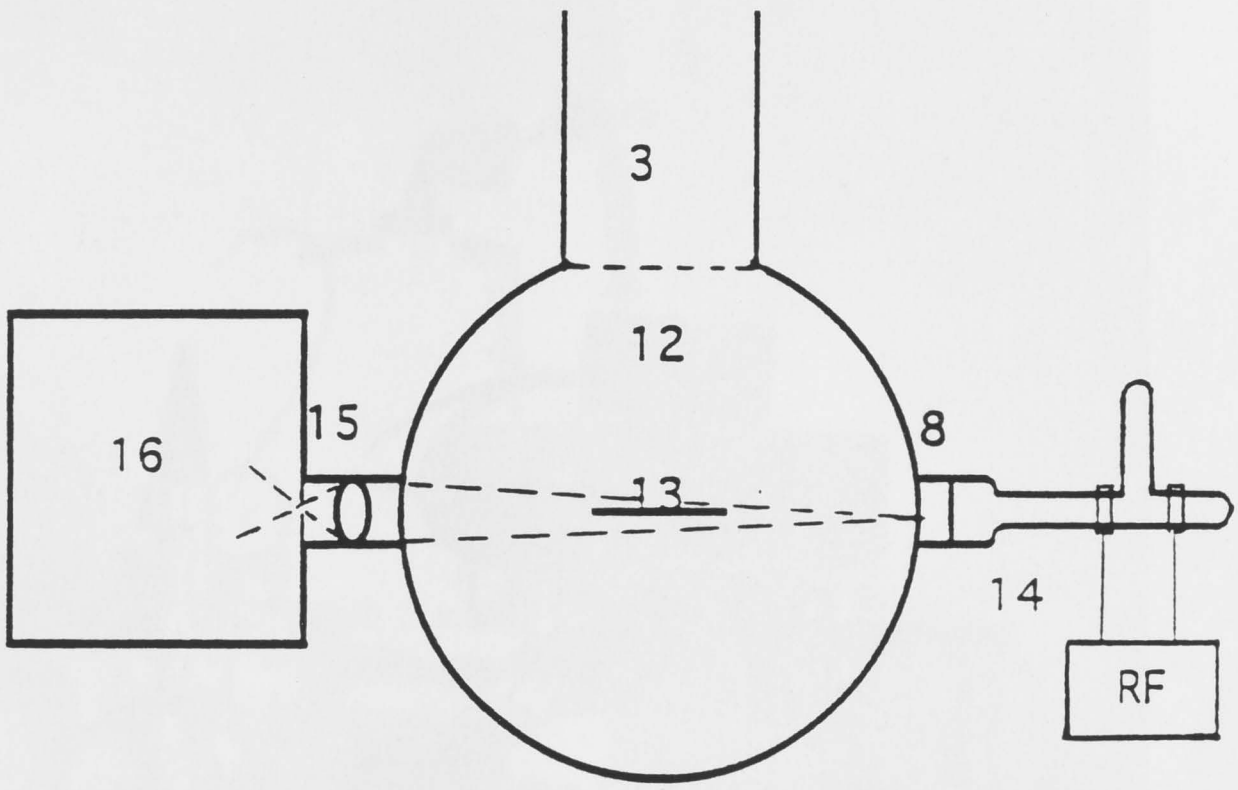

(b)

Fig.2.1(b) optical arrangement for vuv absorption measurement.

argon (purity 99.99%), or industrial hydrogen(99.999%)) is fed in at the top of the source tube via a flow controller at between 6.0 and 12.0 sccm (standard cubic centimeters/minute) to provide a pressure range in the chamber between 10^{-3} and 10^{-1} mbar as measured by a capacitance manometer. An electrodeless discharge is produced by an industrial RF generator (at 13.56MHz) which can supply RF power to the source via an antenna in the range 25 to 300W either continuously or in single pulses of duration between 0.1 and 10 seconds (below 25W, the discharge did not strike reliably at all relevant pressures).

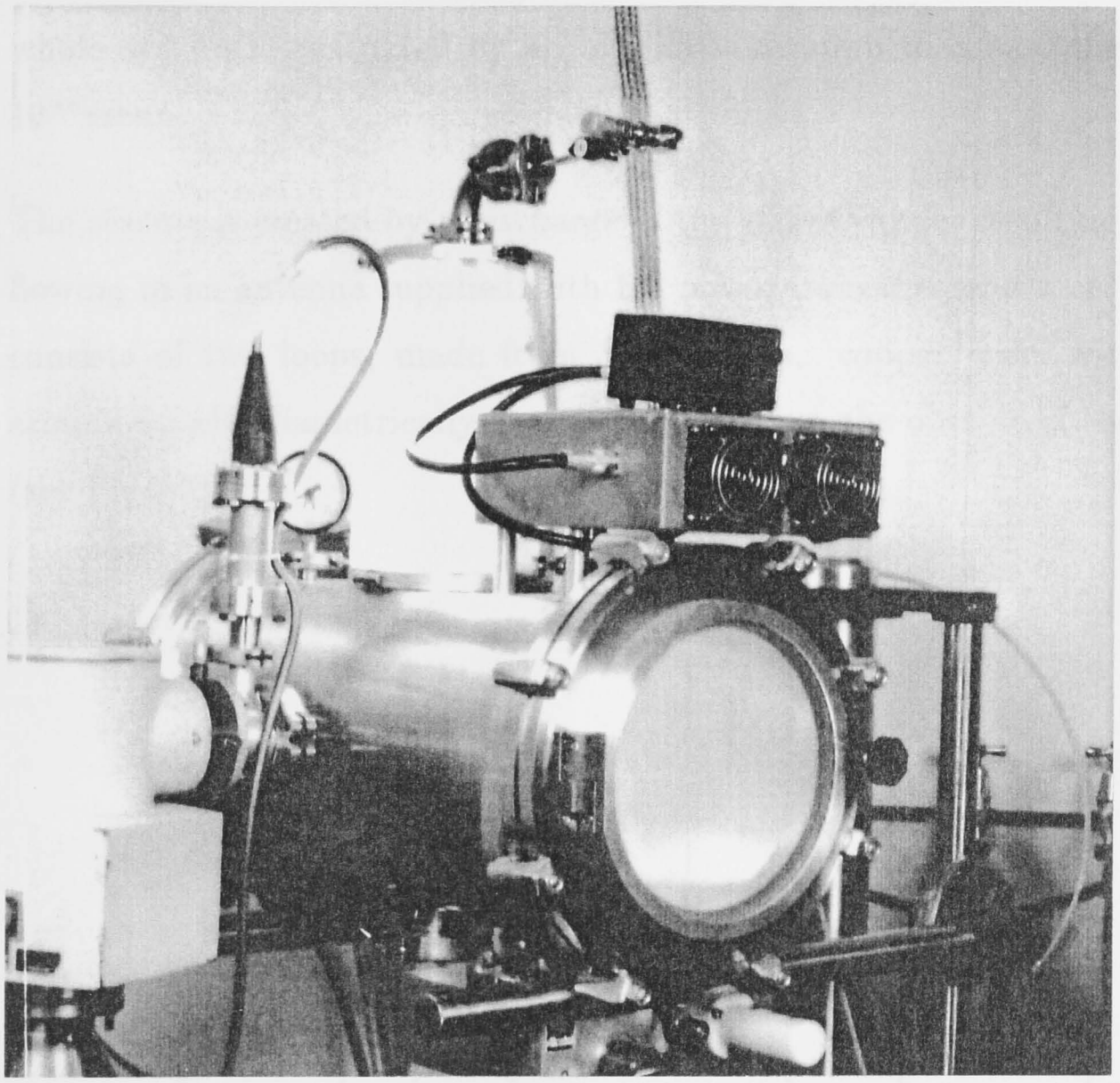

Fig.2.2 Photograph of the apparatus.

Plasma products generated in the source flow into the cylindrical stainless steel reaction chamber, which is 650mm long and 320mm dia. At one end of the chamber a hinged door, fitted with a 250mm dia. glass viewing window, provides access for samples which are located in the chamber about 16 cm below the source on a stainless steel platform. Six ports in the other end-plate and one in the base of the chamber provide access for Langmuir probes used to measure the spatial distribution of the plasma parameters. Two opposing ports in the side of the chamber provide optical access, e.g. for vuv absorption measurements. The

whole system is evacuated by an oil diffusion pump to a base pressure around 10^{-6}mbar.

The plasma is created by a discharge in the glass cylinder resulting from current flowing in an antenna supplied with RF power from the generator. The antenna consists of two loops, made from 3.74mm dia. copper wire, with inductance around 0.8μH, diametrically opposed and held on the outside of the source tube (see Fig.2.3).

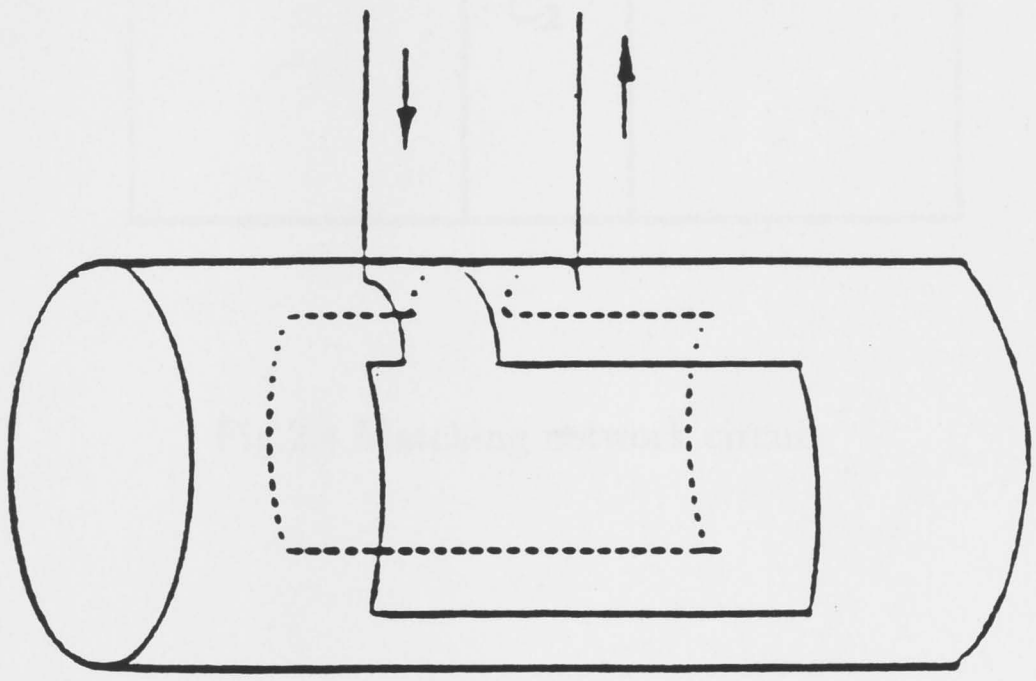

Fig.2.3 Antenna geometry

The completely electrodeless discharge maintained by external excitation has the advantage of maintaining the cleanliness of the system (i.e avoiding electrode erosion and contamination of the plasma with metal vapour) during processing [25, 26]. The plasma source is matched to the RF supply by the matching network shown in Fig.2.4. The resonant circuit is provided by a capacitor C_1 (200pF) in series with the antenna inductance L. The capacitors C_2 (1060pF) and C_1 can be

adjusted to optimise matching. In all the experiments in this study, the tuning is adjusted to keep the standing wave ratio below 1.5. (measured by a SWR meter between the RF generator and the matching network circuit).

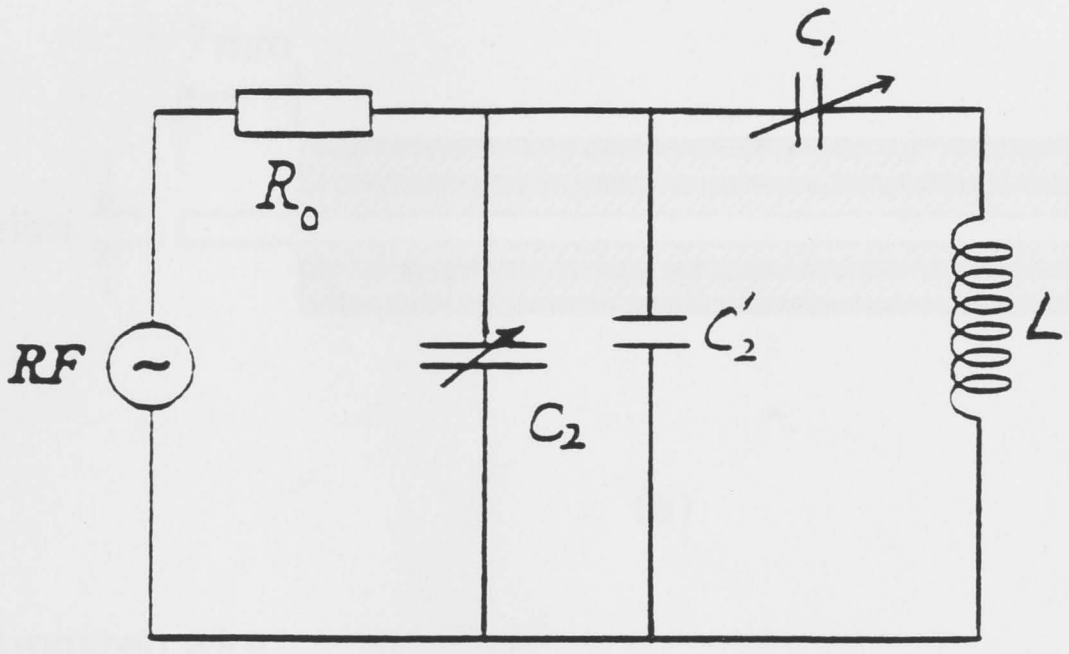

Fig.2.4 Matching network circuit

2.2 LANGMUIR PROBES

Two similar cylindrical Langmuir probes fitted in sliding vacuum seals are used to measure the plasma parameters. One of them (see Fig.2.5(a)) can be moved either along the chamber in a horizontal direction or vertically through the chamber into the plasma source while the other (Fig.2.5(b)) is used to sample the plasma source region along a radius. Fig.2.5 (a) and (b) show the construction of the probes used in these experiments. Both probes are made from 2.5 mm diameter tungsten wire enclosed in ceramic tubing and connected to a copper wire lead. In order to minimize the RF field pick-up during the probe measurements, two stainless steel tubes and a second ceramic tube are used to form double co-axial shields

(see Figures 2.5 (a) and (b)). A 7mm length of the tungsten wire tip is exposed to the plasma and forms the collection electrode.

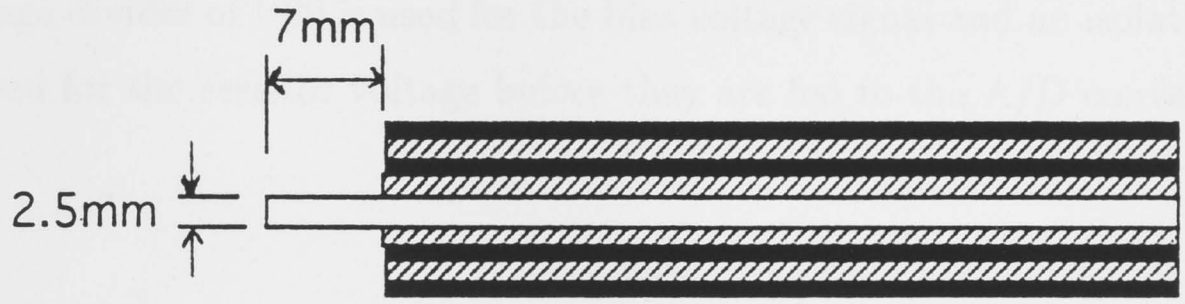

(a)

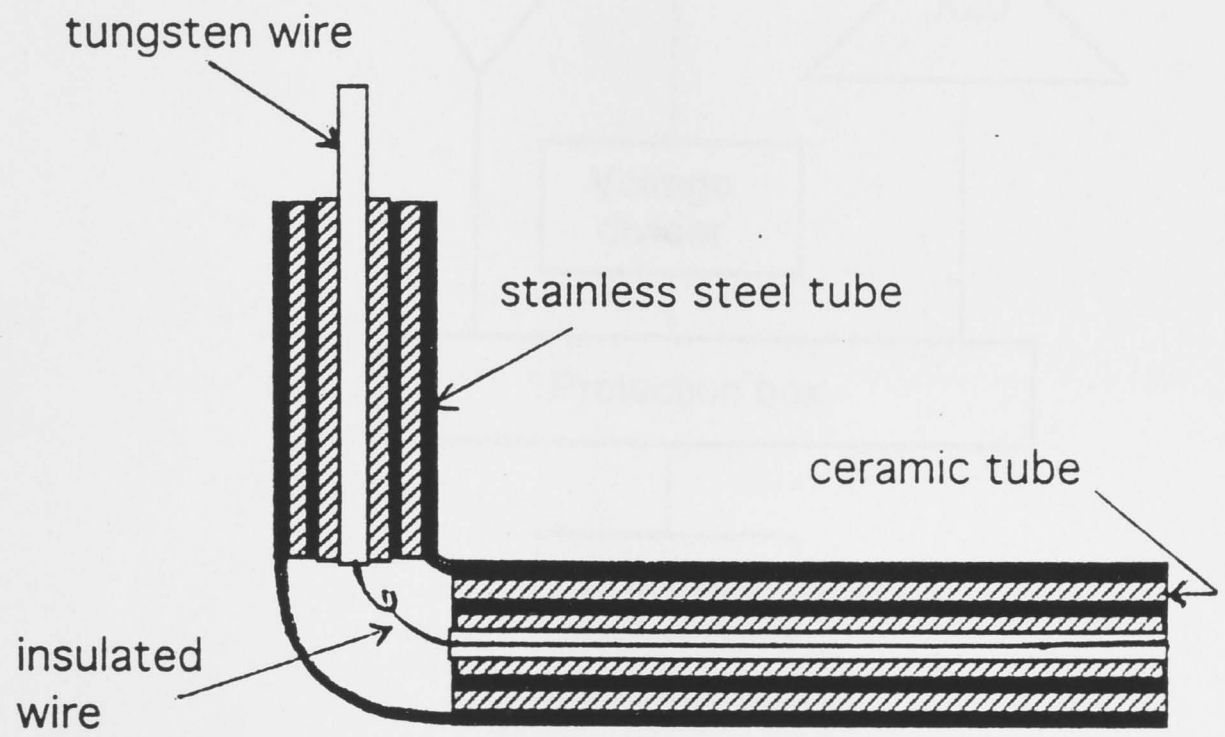

(b)

Fig.2.5 The structure of the Langmuir probes: (a) for measurements in the chamber and from the chamber to the source; (b) for measurement in the source.

The probe data acquisition system is shown in Fig.2.6. The necessary swept bias voltage is generated by a computer, supplied via a D/A converter, amplified and finally applied to the probe, the voltage being swept up to ± 100V. The probe current is measured digitally by the potential drop across the series resistor R_s. A voltage divider of 1:20 is used for the bias voltage signal and an isolation amplifier is used for the resistor voltage before they are fed to the A/D convertor.

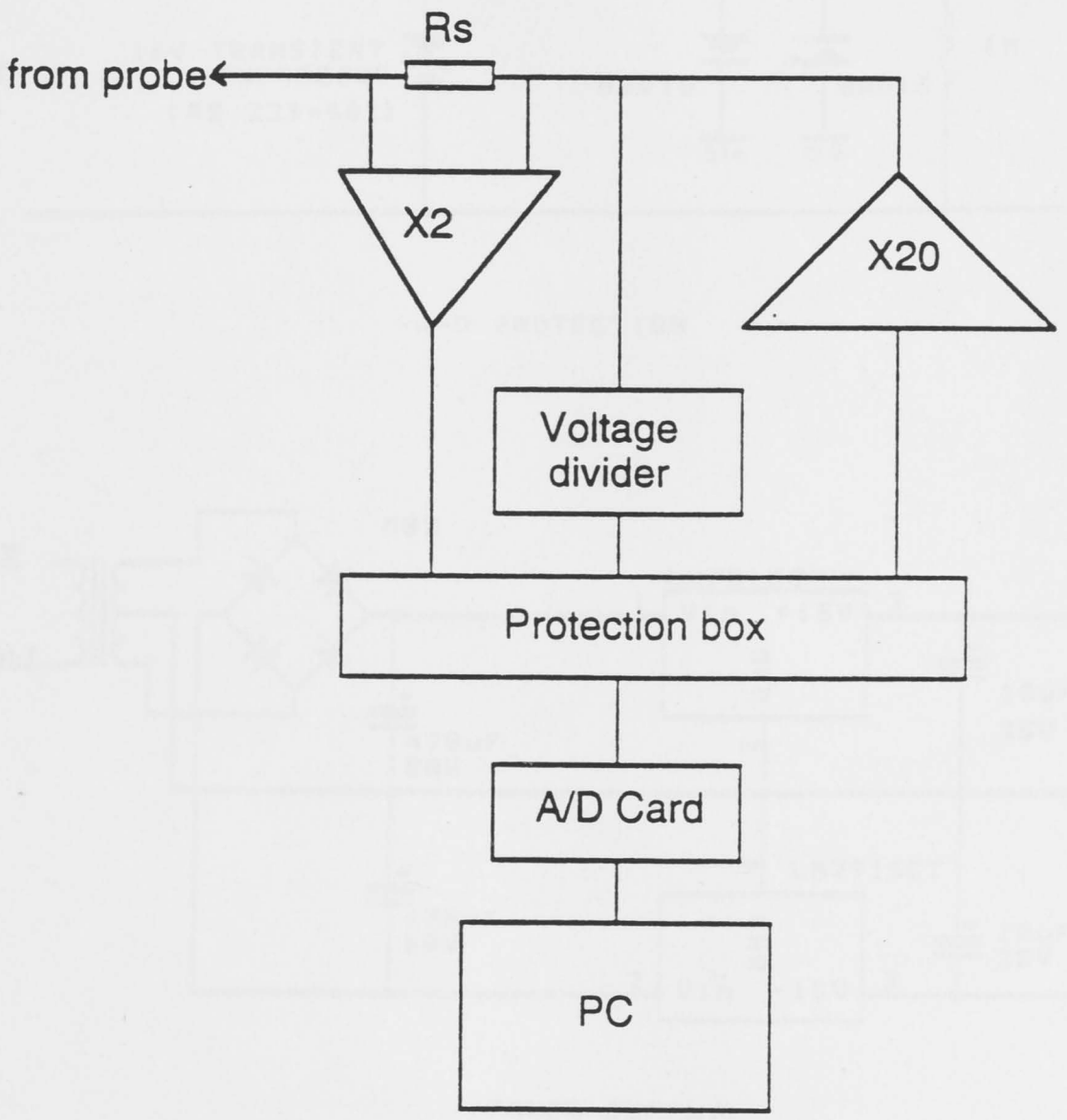

Fig.2.6 The probe data acquisition system

Fig.2.7 shows the arrangement of A/D convertor, with its protection and its power supply. The probe voltage-current characteristics are analysed numerically to obtain the charge density, electron energy distribution function and plasma potential in a standard way [27].

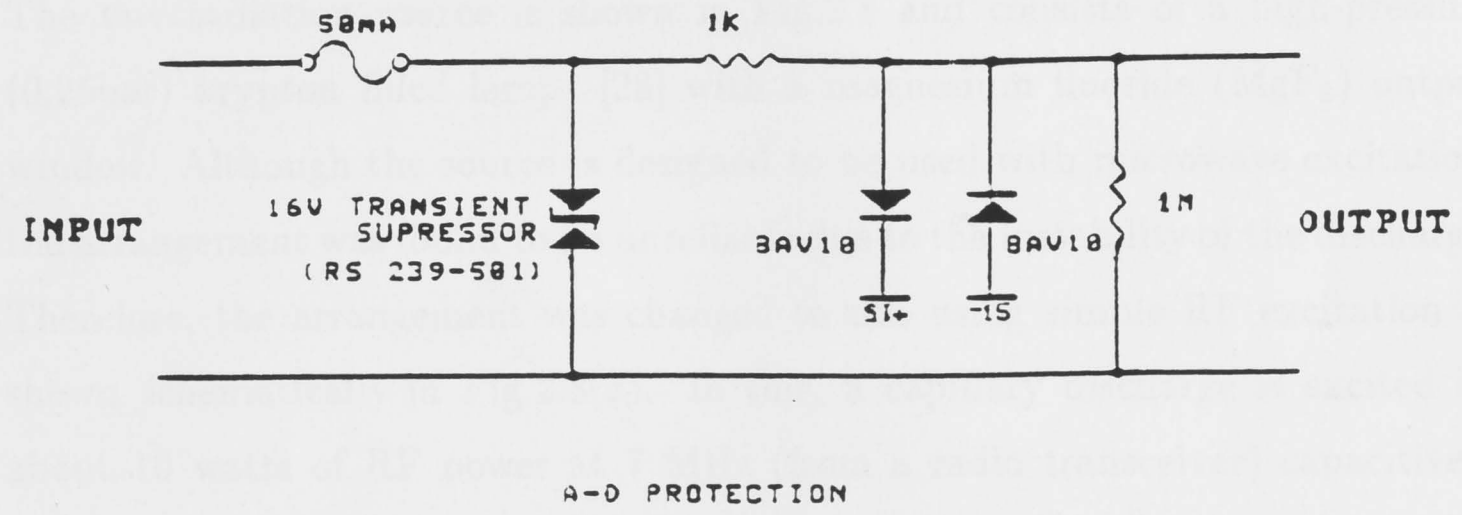

A-D PROTECTION

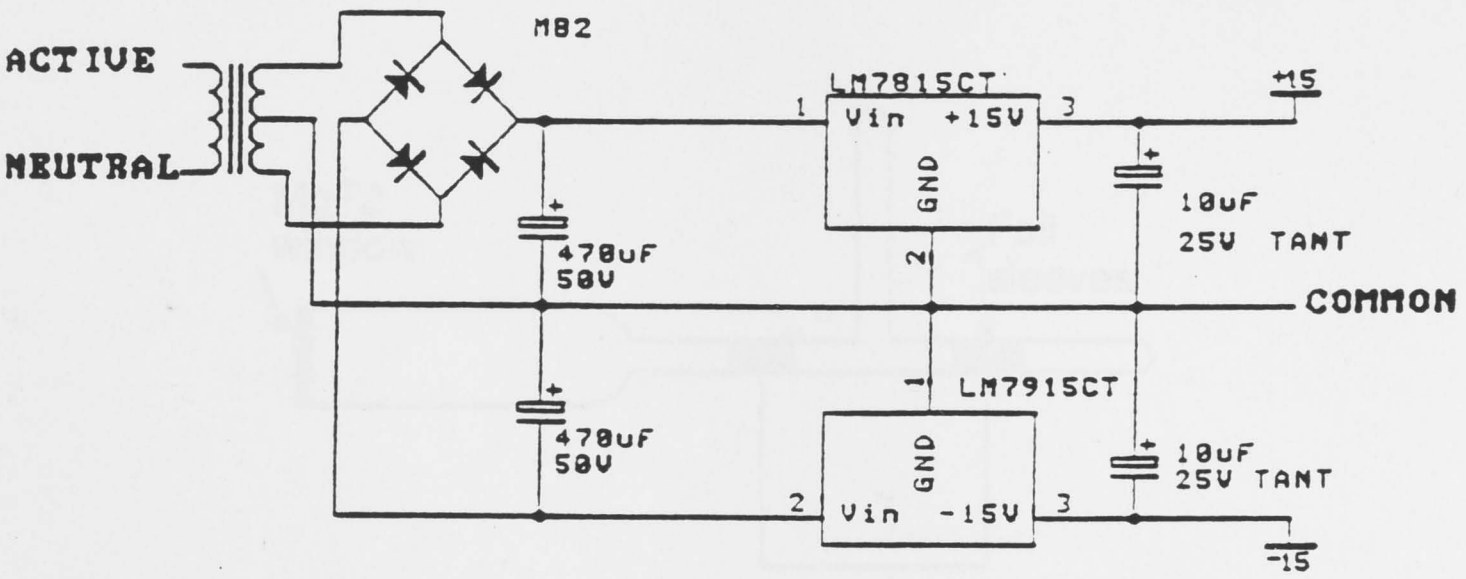

POWER SUPPLY

Fig.2.7 The protection and power supply circuits in A/D card

2.3 VACUUM ULTRA-VIOLET MEASUREMENTS

The concentrations of ground-state ($^3\sum_g$) and singlet ($^1\triangle_a$) molecular oxygen are measured by vuv absorption from a continuum source. The absolute concentration of atomic oxygen is deduced from the reduction in molecular absorption (details in Chapter 4).

The vuv radiation source is shown in Fig.2.8 and consists of a high-pressure (0.25bar) krypton filled lamp [28] with a magnesium fluoride (MgF_2) output window. Although the source is designed to be used with microwave excitation, the arrangement was found to be unreliable due to the instability of the discharge. Therefore, the arrangement was changed to one using simple RF excitation as shown schematically in Fig.2.8(a). In this, a capillary discharge is excited by about 10 watts of RF power at 7 MHz (from a radio transceiver) capacitively coupled to the lamp via close-fitting metal foil sleeves, and modulated at 500Hz. The lamp emits continuum radiation in the range 125-180nm.

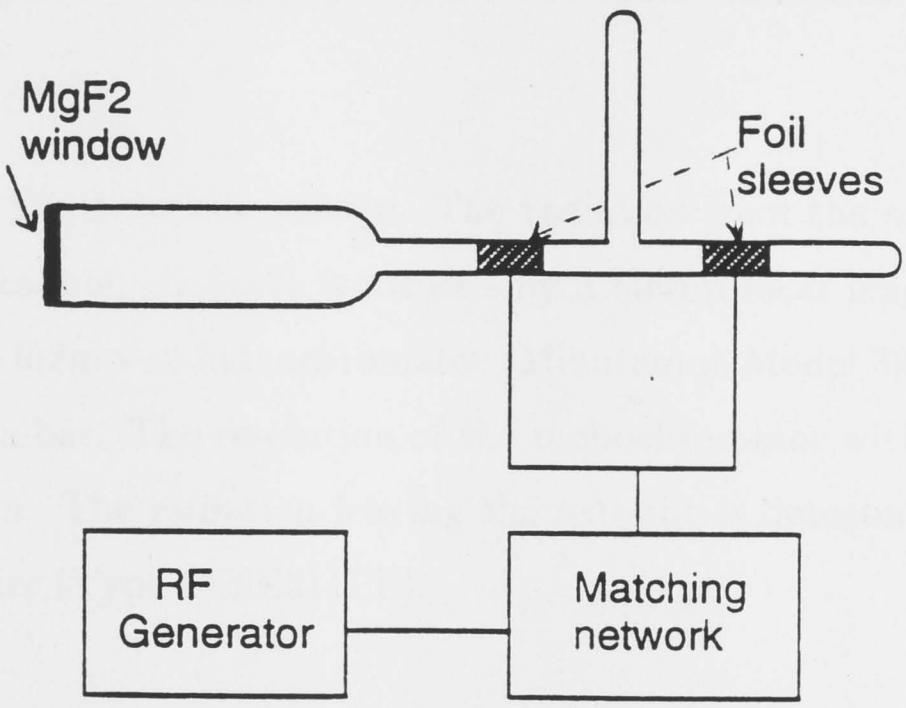

Fig.2.8 (a) The vuv radiation source with RF excitation.

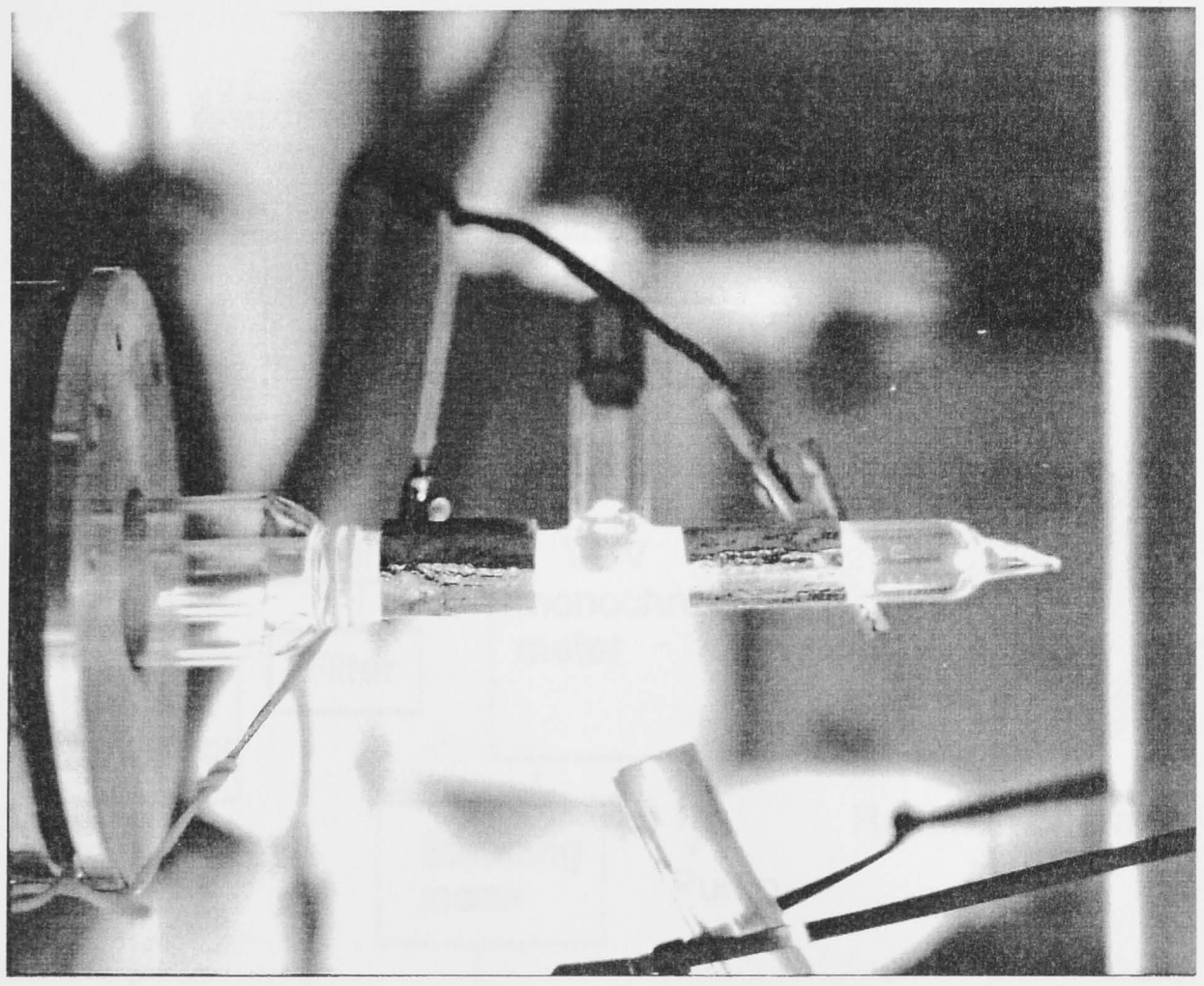

Fig.2.8 (b) Photograph of the vuv radiation source.

Fig.2.9 shows the detection system. The radiation from the source transmitted through the reaction chamber is focused by a 60mm focal length MgF_2 lens on to the slit of a 0.2m vuv monochromator (Minuteman Model 302-VM) evacuated to below 10^{-5}mbar. The resolution of the monochromator with 30μm wide slits is about 0.4nm. The radiation leaving the exit slit is detected by a solar-blind photo-multiplier (Type G26E314LF).

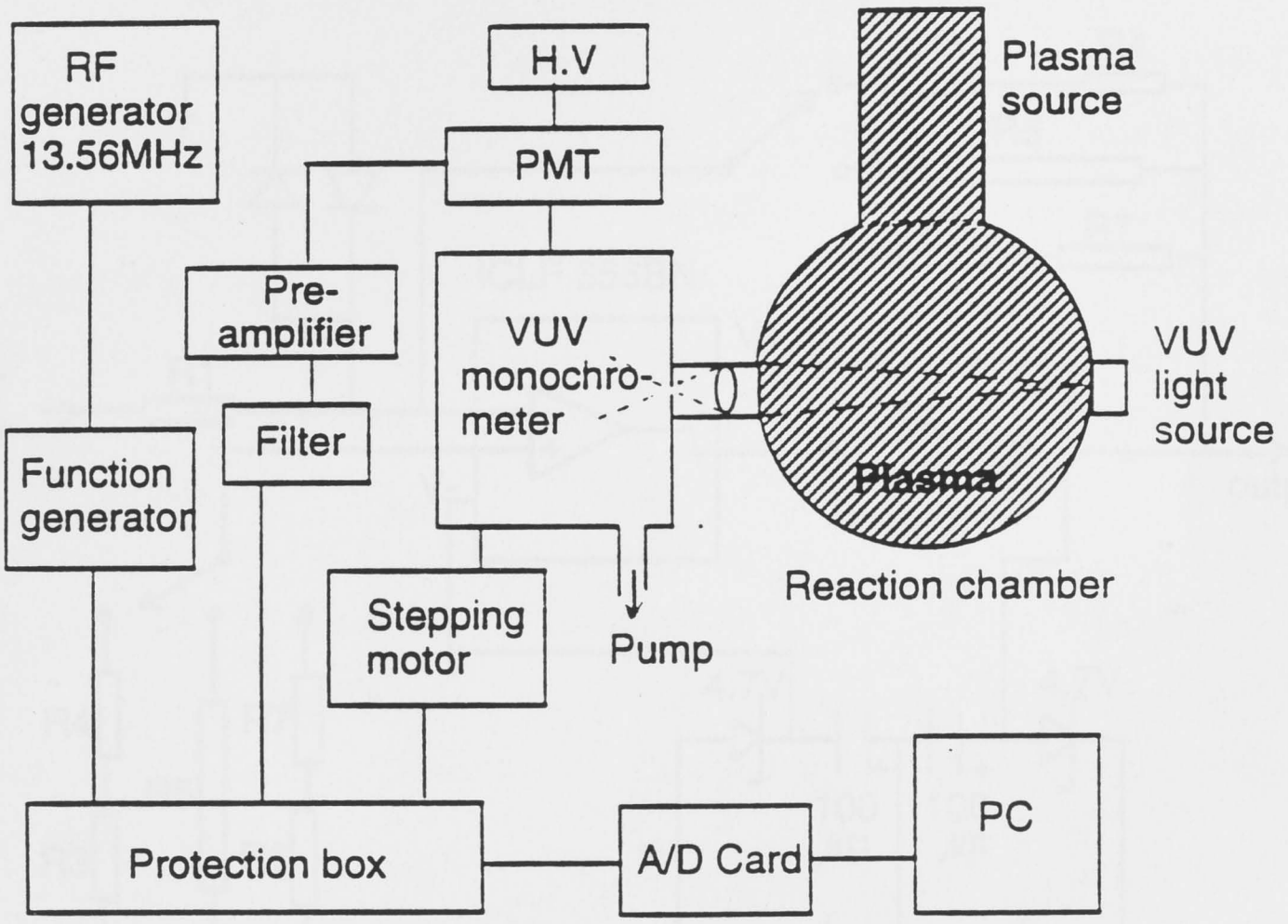

Fig.2.9 The vuv detection system

After pre-amplification (by the circuit shown in Fig.2.10) and low-pass filtering, the digitised photo-multiplier signals (representing the transmitted intensities) are measured using a numerical box-car integration method by computer, averaging over a 15 seconds record for each data point.

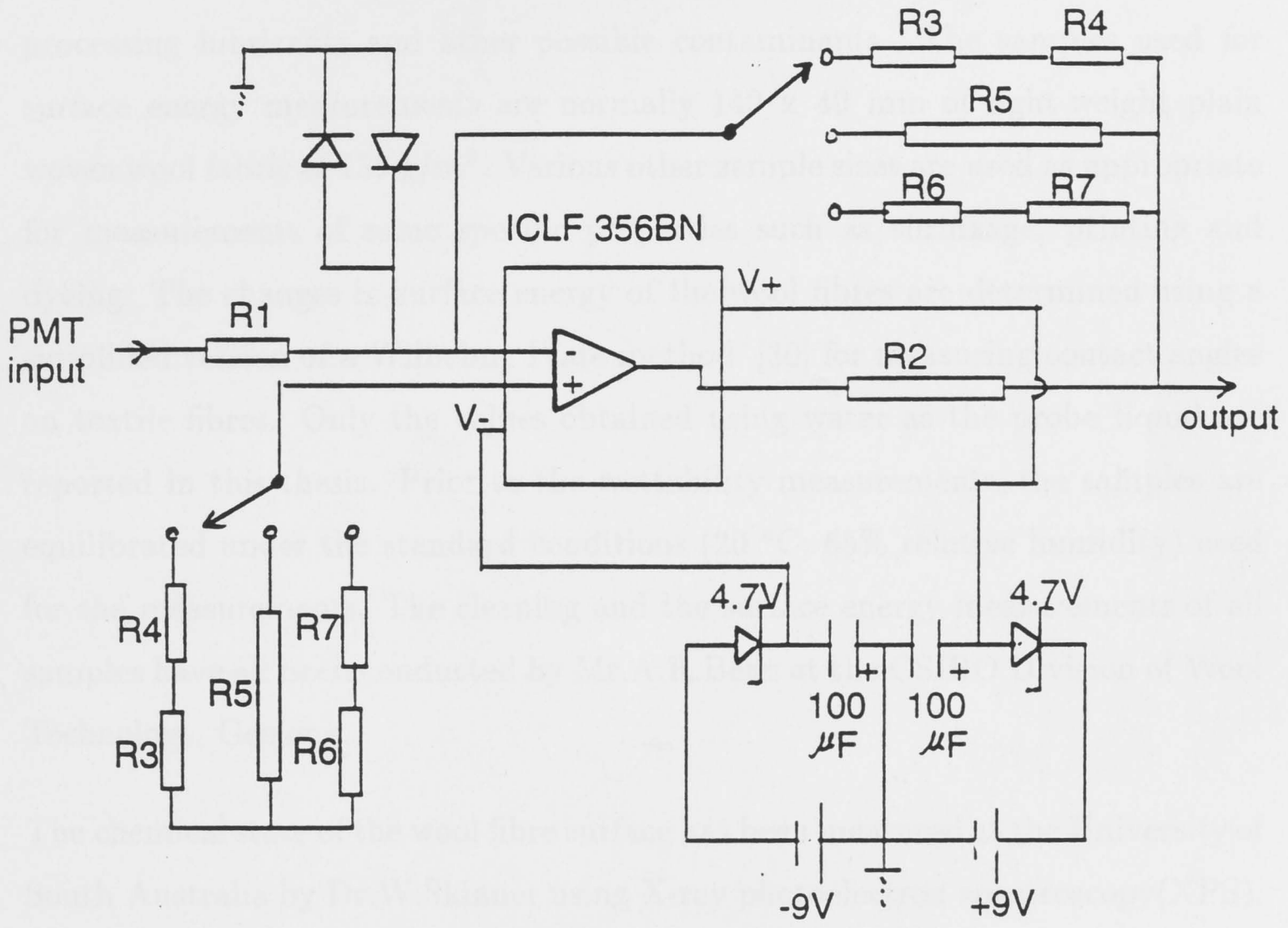

Fig.2.10 Pre-amplifier circuit. R_1=1KΩ; R_2=10KΩ; R_3=100MΩ; R_4=10MΩ; R_5=1000MΩ; R_6=10MΩ; R_7=100KΩ.

2.4 SURFACE ANALYTICAL TECHNIQUES

Before treatment, all wool fabric samples are cleaned in accord with a standard solvent extraction method in dichloromethane [29] for 3 hours to remove residual processing lubricants and other possible contaminants. The samples used for surface energy measurements are normally 140 x 40 mm of light-weight plain woven wool fabric of 155 g/m^2. Various other sample sizes are used as appropriate for measurements of some specific properties such as shrinkage, printing and dyeing. The changes in surface energy of the wool fibres are determined using a simplified version of a Wilhelmy Plate method [30] for measuring contact angles on textile fibres. Only the values obtained using water as the probe liquid are reported in this thesis. Prior to the wettability measurements, the samples are equilibrated under the standard conditions (20 ^{o}C; 65% relative humidity) used for the measurements. The cleaning and the surface energy measurements of all samples have all been conducted by Mr.A.R.Bean at the CSIRO Division of Wool Technology, Geelong.

The chemical state of the wool fibre surface has been measured at the University of South Australia by Dr.W.Skinner using X-ray photoelectron spectroscopy(XPS). XPS spectra are recorded using a PHI Model 5100 spectrometer, with a Mg Kα X-ray source operating at 300 W and with an analyser pass energy of 35eV. The vacuum pressure in the analyzer chamber is always $< 10^{-8}$mbar during analysis with the sample cooled by a liquid nitrogen cold finger. The energy scale is calibrated using the Fermi edge and the Ag $3d_{5/2}$ line (binding energy 367.9eV), whilst the retardation voltage was calibrated noting the position of the peaks corresponding to Cu $2p_{3/2}$ (binding energy 932.67eV) and Cu $3p_{3/2}$ (binding energy 75.13eV). Prior to the XPS measurements, the treated samples are stored in sealed containers.

Morphological changes to the wool fibre surface have been measured at the CSIRO Division of Wool Technology, Geelong by Mr.Bean using a Hitachi S4100 Field Emission Scanning Electron Microscope (FESEM). For imaging the beam energy is 1 keV, a working distance of 5mm is used, with a beam current around 2.5pA, an emission current of 10μA and an objective aperture of 20μm.

Free radicals formed on wool surface have been measured at the Research School of Chemistry of the Australian National University by Dr. Deming Wang using Electron Paramagnetic Resonance (EPR) spectra . All spectra have been measured at room temperature by a Varian X-band ($\sim$ 9.0GHz) V4500 spectrometer.

3

CHARGED PARTICLE STUDIES

3.1 INTRODUCTION

Low temperature plasmas consist predominantly of neutral particles with a relatively small proportion of charged particles. The gas is ionized, excited, and dissociated by electron collisions with the neutral particles, thus creating the various chemically active species. The main active species assumed to be important in oxygen discharges are atomic oxygen O, excited singlet oxygen molecules $O_2(a^1\Delta_g)$, positive ions O_2^+, and negative ions O^- [31]. As the active species are created by electron-neutral collision, it is important to study the electron energy distribution function. In this chapter only the charged particles are considered. We concentrate on the studies of the electron energy distribution function (EEDF) and the positive ion number density (N_i) in an oxygen plasma as they are essential to understand how the active neutrals are produced and the reaction mechanisms between them and the wool. Negative ions O^- have not been considered here since any O^- formed would recombine very quickly [32], it would not be available. This assumption is consistent with the model calculations in Chapter 5.

This chapter describes the study of the charged particles in the oxygen plasma both inside the plasma source itself and in the reaction chamber. Section 3.2 describes how the plasma density depends on the gas pressure and RF power,

the spatial distribution of the plasma parameters, and the effect of inserting a wire mesh baffle between the source and the chamber. The emphasis placed on determining the EEDF (Section 3.3) is because the main production of reactive species in the plasma is by electron impact excitation, ionization, or dissociation, all of which depend on the kinetic energy of the electrons. The measured EEDFs are then compared with the commonly assumed Maxwell-Boltzmann and Druyvesteyn functions.

3.2 CHARGED PARTICLE CHARACTERISTICS

The experimental apparatus, Langmuir probes and data acquisition system have been described in Chapter 2. In order to describe clearly the spatial distribution of the particles, a laboratory coordinate system is defined in Fig.3.1. The origin 0 is chosen to be at the axis of the source 2cm above the exit of the source (for reasons given in Section 3.2.2). The wool sample position is at z=16cm (the chamber centre), i.e. 16cm below the origin 0.

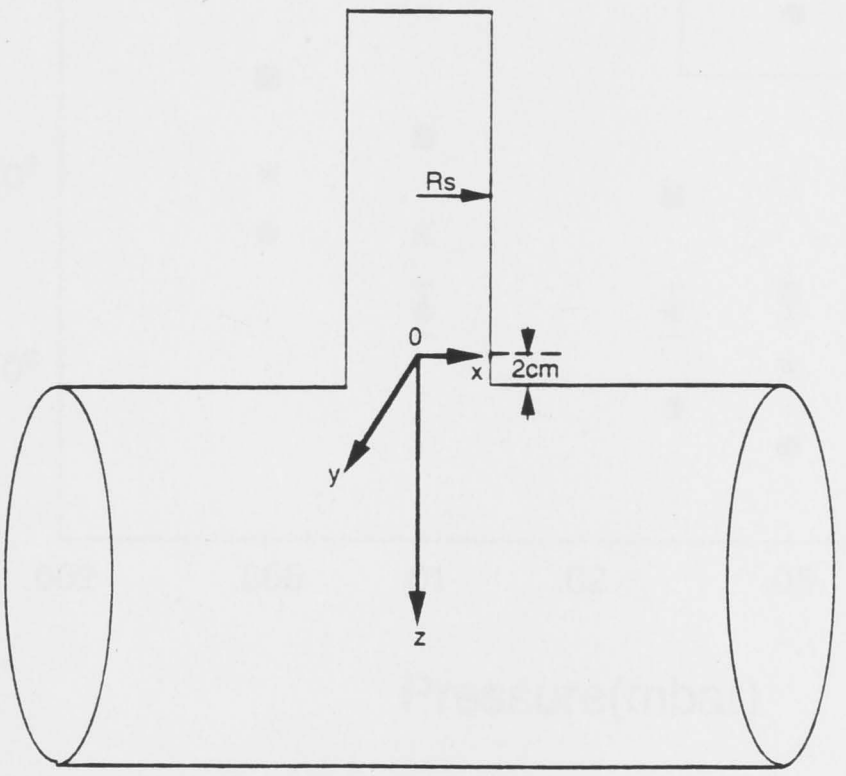

Fig.3.1 Coordinate system

3.2.1 Effects of Gas Pressure and Radio-Frequency Power

As gas pressure p and RF power P are the principal external controls for plasma production, the effects are first studied of their variation on the plasma density at two positions: in the chamber (z=16cm) corresponding to the centre of the wool samples, and at the origin 0 inside the source. Because of limits to the range adjustment of the RF matching box, the two experimental parameters are restricted to pressures between 0.005mbar and 0.1mbar and powers between 50W and 300W.

Fig.3.2 shows the effects of p and P on the ion density N_i in the chamber for pressures from 0.005 to 0.1mbar at three RF powers, 50W, 100W, and 150W. It

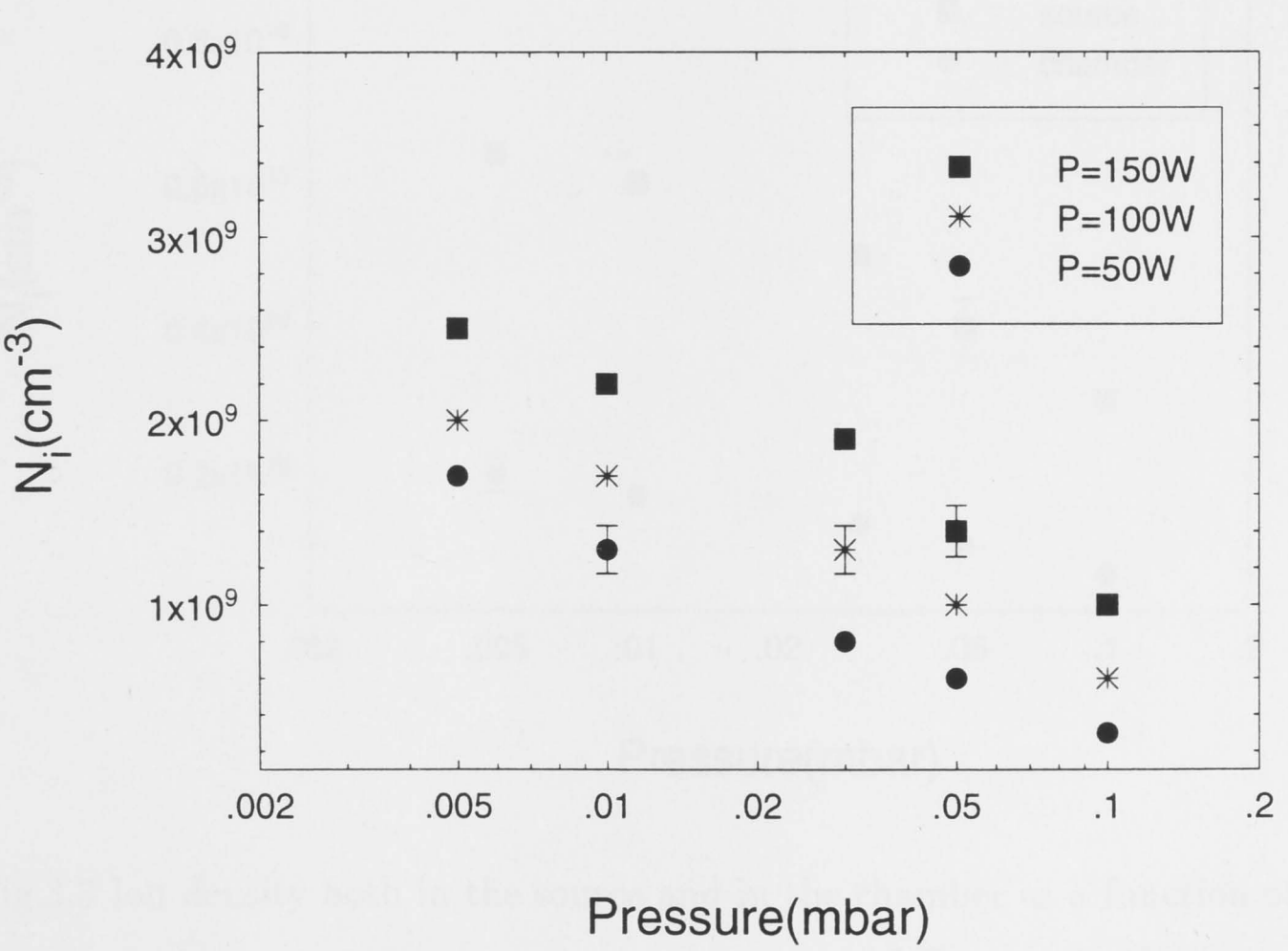

Fig.3.2 Ion density as a function of pressure for three RF power levels

can be seen that N_i in the chamber always decreases as the pressure increases for all three RF powers, but increases with RF power at all pressures.

The density N_i in the plasma source and the reaction chamber as a function of pressure is shown in Fig.3.3. It is noted that the ratio of N_{ic} (the ion density in the chamber) and N_{is} (ion density in the source) shows a slight decrease as the pressure increases (Fig.3.4). This can be explained by the electron mean free path (λ_e) being inversely proportional to gas pressure [33]. The plasma in the

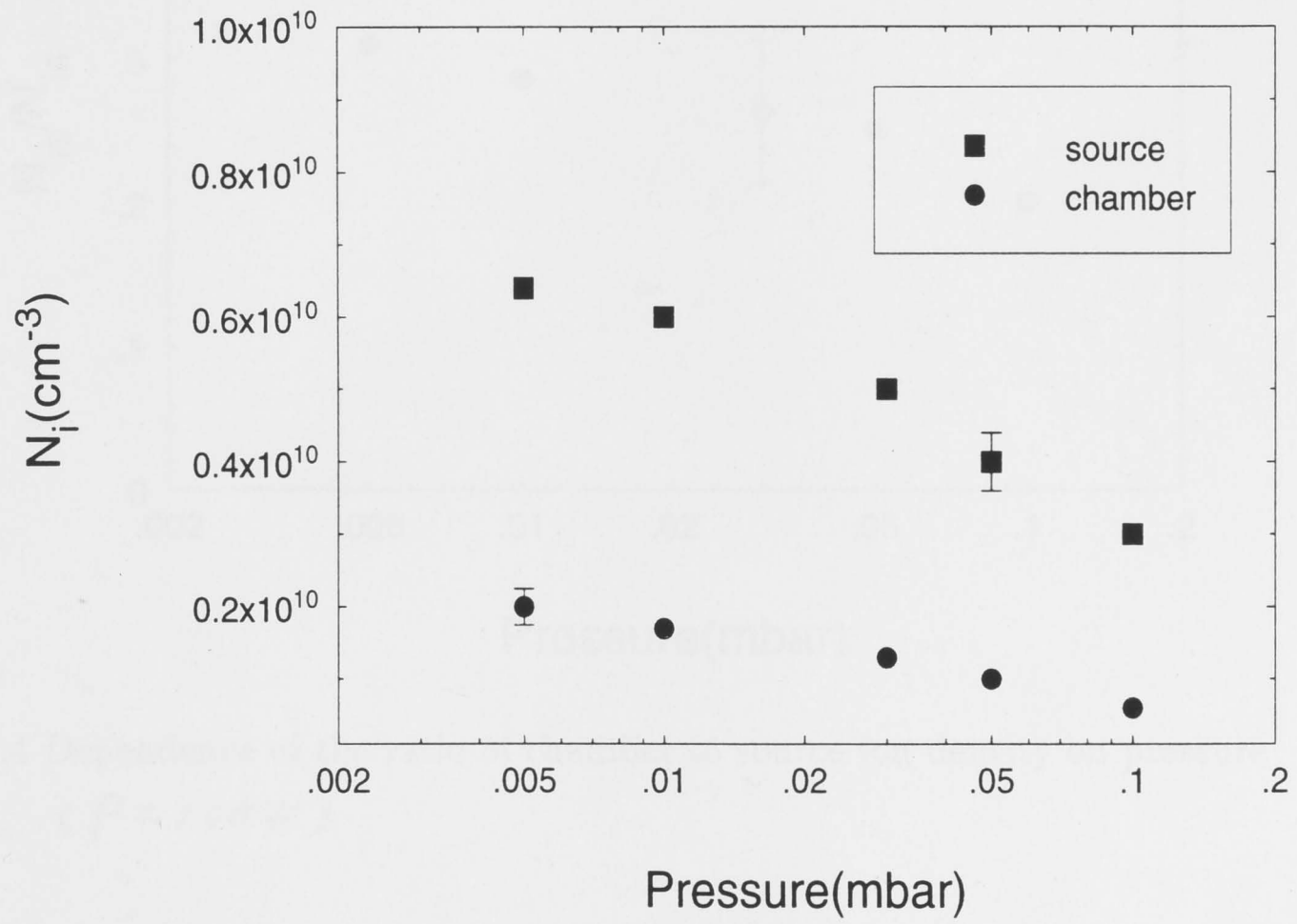

Fig.3.3 Ion density both in the source and in the chamber as a function of pressure (P= 100 W)

chamber must come mainly from the source since there is negligible RF power in the chamber. The increased collisionality results in both more rapid electron cooling, and thus reduced re-ionization, and enhanced recombination of the charged particles.

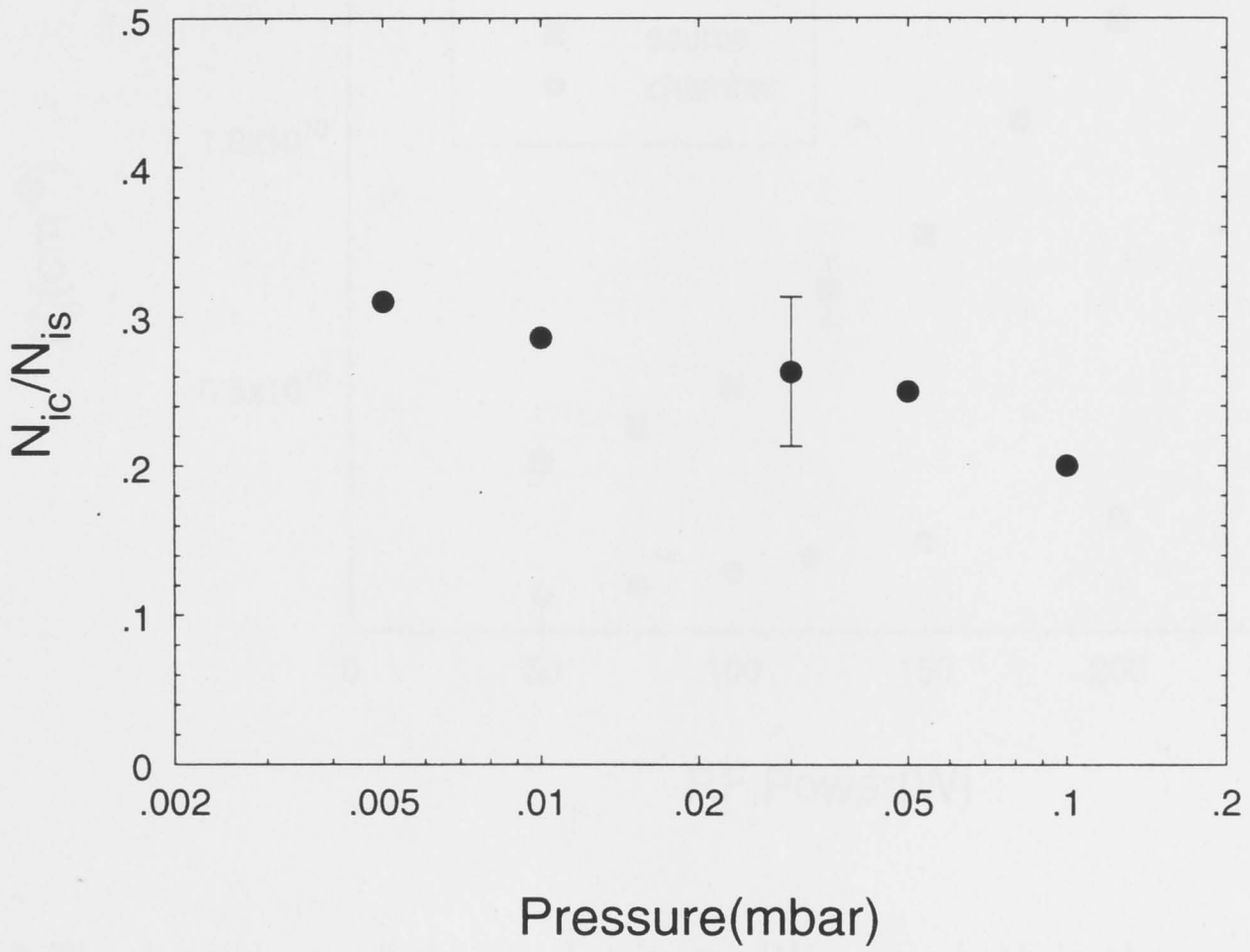

Fig.3.4 Dependence of the ratio of chamber to source ion density on pressure (P=100W)

The effects of RF power on N_i in both the source and the chamber at a fixed gas pressure, p=0.03mbar, are shown in Fig.3.5. It is interesting that the ratio of N_{ic} and N_{is} remains nearly constant, as shown in Fig.3.6. It shows that there is no alteration in power deposition when RF power is varied.

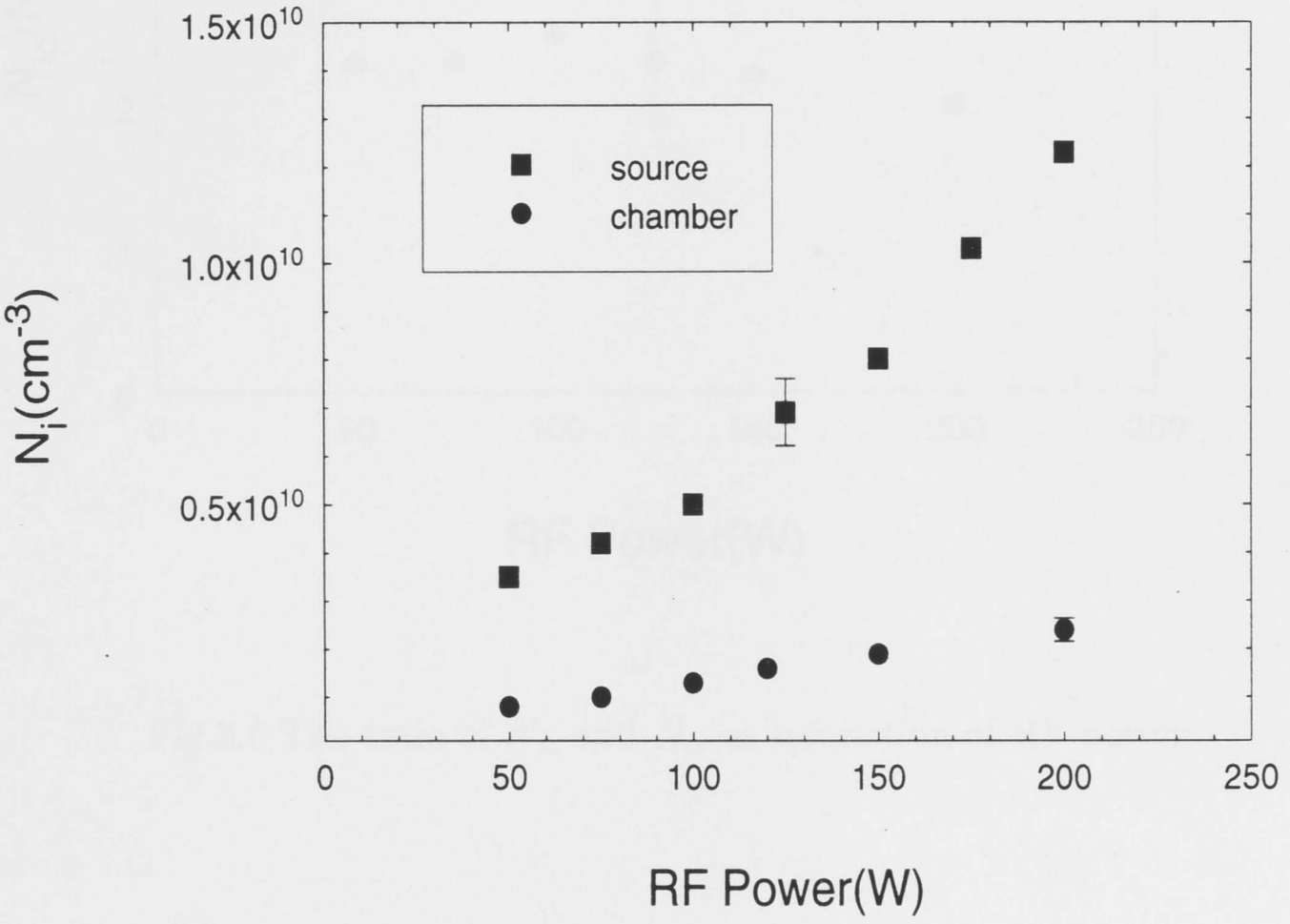

Fig.3.5 The dependence of the ion density on RF power both in the source and in the chamber

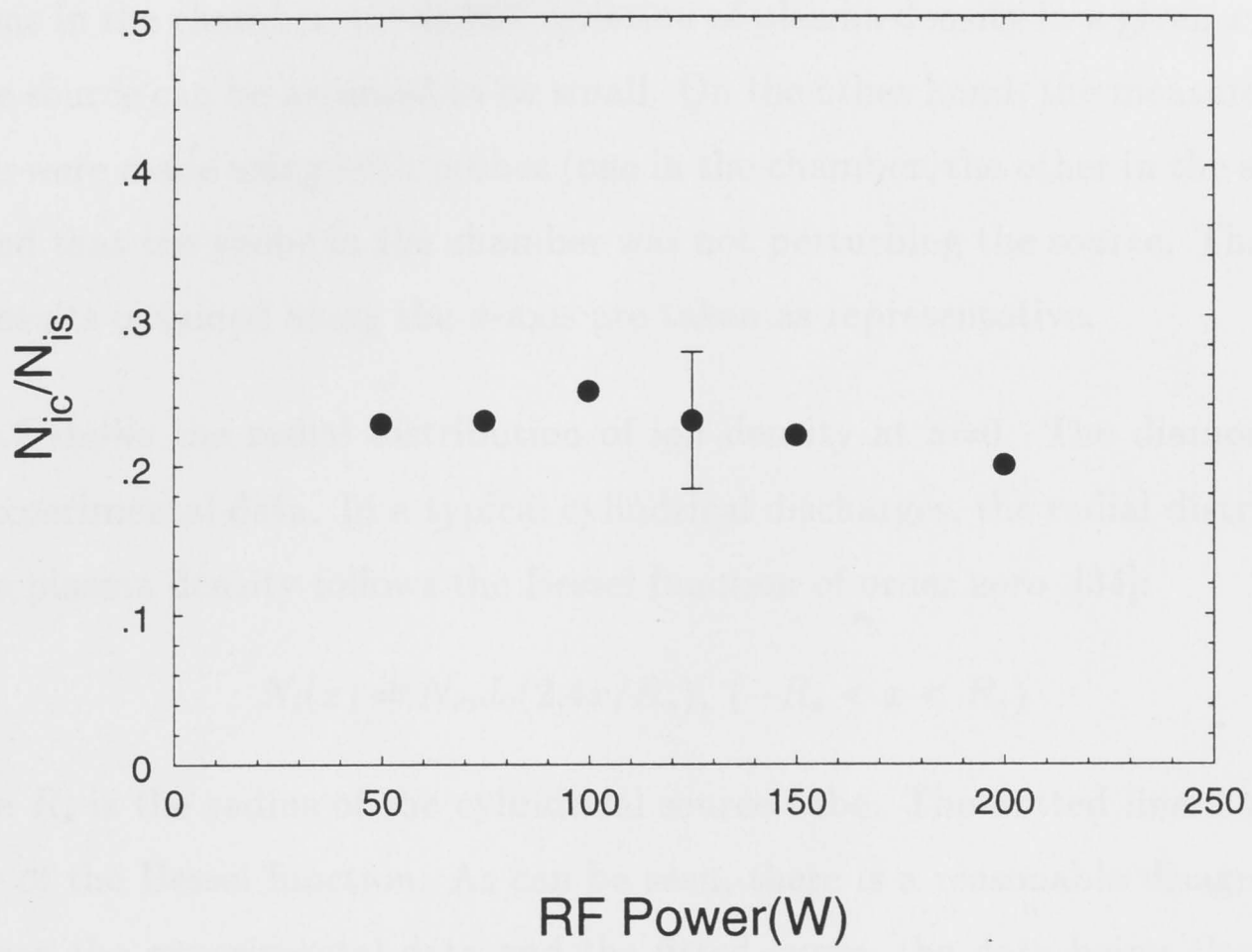

Fig.3.6 The ratio of N_{ic} and N_{is} as a function of RF power

3.2.2 Spatial Profiles

In a more detailed study, the spatial profiles of the plasma parameters have been measured at a gas pressure and RF power (0.03mbar and 100W) chosen as the optimum conditions for plasma-wool processing (see following chapters).

In the Source:

Due to the limited access for the Langmuir probe, the plasma parameters in the source could be measured only along the x-axis . However, from the cylindrical

symmetry of the plasma source and as suggested by the measured spatial distributions in the chamber, the ~~radial~~ poloidal variation of plasma density in a given xy plane in the source can be assumed to be small. On the other hand, the measurements, which were made using both probes (one in the chamber, the other in the source), showed that the probe in the chamber was not perturbing the source. Therefore, the results obtained along the x-axis are taken as representative.

Fig.3.7 shows the radial distribution of ion density at z=0. The diamonds are the experimental data. In a typical cylindrical discharges, the radial distribution of the plasma density follows the Bessel function of order zero [34]:

$$N_i(x) = N_{i0} J_0(2.4x/R_s), \ (-R_s < x < R_s) \tag{3.1}$$

where R_s is the radius of the cylindrical source tube. The dotted line is a fitted curve of the Bessel function. As can be seen, there is a reasonable disagreement between the experimental data and the fitted curve, the data being closer to a cosine function (the solid line). This result is in good agreement with previous experiment [35] in a similar apparatus. The slightly higher charged particle density towards the outside is probably caused by the antenna being close to the cylindrical source tube walls, which results in a strong field at the edge of the tube.

In the Reaction Chamber:

The ion densities were measured along the x and y directions at z=16cm (the chamber centre). The results are presented in Fig.3.8 (a) and (b) respectively.

It should be noted that N_i is roughly constant (N_i=1.26 $\pm$ 0.04)x10^9 cm^{-3} in the region of interest ($-R_s < (x, y) < R_s$). This type of distribution means that N_i can be assumed to be constant over the wool samples and also along the only available optical path for the vacuum ultra-violet absorption measurements,

which uses the two opposing ports (along the y-axis) in the side of the cylindrical chamber (see Fig.2.1 (b)). Since at least some of the active neutrals will be formed by electron collisions in the chamber, the fact that the charged particle distribution in the region of the sample is fairly uniform is very useful and will be discussed in later chapters.

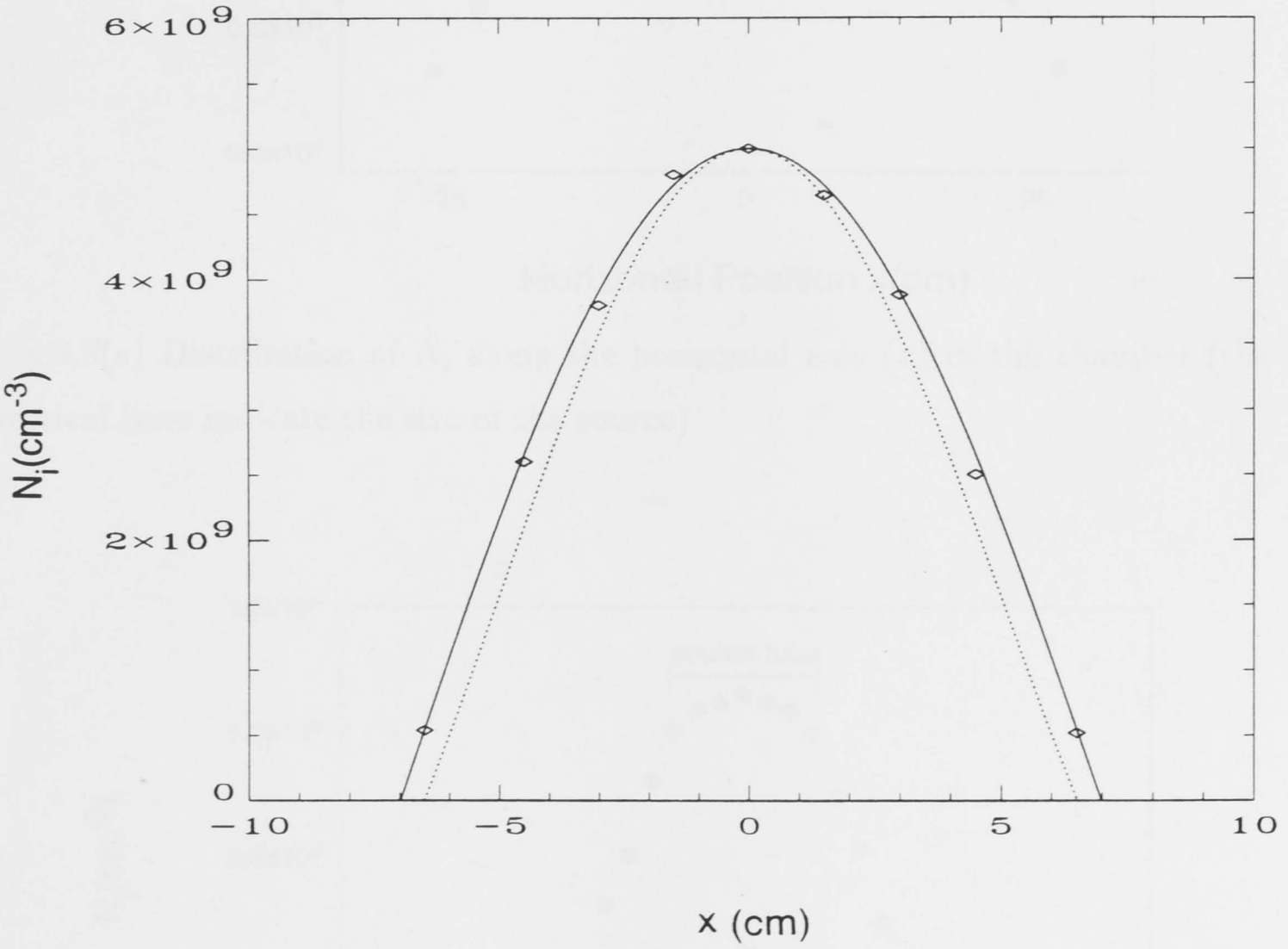

Fig.3.7 Radial distribution of N_i in the source

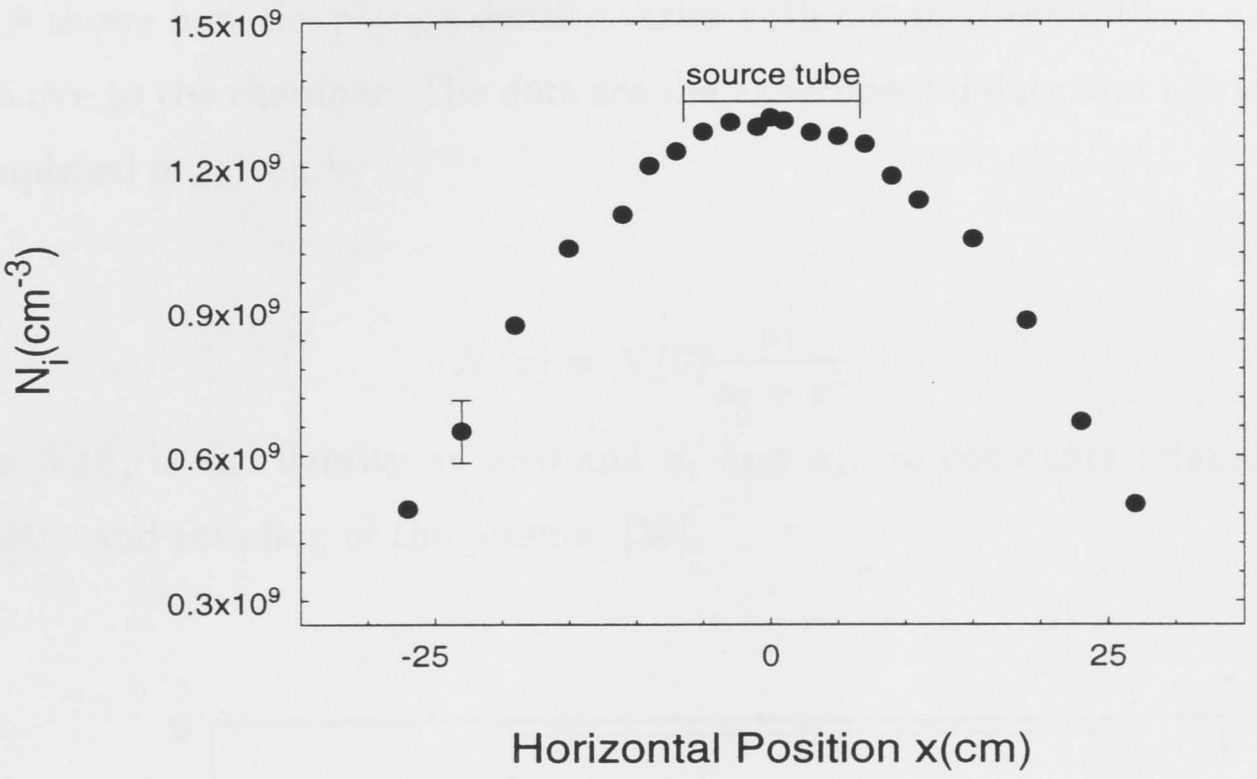

Fig.3.8(a) Distribution of N_i along the horizontal axis (x) in the chamber (the vertical lines indicate the size of the source)

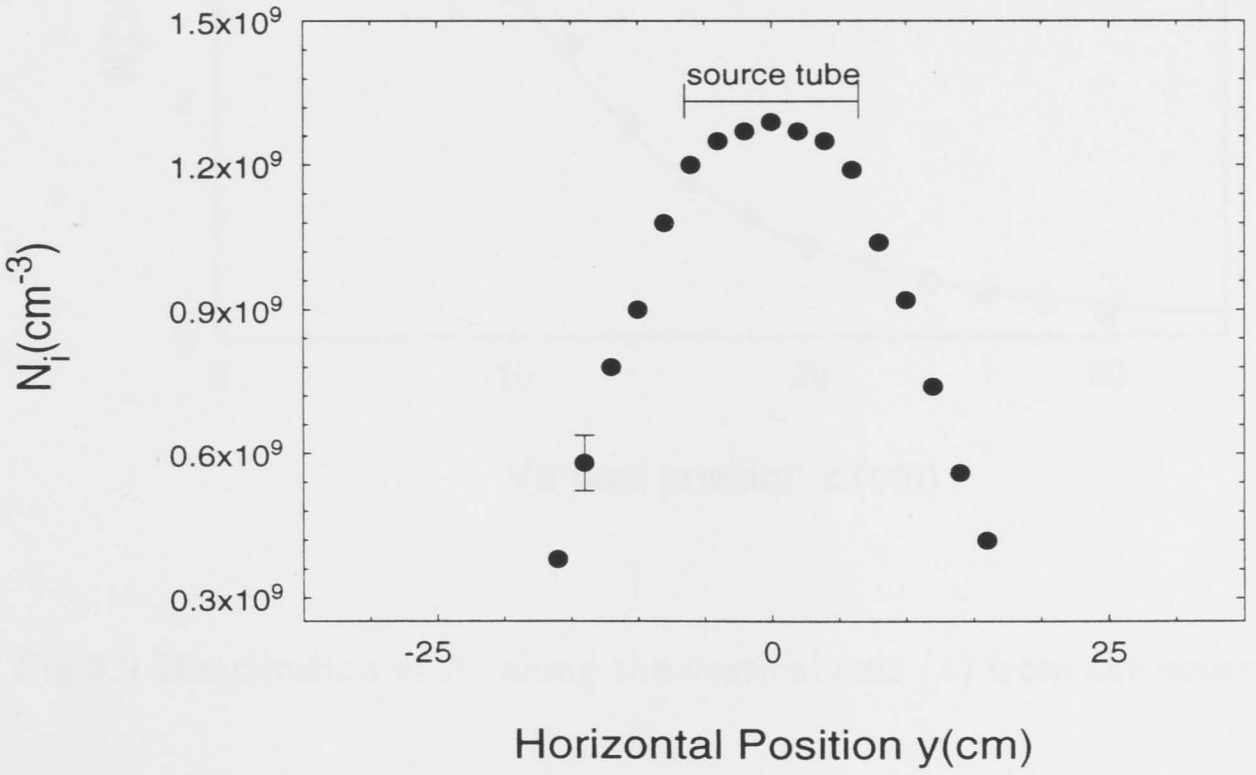

Fig.3.8(b) Distribution of N_i along the horizontal axis (y) in the chamber

Transport of Charged Particles from the Source to the Reaction Chamber

Fig.3.9 shows how the plasma density varies with distance along the z-axis from the source to the chamber. The dots are the experimental data and the solid line an empirical fit, given by

$$N_i(z) = N_i(0)\frac{a_1}{a_2 + z^3} \tag{3.2}$$

where $N_i(0)$ is the density at z=0 and a_1 and a_2 are constants related to the geometry and coupling of the plasma [36].

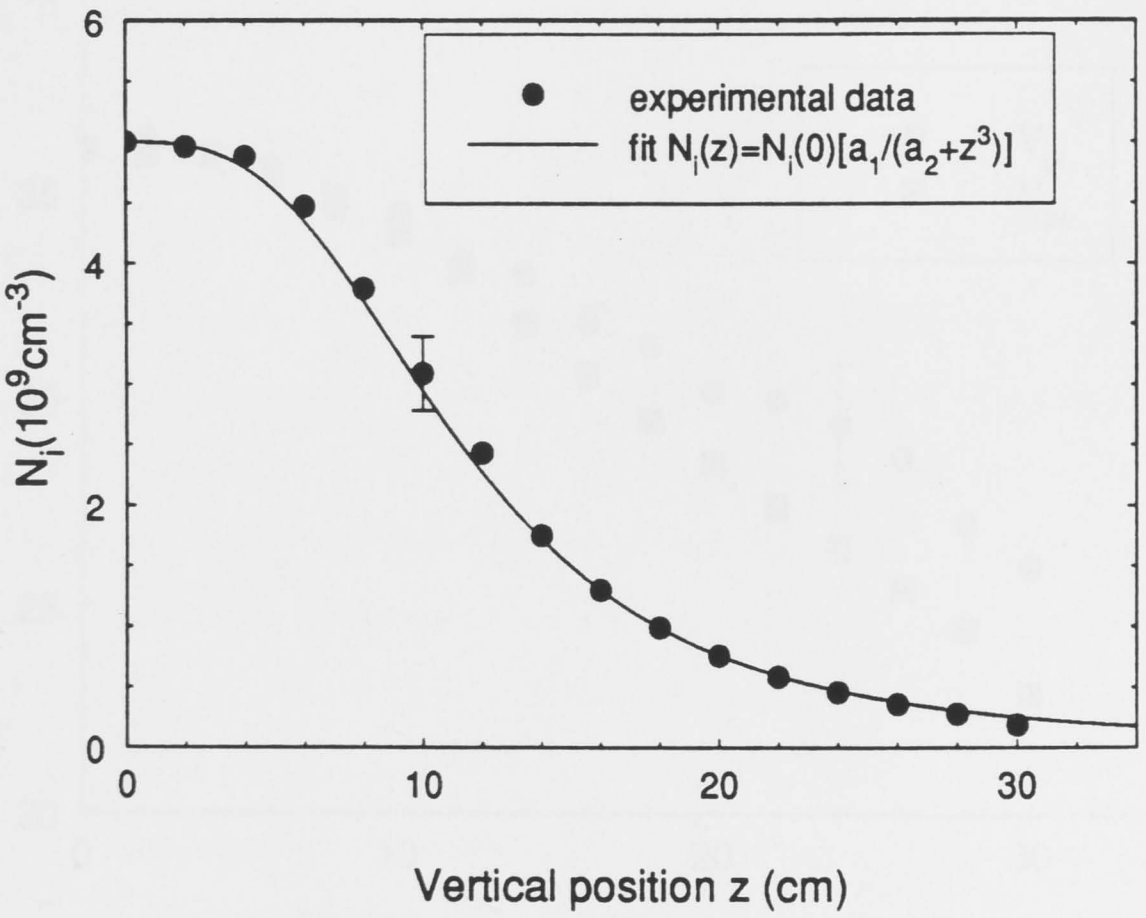

Fig.3.9 Distribution of N_i along the vertical axis (z) from the source to the chamber

Since v_i (the ion drift velocity) is approximately constant [37] , we can explain this transport behaviour by assuming that charged particle flux conservation of the plasma drifting from the source undergoes an expansion as a function of z^3.

To maintain approximate charge neutrality, the self-consistent field generated in the diffusion region is given by the Boltzmann relation [38]:

$$V_p(z) = V_p(0) + \frac{k_B T_e}{e} ln \frac{N_i(z)}{N_i(0)} \tag{3.3}$$

if the EEDF is Maxwellian with electron temperature T_e, where k_B is the Boltzmann constant and e is the electron charge.

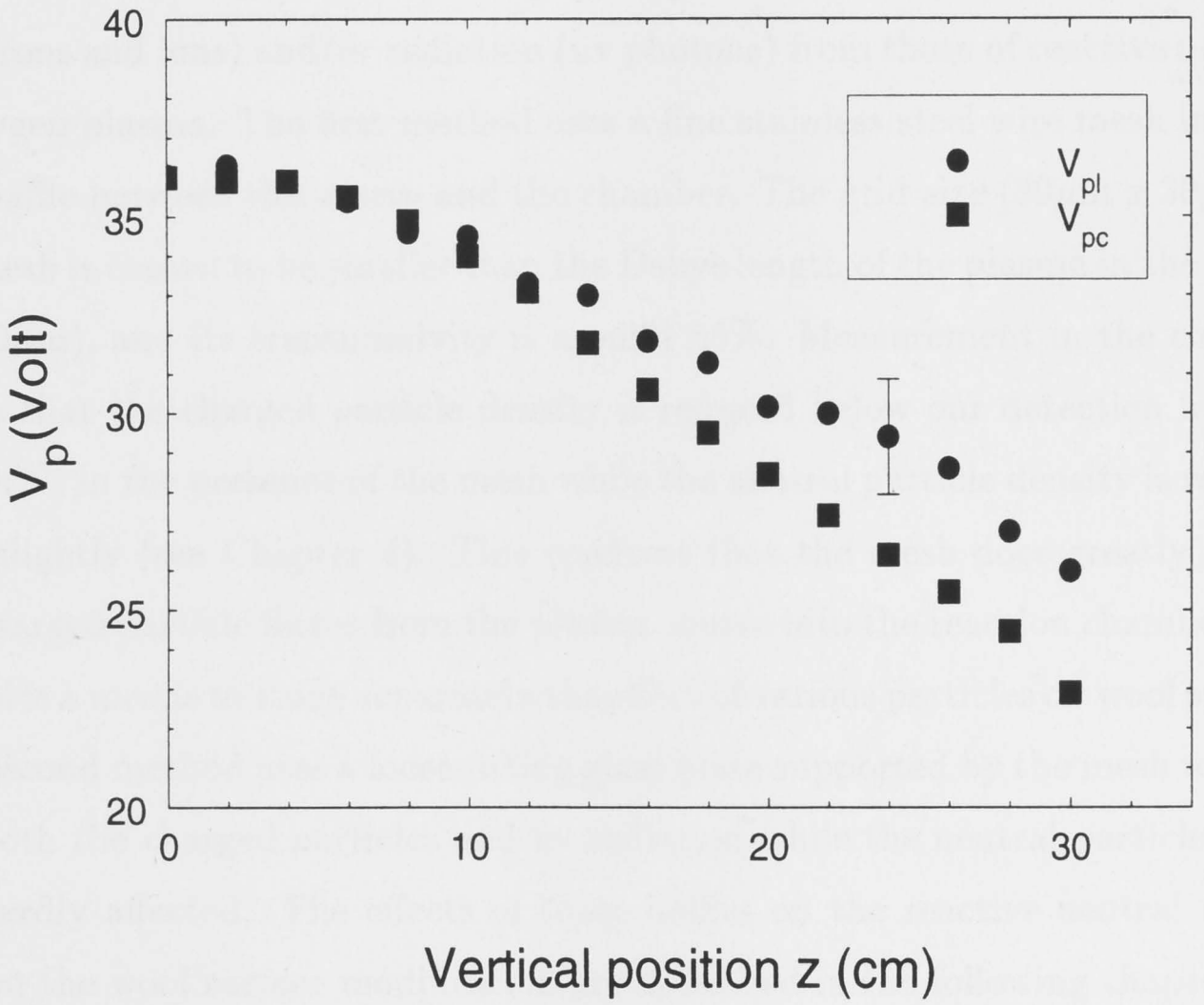

Fig.3.10 Distribution of plasma potential along the vertical axis (z)

Fig.3.10 shows the variation in plasma potential along the z-axis. The subscript '*pl*' is used to denote the value determined by the standard Langmuir probe

method and '*pc*' is the value according to Eq.(3.3) where T_e is as measured by a Langmuir probe assuming a Maxwellian EEDF. It can be seen that V_{pc} becomes a little different from V_{pl} as we move along the z away from the origin 0. This discrepancy may be related to the fact that the EEDF is not actually Maxwellian. This is discussed in Section 3.3.

3.2.3 Use of Selective Baffles

In order to identify the main reactive species in the plasma responsible for the modification of wool surface, two methods are used to control flow between the source and the chamber and to help distinguish the effects of charged particles (electrons and ions) and/or radiation (uv photons) from those of reactive neutrals in oxygen plasma. The first method uses a fine stainless steel wire mesh inserted as a baffle between the source and the chamber. The grid size (30μm x 30μm) of the mesh is chosen to be smaller than the Debye length of the plasma in the source ($\sim 200\mu$m), and its transmissivity is around 55%. Measurement in the chamber shows that the charged particle density is reduced below our detection level ($< 10^8 \mathrm{cm}^{-3}$) in the presence of the mesh while the neutral particle density is reduced only slightly (see Chapter 4). This confirms that the mesh does greatly reduce the charged particle fluxes from the plasma source into the reaction chamber, and provides a means to study separately the effect of various particles on wool surface. The second method uses a loose-fitting glass plate supported by the mesh to block out both the charged particles and uv radiation while the neutral particle fluxes are hardly affected. The effects of these baffles on the reactive neutral species and on the wool surface modification are described in the following chapters.

3.3 ELECTRON ENERGY DISTRIBUTION FUNCTION

The importance of knowing the electron energy distribution has been mentioned in section 3.1. Usually, the standard Langmuir probe method is used to derive the plasma potential, the plasma density, and the electron temperature. However, the very term 'electron temperature' implies that the plasma has a Maxwellian distribution of electron energies. For our purpose, it is important to have a more accurate knowledge of the EEDF because the chemical kinetics are sensitive to the energy distribution. For this reason, the Druyvesteyn method [39] (also known as the second derivative technique) is used to determine the actual distribution function.

3.3.1 Modelling the Distribution

The electron energy distribution ($F(E)$) can be represented as the product of the electron density (N_e) and a normalized electron energy distribution function ($f(E)$):

$$F(E) = N_e f(E) \tag{3.4}$$

and

$$\int_0^\infty f(E)dE = 1 \tag{3.5}$$

Druyvesteyn showed that the EEDF is related to the second derivative of the Langmuir I-V characteristic in the voltage region just below the plasma potential:

$$f(E) \propto \sqrt{E}\frac{d^2 I_e}{dV^2} \tag{3.6}$$

$$E = V_p - V \tag{3.7}$$

where V is the potential applied to the probe, V_p is the plasma potential, E is the electron energy, and I_e is the electron current collected by the probe.

In this work, the second derivative is obtained by modelling from the $I-V$ curve measured using Langmuir probes.

The modelling is carried out using the following procedure:

(1) The net electron current is obtained from a straight-line extrapolation of the ion current which is subtracted (see Fig.3.11 and Fig.3.12).

$$I_e = I - I_{i0}; \tag{3.8}$$

(2) The second deviative, d^2I_e/dV^2, is calculated numerically;

(3)$\sqrt{E}(d^2I_e/dV^2)$ is plotted as a function of E;

(4)An analytical function is fitted to the resulting distribution:

$$f(E) = a\sqrt{E}exp(-bE^c) \tag{3.9}$$

where a is a normalization constant, b and c are fitting parameters. This analytical function was introduced by Rundle [40].

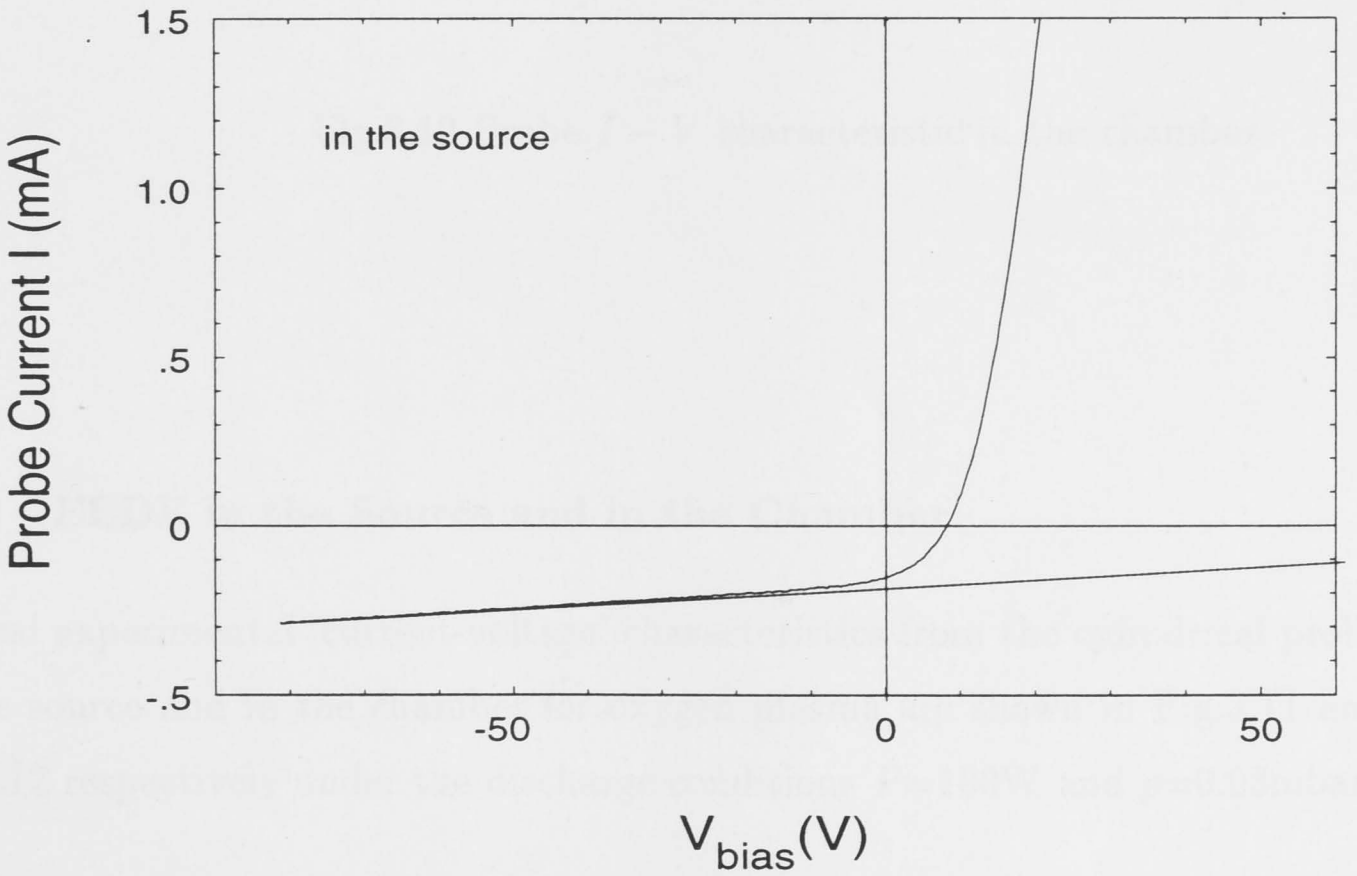

Fig.3.11 Probe $I-V$ characteristic in the source

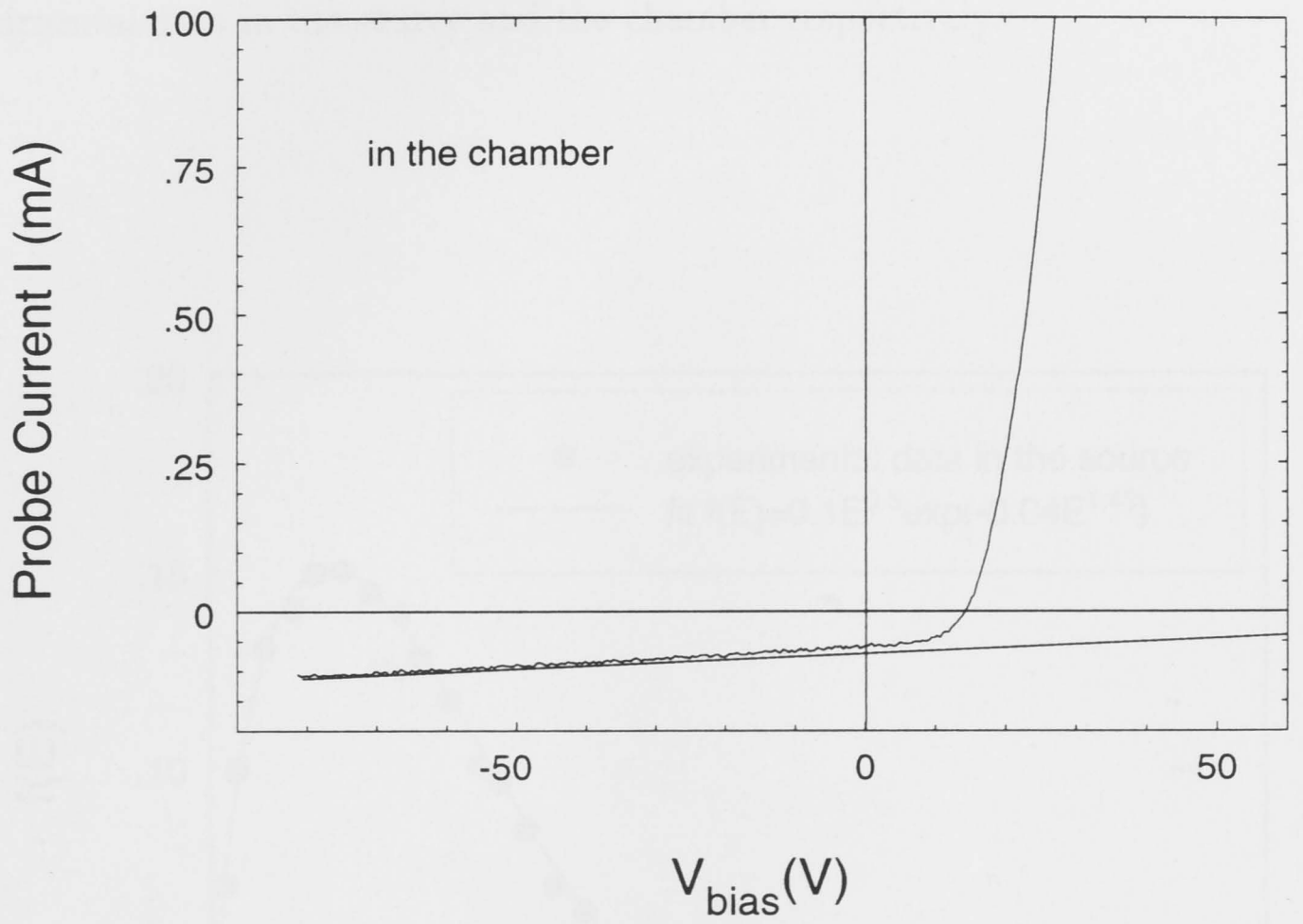

Fig.3.12 Probe $I - V$ characteristic in the chamber

3.3.2 EEDF in the Source and in the Chamber

Typical experimental 'current-voltage' characteristics from the cylindrical probe in the source and in the chamber for oxygen plasma are shown in Fig.3.11 and Fig.3.12 respectively under the discharge conditions P=100W and p=0.03mbar.

Fig.3.13 and Fig.3.14 illustrate a typical fit of the model function (3.9) to the experimental data in the source and the chamber respectively.

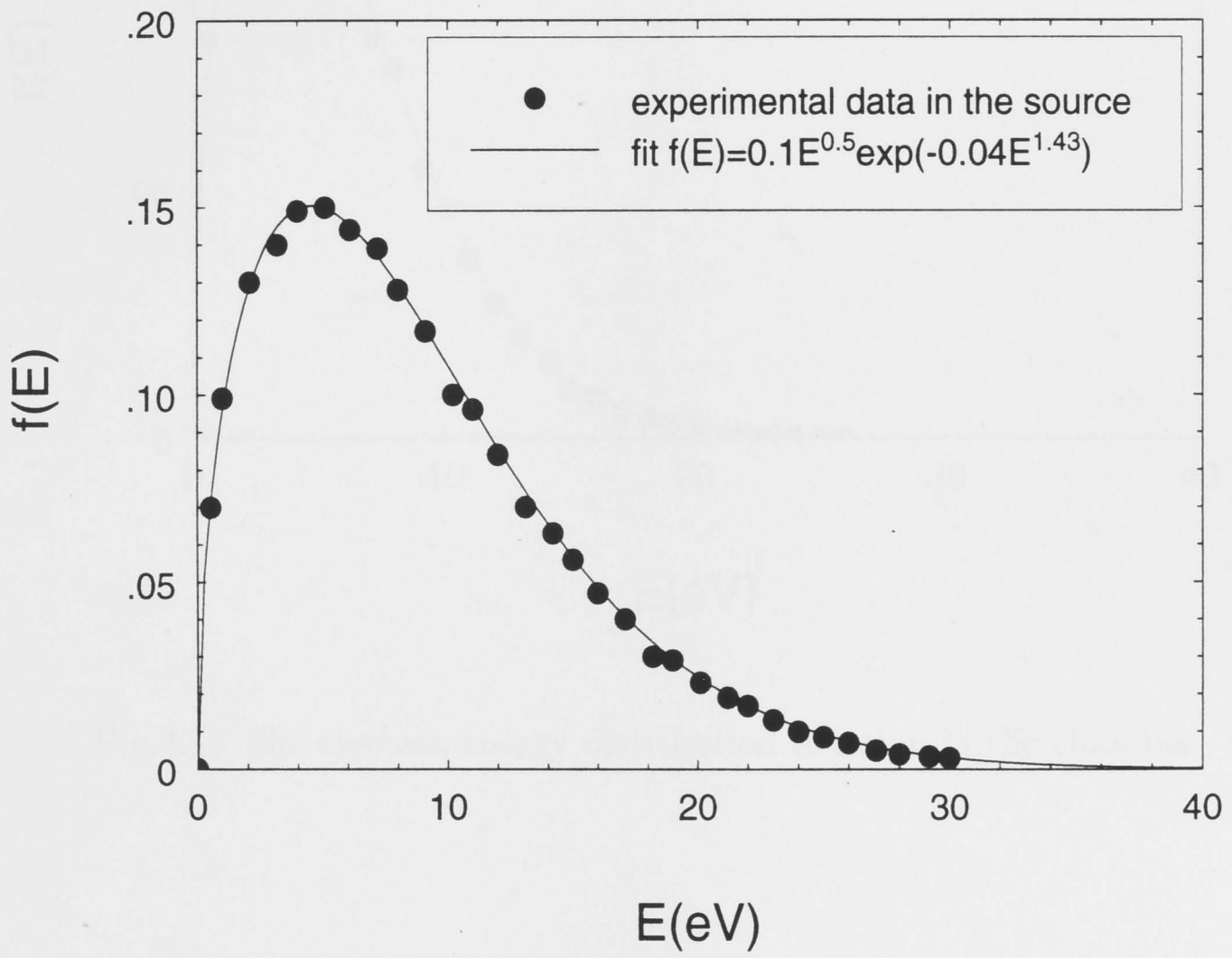

Fig.3.13 The electron energy distribution function in the source

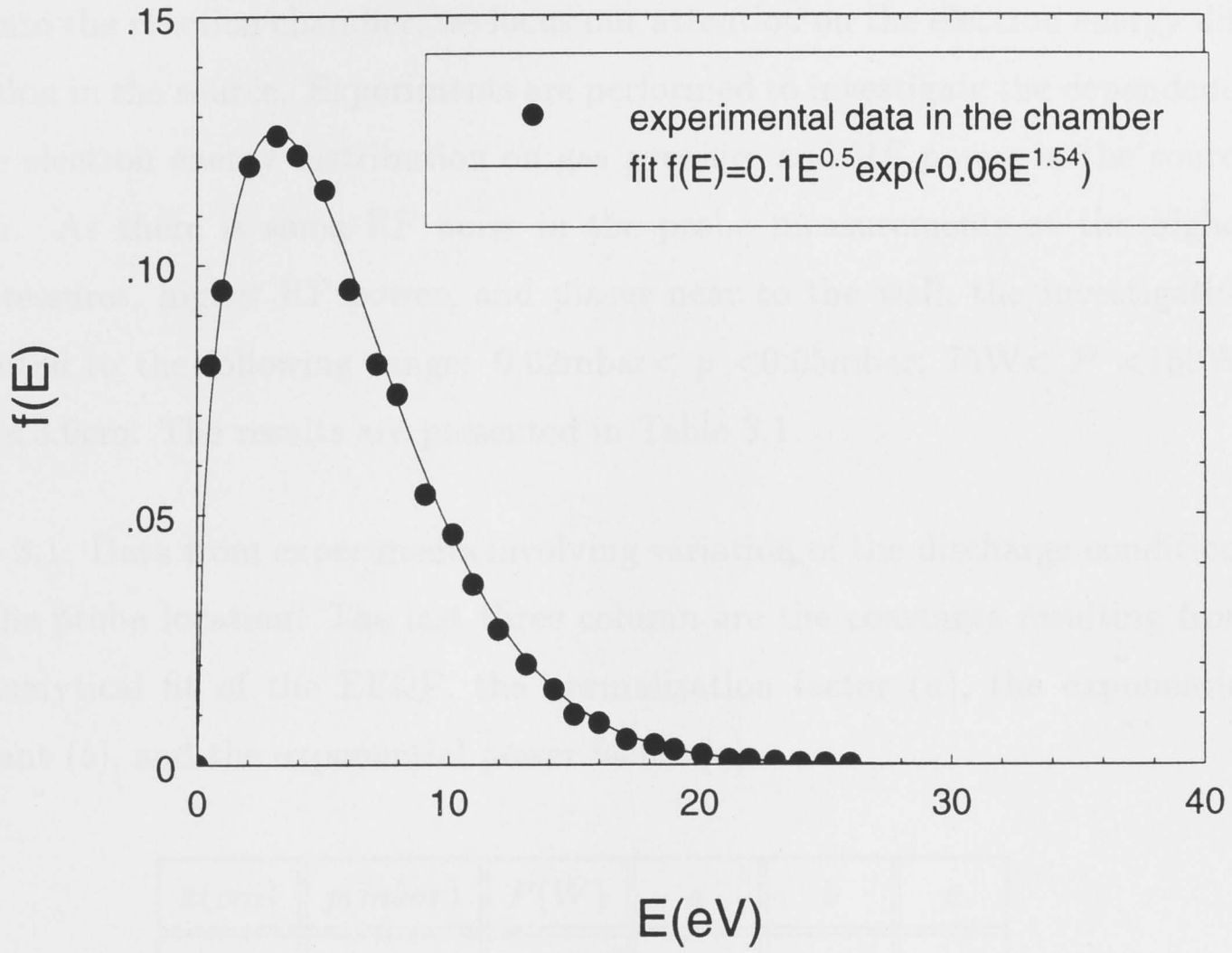

Fig.3.14 The electron energy distribution function in the chamber

The fit of the function inside the source is

$$f(E) = 0.1\sqrt{E}exp(-0.04E^{1.43}) \tag{3.10}$$

and inside the chamber

$$f(E) = 0.1\sqrt{E}exp(-0.06E^{1.54}). \tag{3.11}$$

The distributions show there are relatively more higher-energy electrons in the source than in the chamber.

Since most plasma components are produced in the source region, which then flow into the reaction chamber, we focus our attention on the electron energy distribution in the source. Experiments are performed to investigate the dependence of the electron energy distribution on gas pressure and RF power in the source region. As there is some RF noise in the probe measurements at the higher gas pressures, higher RF power, and places near to the wall, the investigation is limited to the following range: 0.02mbar$< p <$0.05mbar; 75W$< P <$150W; $0< x <$3.0cm. The results are presented in Table 3.1.

Table 3.1: Data from experiments involving variation of the discharge conditions and the probe location. The last three column are the constants resulting from the analytical fit of the EEDF, the normalization factor (a), the exponential constant (b), and the exponential power factor (c).

$x(cm)$	$p(mbar)$	$P(W)$	a	b	c
0.0	0.02	100	0.095	0.035	1.45
0.0	0.03	100	0.100	0.040	1.43
0.0	0.05	100	0.120	0.057	1.39
0.0	0.03	75	0.115	0.049	1.42
0.0	0.03	150	0.090	0.030	1.48
1.5	0.03	100	0.110	0.045	1.41
3.0	0.03	100	0.115	0.055	1.38

The first column in the table is the location of the probe tip. The EEDFs are characterized by the three parameters a, b, and c (Eq. 3.9). Overall, the values for a, b, and c vary only slightly over the range of the discharge conditions. For example, the values of the exponent c are all within 1.43 ± 0.05. This indicates that the electron energy distribution is approximately constant in the source

region for the discharge conditions investigated. Furthermore, from the Langmuir probe measurements, the electron temperature is nearly constant in the range (0.01mbar$< p <$0.08mbar; 50W$< P <$150W; $-6.0 < x < 6.0$cm). This suggests that the measured EEDF may hold for the parameters range over which only the temperature was measured.

Since the processes of dissociation, excitation, and ionization by electrons all depend on the kinetic energy of the plasma electrons, it is of interest to calculate the average electron energy from the electron energy distribution:

$$< E >= \int_0^\infty Ef(E)dE \tag{3.12}$$

The value is about (6.0 ± 0.5)eV in the chamber and (9.0 ± 0.5)eV in the source over the range of plasma conditions listed in Table 3.1.

3.3.3 Comparison with Standard Distributions

The distribution function for the particles represents a solution of the Boltzmann equation of kinetic theory. The Maxwellian and Druyvesteyn velocity distribution functions are respectively two possible solutions of the Boltzmann equation in a collision-dominated plasma. If we consider a homogeneous, isotropic plasma in the presence of an alternating electric field $\vec{\mathbf{E_0}}e^{-iwt}$, and if the value of $\mathbf{E_0}$ is set to zero and inelastic losses are neglected, the distribution function becomes the Maxwellian and has the form [34]:

$$f(v) \propto e^{-mv^2/2k_BT_e} \tag{3.13}$$

where v is electron velocity. If it is expressed as a function of energy, the Maxwellian distribution is:

$$f(E) = aexp(-bE)\sqrt{E} \tag{3.14}$$

Here, the exponent in Eq. (3.9) c=1.

If the electron energy acquired from the applied electric field is much greater than $k_B T_g$ (T_g is gas temperature), the frequency for the applied field is sufficiently low such that $w^2 << \nu_m^2$, and the momentum transfer collision frequency ν_m is independent of velocity, the resulting distribution function becomes the Druyvesteyn which has the form [41]:

$$f(v) \propto exp(-\frac{(mv^2/2)^2}{e^2 E_0^2 M/6mN^2\sigma_m^2}) \tag{3.15}$$

where m and M are the masses of the electrons and target molecules respectively, N is the total gas density, and σ_m is the momentum transfer collision cross-section. If it is expressed as a function of energy, the Druyvesteyn distribution is:

$$f(E) = aexp(-bE^2)\sqrt{E} \tag{3.16}$$

Here, the exponent c=2.

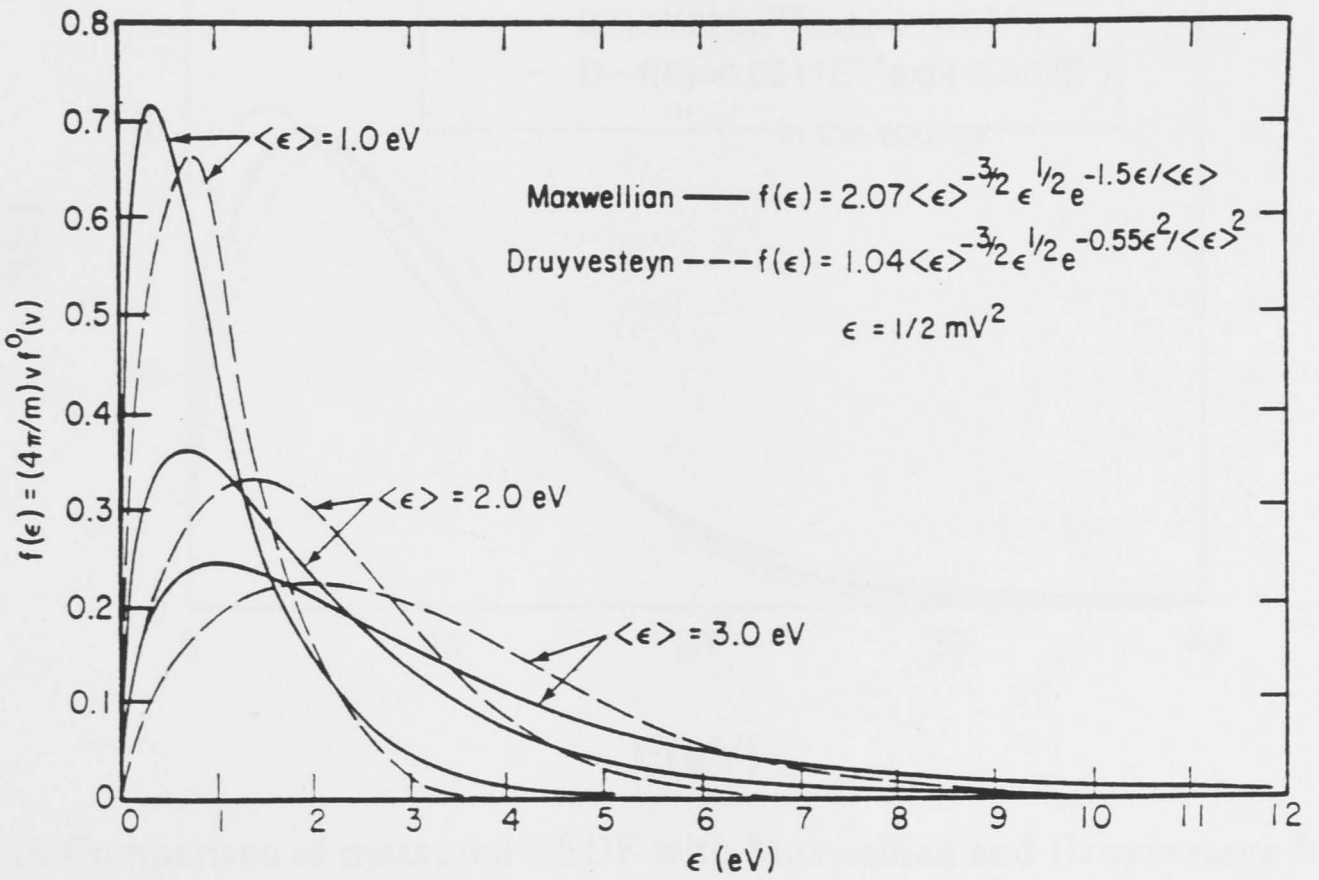

Fig.3.15 Comparison of Maxwellian and Druyvesteyn energy distribution functions (reproduced from [5])

Since the Druyvesteyn distribution varies as $exp(-bE^2)$, the tail of this distribution decreases more rapidly than in a Maxwellian distribution. Fig.3.15 [5] shows that, for a plasma with a given mean energy, the Druyvesteyn distribution has fewer high-energy electrons than does the Maxwellian distribution.

It is very interesting to compare the measured EEDF in our plasma and the models of Maxwell-Boltzmann and Druyvesteyn respectively in both the source and the chamber. They are presented in Fig.3.16 and Fig.3.17, and show that the measured EEDF in our plasma is intermediate between the Maxwellian and Druyvesteyn distributions.

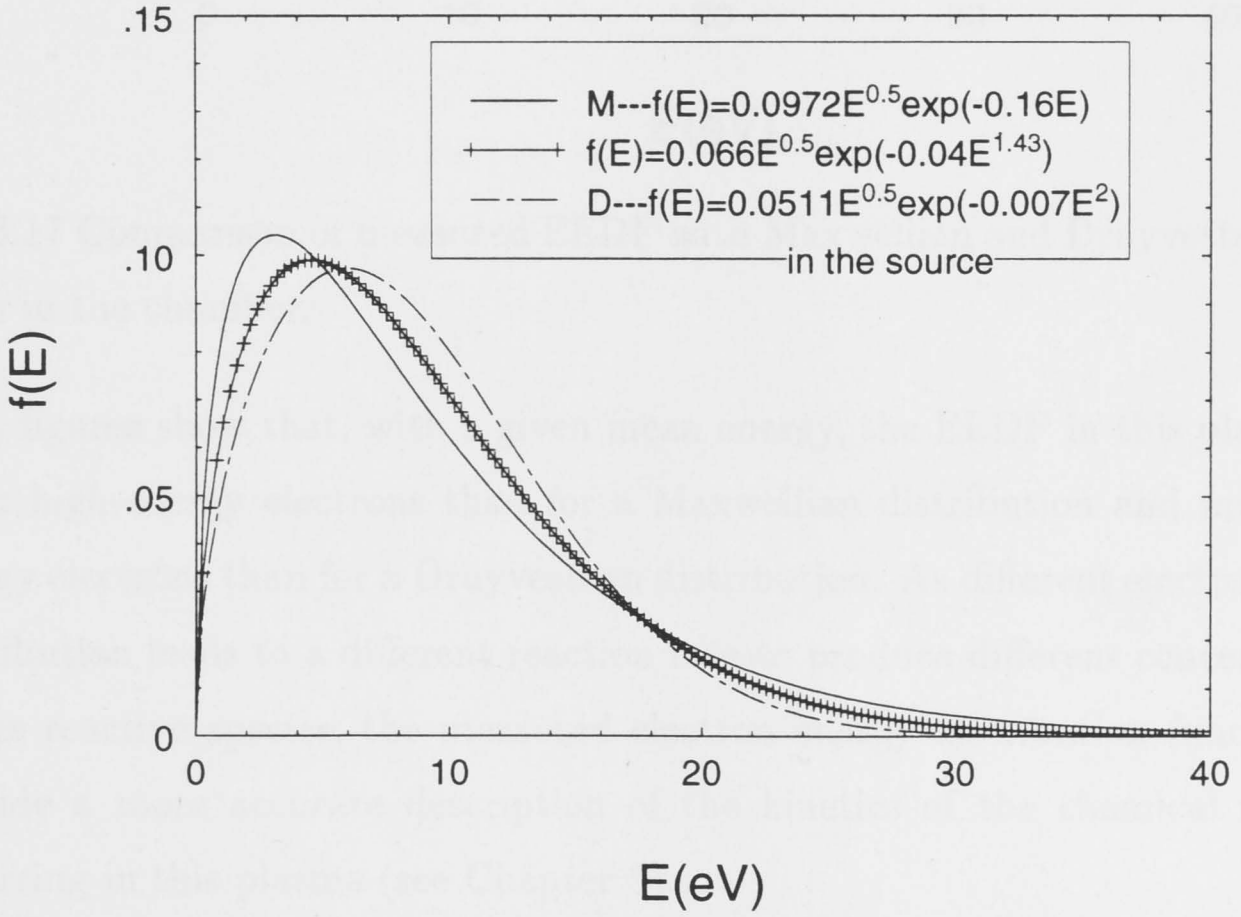

Fig.3.16 Comparison of measured EEDF with Maxwellian and Druyvesteyn functions in the source

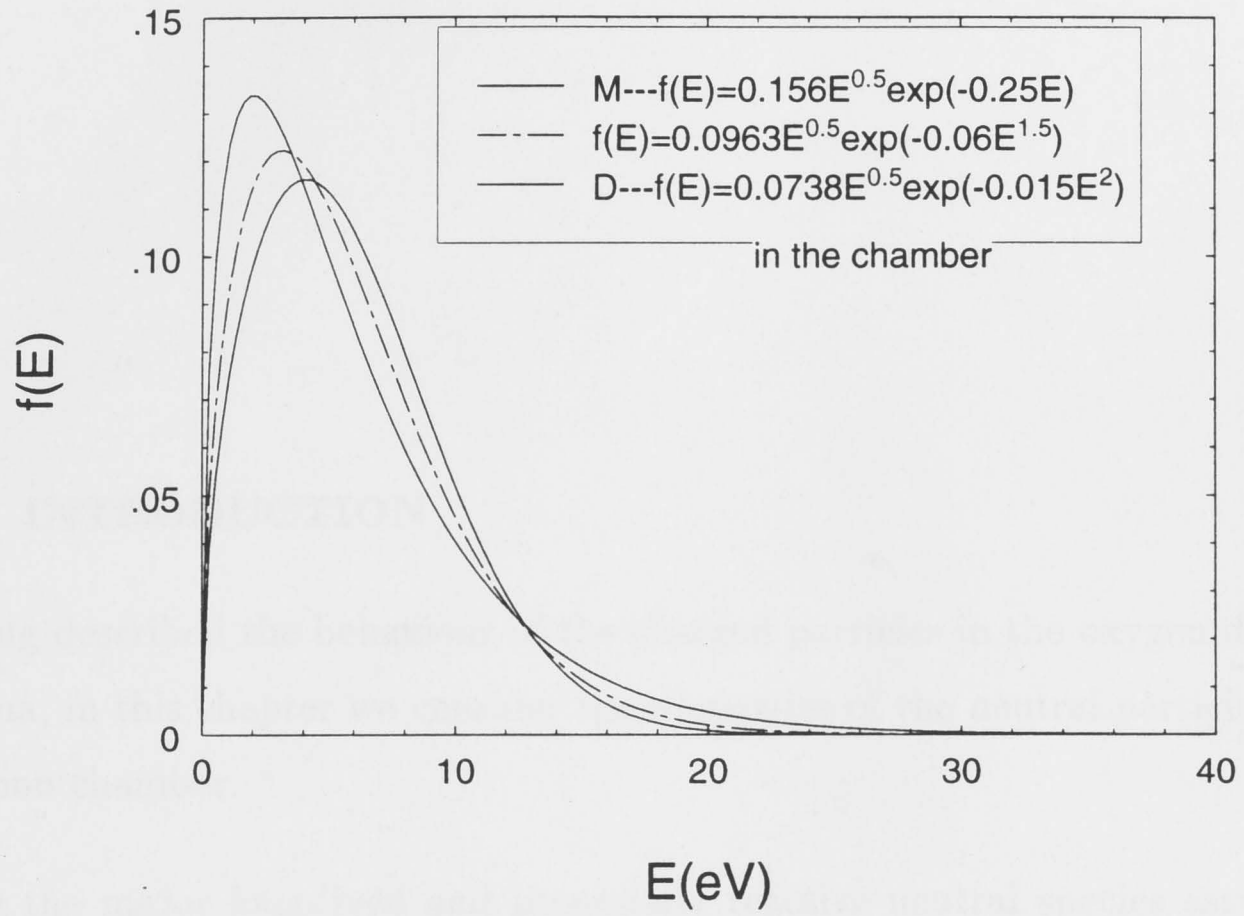

Fig.3.17 Comparison of measured EEDF with Maxwellian and Druyvesteyn functions in the chamber.

Both figures show that, with a given mean energy, the EEDF in this plasma has fewer high-energy electrons than for a Maxwellian distribution and more high-energy electrons than for a Druyvesteyn distribution. As different electron energy distribution leads to a different reaction rate to produce different concentrations of the reactive species, the measured electron energy distribution function will provide a more accurate description of the kinetics of the chemical reactions occurring in this plasma (see Chapter 5).

4

NEUTRAL PARTICLE STUDIES

4.1 INTRODUCTION

Having described the behaviour of the charged particles in the oxygen discharge plasma, in this chapter we consider the properties of the neutral particles in the reaction chamber.

Since the major long-lived and potentially reactive neutral species assumed to be important in oxygen discharge are atomic oxygen O and metastable excited molecular oxygen $O_2(a^1\Delta_g)$ [31, 42], we concentrate on the study of these two active species. Various diagnostic techniques have been used to determine the concentration of the two species in oxygen plasmas. The atomic concentration $N[O]$ has been determined by titration with NO_2 [43, 44], or by calorimetry [45] downstream of a discharge. Localized measurements of $N[O]$ have been made by two-photon laser-induced fluorescence [46, 47], and by an actinometric technique [48, 49]. The concentration of the metastable molecule $N[O_2^*]$ has been measured using calorimetry [50], optical emission of the forbidden line at 1.25 μm, and luminescence at 634nm [51]. Although vuv absorption techniques have also been used to measure concentrations of these reactive species [31, 52, 53], no complete investigations have been presented.

In this work, most effort has been devoted to measurements based on continuum vuv absorption, made possible by the development of an improved light source. These measurements are described in section 4.2. Section 4.3 presents the measured concentrations of the main reactive species $N[\mathrm{O}]$ and $N[\mathrm{O}_2^*]$ for various plasma conditions. Finally, a summary is presented in section 4.4.

4.2 MEASUREMENT METHODS

4.2.1 Actinometry

Among several optical techniques considered to measure the concentration of O, actinometry was first because of its experimental simplicity and ease of application compared to other optical diagnostic techniques. The technique is based on the assumption that the emitting excited state atoms are produced solely by electron impact upon the ground-state atoms:

$$\mathrm{O}(2p^4\ {}^3P) + e \longrightarrow \mathrm{O}^*(3p\ {}^3P) + e \tag{4.1}$$

$$\mathrm{O}^*(3p\ {}^3P) \longrightarrow \mathrm{O}^*(3s\ {}^3S) + h\nu(844\mathrm{nm}) \tag{4.2}$$

The schematic diagram of the energy levels of oxygen atoms concerned in the process is shown in Fig 4.1.

The intensity of the 844nm emission is directly proportional to the $\mathrm{O}^*(3p^3P)$ concentration. It is given by

$$I_{N[\mathrm{O}]} = N[\mathrm{O}^*]A_{ij} \tag{4.3}$$

where $I_{N[O]}$ is the number of photons emitted per unit volume and A_{ij} is the Einstein coefficient for the observed $(i \rightarrow j)$ transition. The density of the emitting

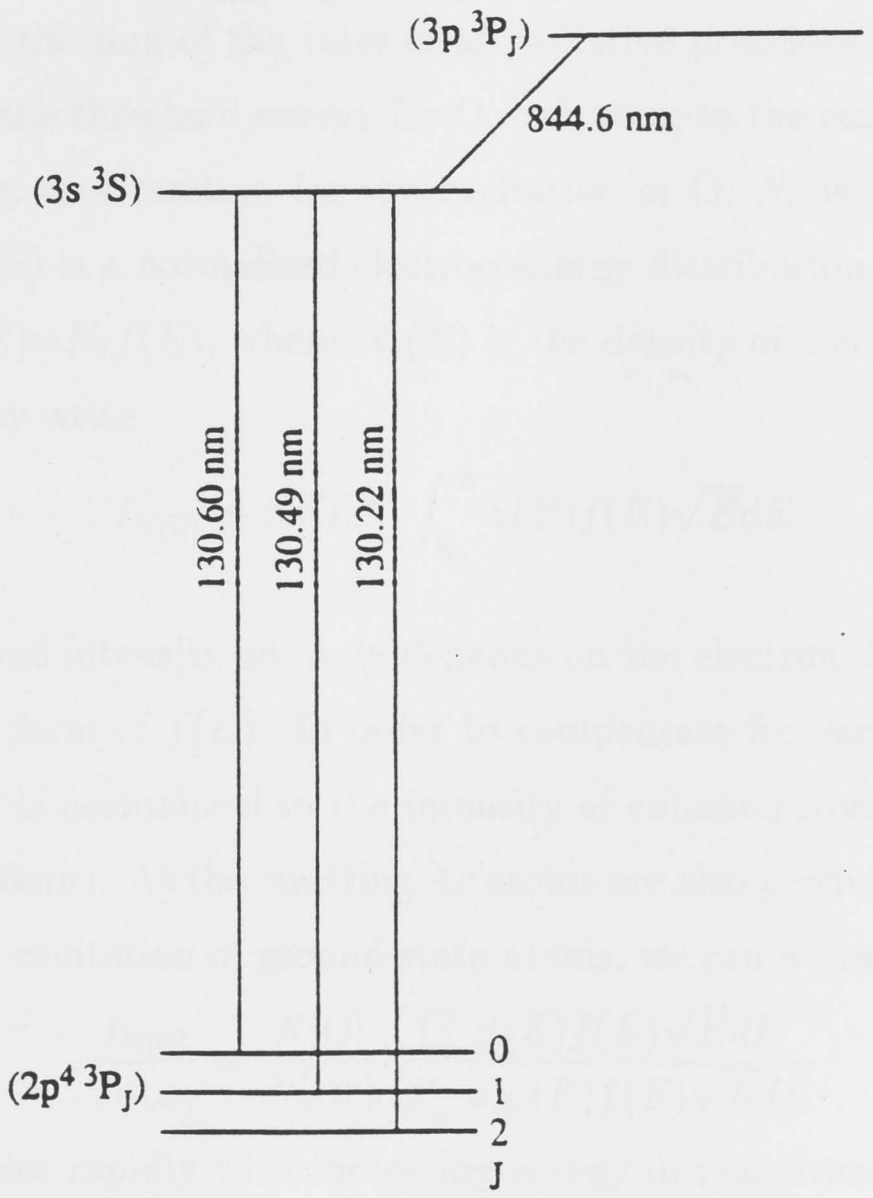

Fig.4.1 Energy levels and transition wavelengths in atomic oxygen relevant to this study.

atoms $N[O^*]$ is related to the ground-state atom concentration $N[O]$ by the rate of electron impact excitation [54]:

$$N[O^*] = \frac{N[O]}{\sum_j A_{ij}} \int_{E_o}^{\infty} \sigma(E) N_e f(E) \sqrt{2E/m} dE \tag{4.4}$$

where $\sum_j A_{ij}$ is the sum of the rates of all radiative processes undergone by the state O^*, E_o is the threshold energy for O excitation to the emitting state, $\sigma(E)$ is the excitation cross section for the excitation of O, N_e is the total electron density, and $f(E)$ is a normalized electron energy distribution function which is defined as $N_e(E)=N_e f(E)$, where $N_e(E)$ is the density of electrons with energy E. Then we may write

$$I_{N[O]} \propto N[O] N_e \int_{E_o}^{\infty} \sigma(E) f(E) \sqrt{E} dE \tag{4.5}$$

Thus the observed intensity not only depends on the electron density, but also is sensitive to the form of $f(E)$. In order to compensate for variations in N_e and $f(E)$ the signal is normalized to the intensity of emission from an excited state of Ar atoms (750nm). As the emitting Ar atoms are also produced only by direct electron impact excitation of ground-state atoms, we can write:

$$\frac{I_{N[O]}}{I_{N[Ar]}} \propto \frac{N[O]}{N[Ar]} \frac{\int_{E_o}^{\infty} \sigma(E) f(E) \sqrt{E} dE}{\int_{E_{Ar}}^{\infty} \sigma_{Ar}(E) f(E) \sqrt{E} dE} \tag{4.6}$$

As $f(E)$ decreases rapidly with increasing energy in real situations, the form of the cross sections is relatively unimportant. As the energy thresholds E_o(11eV) and E_{Ar}(13.5eV) are roughly similar, then it is reasonable to assume:

$$\frac{I_{N[O]}}{I_{N[Ar]}} = k' \frac{N[O]}{N[Ar]} \tag{4.7}$$

where k' is a constant. Thus $N[O]$ can be obtained by the ratio of the emission intensity using a known quantity of Ar.

Although measurable signals at 844nm and 750nm have been successfully obtained via an optical fibre in this experiment, a problem with this technique is

that O^* is also produced by dissociative excitation of O_2 in the plasma [55]:

$$O_2 + e \longrightarrow O^* + O + e \tag{4.8}$$

The dissociative excitation contribution to the observed intensity may be represented by adding a second term to Eq.(4.7) [49]:

$$\frac{I_{N[O]}}{I_{N[Ar]}} = k' \frac{N[O]}{N[Ar]} + k'' \frac{N[O_2]}{N[Ar]} \tag{4.9}$$

As a result, the reliability of oxygen atom actinometry is difficult to ascertain from the two processes [56, 57]. We therefore decided to abandon this experimental method to measure atomic oxygen. In order to obtain a more reliable measurement, a vuv absorption technique was chosen as it is at least a partially localized method which yields absolute values.

4.2.2 Vacuum Ultra-violet Measurements

Although in principle it is possible to obtain the absolute concentration of atomic oxygen by resonance line absorption [58], the method suffers from many practical difficulties. For example, it is necessary to know the line profile of the resonance line emitted from the source, which will inevitably suffer from some self absorption, with a precision obtainable only with an extremely high resolution instrument not available to us. The low resolution spectrometer which was available (0.4nm with 30μm slits) was not able to resolve the atomic absorption line from a continuum source, so this method could not be used either.

It was therefore decided to base absorption measurement on the photo-dissociation continuum of the molecular species, which does not require high resolution, and rely on the reduction in absorption resulting from dissociation caused by the plasma to deduce the atomic concentration. This was supplemented by measurements of the OI resonance line emission for low O concentrations.

The method is to measure the concentrations with and without the discharge of both ground-state molecular oxygen (O_2), and singlet (excited) molecular oxygen (O_2^*) using vuv absorption from a continuum source (for details of the radiation source see section 4.2.3). The absolute concentration of atomic oxygen is deduced from the reduction in molecular absorption resulting from dissociation, and at low concentrations from relative intensity measurements of the OI resonance line emission at 130nm after calibration against absorption (see Fig.4.3).

We denote the concentration of oxygen molecules inside the reaction chamber in the ground state ($^3\sum_g$) and in its metastable excited state($^1\Delta_a$) by $N[O_2]$ and $N[O_2^*]$ respectively, and use the subscript p to denote its value when the plasma source is switched 'on'. We denote $I_0(\lambda)$ as the intensity measured when the chamber is evacuated (i.e. with $N[O_2]$=$N[O_2^*]$=0), and $I(\lambda)$ and $I_p(\lambda)$ the intensity with the same gas flow but with the plasma source off and on respectively. From the Beer-Lambert law [59]:

$$I(\lambda) = I_0(\lambda)exp(-N\sigma(\lambda)l) \tag{4.10}$$

where $I(\lambda)$ is the transmitted light intensity, $I_0(\lambda)$ is the intensity of the parallel beam of purely monochromatic light, N is the number of molecules per cm^{-3}, $\sigma(\lambda)$ is the absorption cross-section, and l is the absorption path length. We then have

without plasma:

$$ln(I_0(\lambda)/I(\lambda)) = N[O_2]\sigma_x(\lambda)l \tag{4.11}$$

with plasma:

$$ln(I_0(\lambda)/I_p(\lambda)) = N_p[O_2]\sigma_x(\lambda)l + N[O_2^*]\sigma_a(\lambda)l \tag{4.12}$$

where $\sigma_x(\lambda)$ and $\sigma_a(\lambda)$ are respectively the absorption cross-sections for ground-state and metastable excited molecules, which are both assumed to be uniformly distributed in the chamber along the beam path of $l = 43$cm.

In order to obtain all three quantities, $N[O_2]$, $N_p[O_2]$ and $N[O_2^*]$ from the equations above, two wavelengths λ_1, λ_2 are chosen (see Table 4.1) for which the singlet oxygen absorption cross-section σ_a is significantly different and the ground-state absorption cross-section σ_x is nearly the same in the two wavelengths.

Table 4.1: Experimental vuv absorption wavelengths and corresponding cross-sections.

λ (nm)	σ_x (10^{-17} cm^2)	σ_a (10^{-17} cm^2)
140	1.42	0
144	1.40	8.2

The mean atomic oxygen density $N[O]$ is then estimated from the reduction in total molecular concentration measured,

$$N[O] = 2(N[O_2] - N_p[O_2] - N[O_2^*]) \tag{4.13}$$

with the assumption that the oxygen flow rate is constant and the pumping speed is unchanged.

As $N[O_2]=p/k_BT_g$, from eq.(4.11) $ln(I_0/I)$ is proportional to p (gas pressure) at the fixed wavelength λ=140nm with other quantities kept constant. From the slope ($\sigma_x l/k_BT_g$) of the straight line and given l, k_B, and T_g, the cross-section σ_x can be obtained. The results can be seen in Fig.4.2, in which the dots are experimental data and the solid line is the best fit. Comparing the cross-section for ground-state O_2 at 140nm derived in this way, namely $\sigma_x = (1.43 \pm 0.15)\text{x}10^{-17}\text{cm}^2$, with the best available measurement $\sigma_x = (1.42 \pm 0.06)\text{x}10^{-17}\text{cm}^2$ [60], lends confidence in the accuracy of these optical and initial concentration measurements.

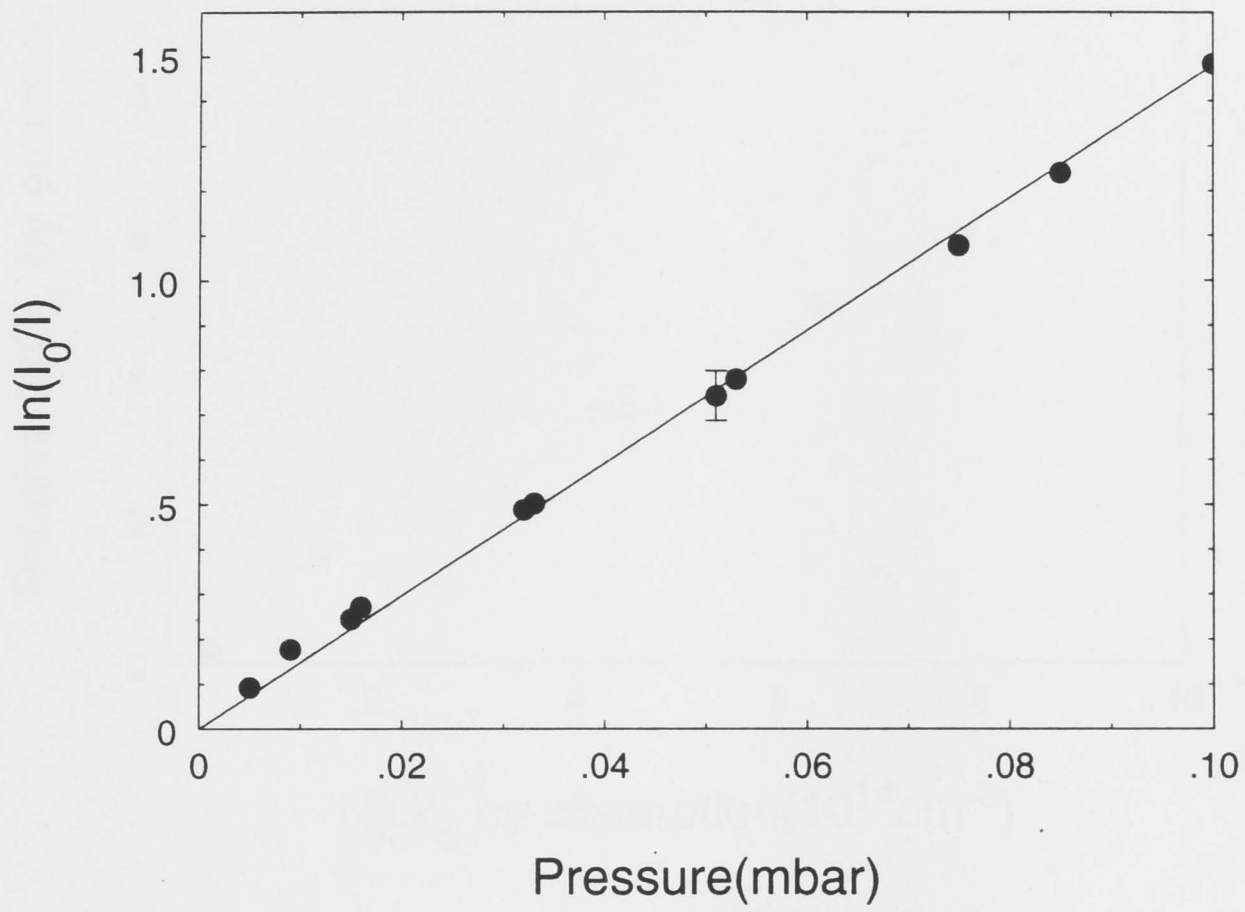

Fig.4.2 $ln(I_0/I)$ as a function of gas pressure at λ=140nm.

The OI resonance line emission of oxygen plasma at 130nm in the reaction chamber has been measured to compare with the absolute value of N[O] from the absorption measurements. According to equations (4.3) and (4.5), the emission intensity at 130nm is directly proportion to the concentration of atomic oxygen in the absence of self-absorption. Fig.4.3 shows how the relative intensity of the observed line emission depends on atomic density N[O] as measured by absorption. The lack of proportionality at the higher densities results from self-absorption of the line radiation.

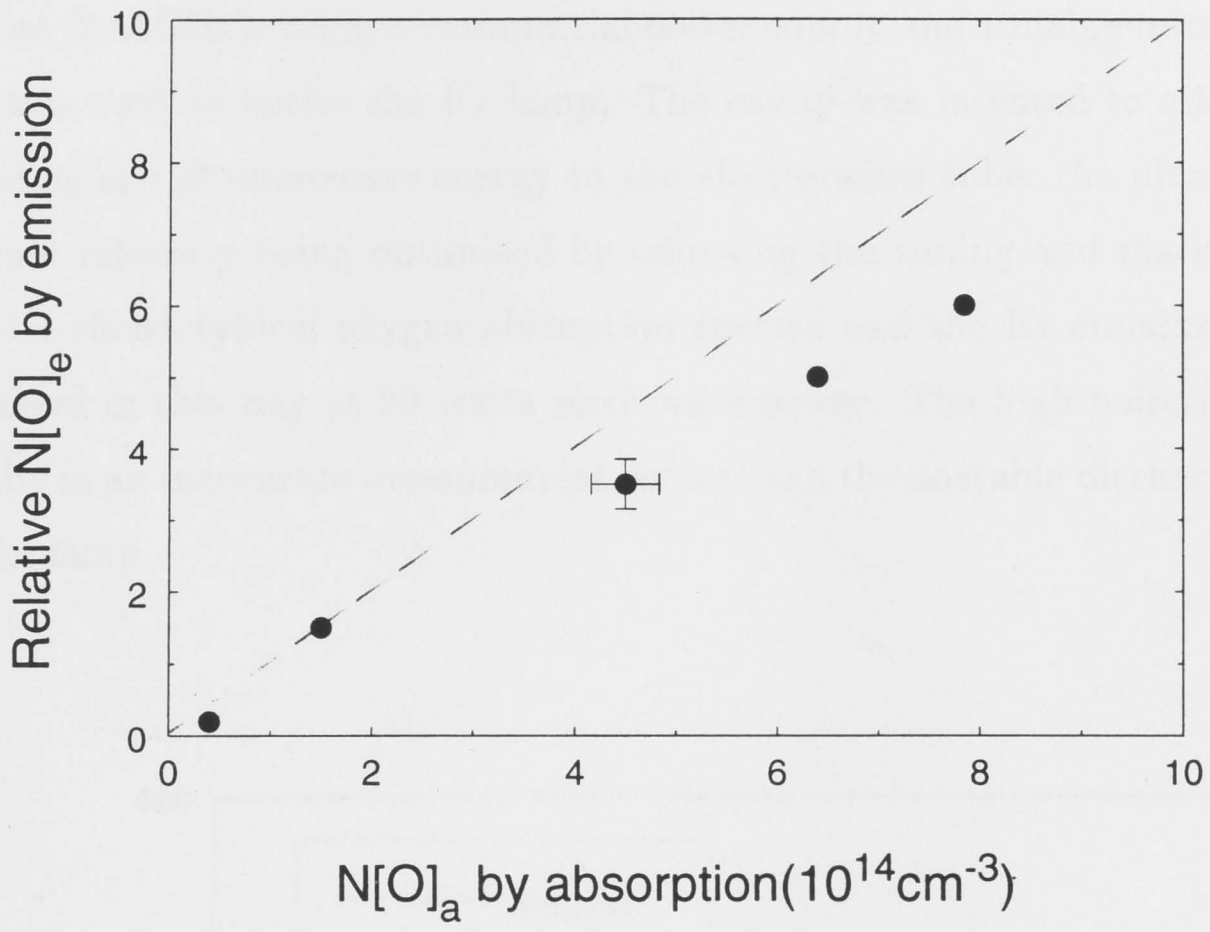

Fig.4.3 Comparing the relative values of N[O] from the emission measurements with the absolute values of N[O] from the absorption measurements.
(p=0·03 mbar. P=50-200 W)

4.2.3 Vuv Continuum Radiation Source

The study of emission continua from rare gas discharges has proven them to be very valuable as spectroscopic absorption background sources [61]. At sufficiently high pressure all the rare gases, when properly excited, emit continuous spectra with little or no structure except for a few emission lines which prove useful as wavelength standards. For this reason, the commercially available high-pressure krypton lamp (0.25bar) was chosen for our study (see Chapter 2).

Another matter is the choice of discharge used to excite such continua with respect to its suitability for photoelectric detection. Hitherto, only condensed

discharges and microwave discharges have been used. Initially, a microwave discharge (2.45GHz), using a commercial power supply and tunable microwave cavity, was used to excite the Kr lamp. The cavity was intented to allow efficient coupling of the microwave energy to the electrodeless tube, the ultraviolet continuum intensity being optimized by adjusting the tuning and matching stubs. Fig.4.4 shows typical oxygen absorption spectra and the Kr emission spectrum obtained in this way at 20 watts microwave power. The high noise level, which results in an inaccurate measurement, arises from the unstable discharge channels in the lamp.

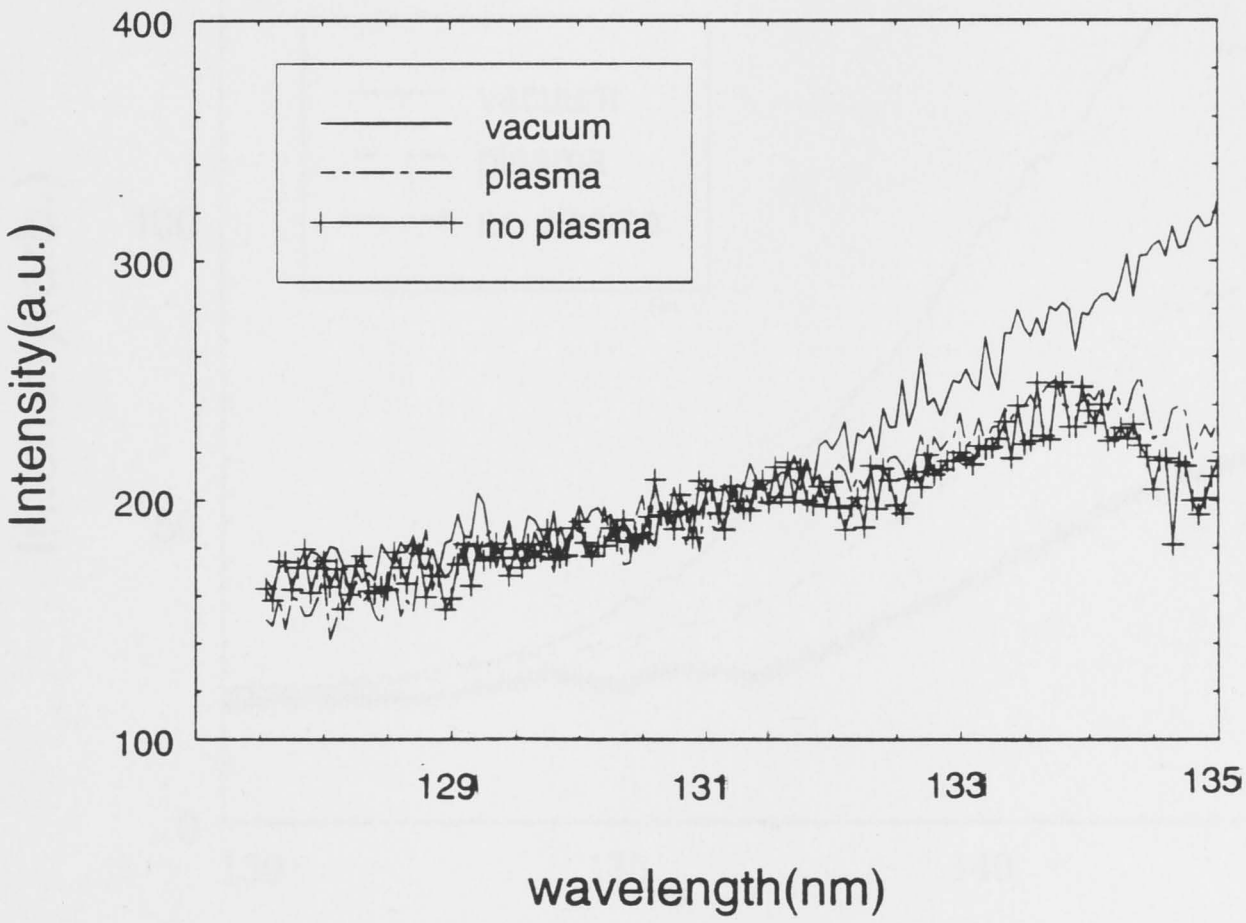

Fig.4.4 Typical oxygen absorption spectra (the line of crosses for oxygen and the dotted line for oxygen plasma) and the Kr emission spectrum (the solid line) at 20W microwave power.

In order to solve this problem, it was decided to excite the lamp using RF instead of microwaves, using the arrangement described in Chapter 2 (Fig.2.8). The spectra of emission from the lamp and after absorption through oxygen (with and without plasma) are shown in Fig.4.5. It can be seen that the noise is greatly reduced. It clearly shows that when the plasma is 'on' there is an obvious reduction in absorption by O_2 which means that much O_2 has been dissociated, and that there is an obvious increased of absorption by O_2^* at $\lambda = 144$nm.

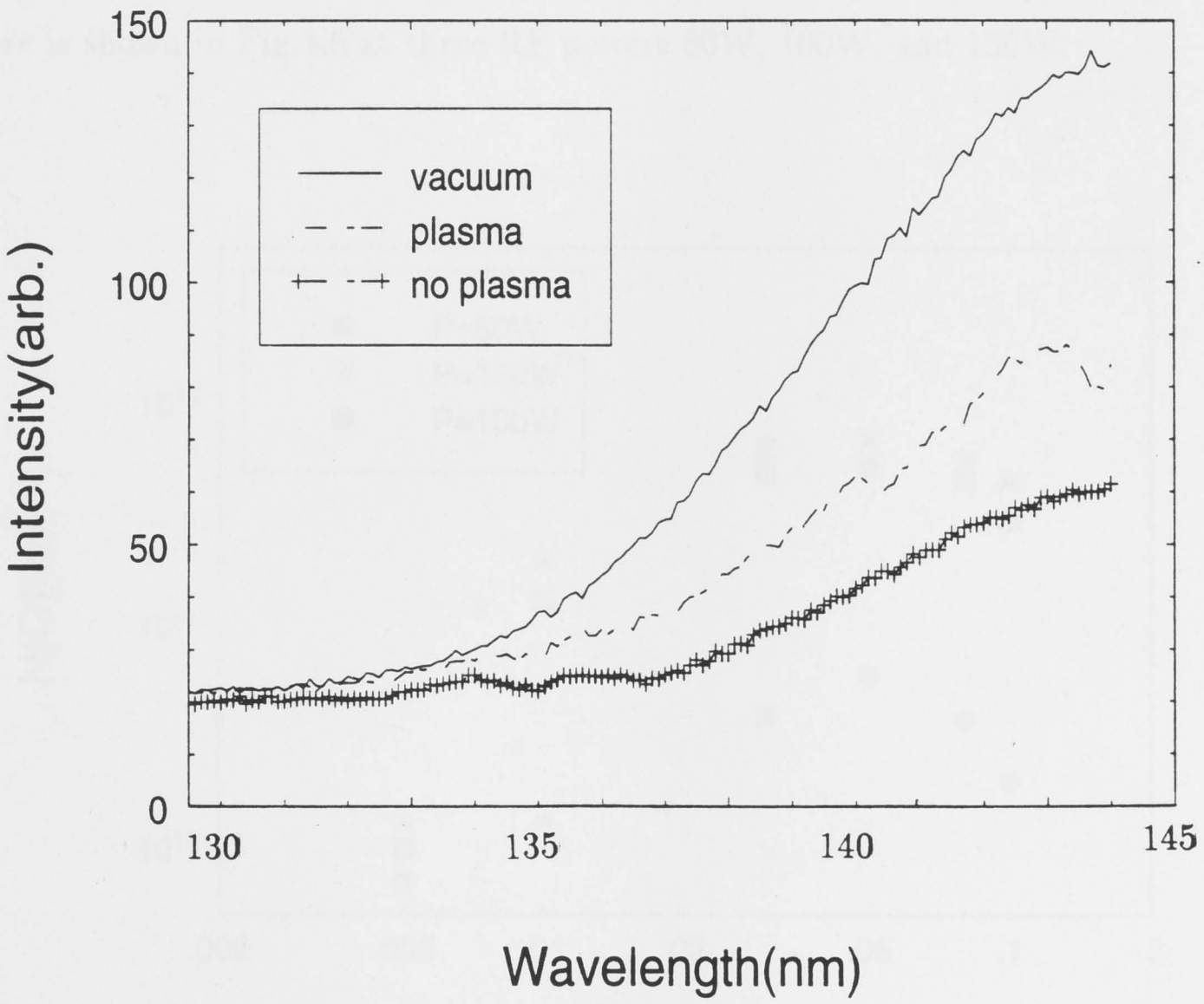

Fig.4.5 Typical oxygen absorption spectra (the line of crosses for oxygen and the dotted line for oxygen plasma) and the Kr emission spectrum (the solid line) at 10W RF power.

Compared to the microwave discharge, the RF discharge has the following advantages: higher stability, lower power requirements (only 10W needed), and easier control. It should be emphasised that it is this improved source operation that has made accurate measurements possible.

4.3 RESULTS

4.3.1 Effects of Gas Pressure

The dependence of the concentration of oxygen atoms in the chamber on gas pressure is shown in Fig.4.6 at three RF powers 50W, 100W, and 150W.

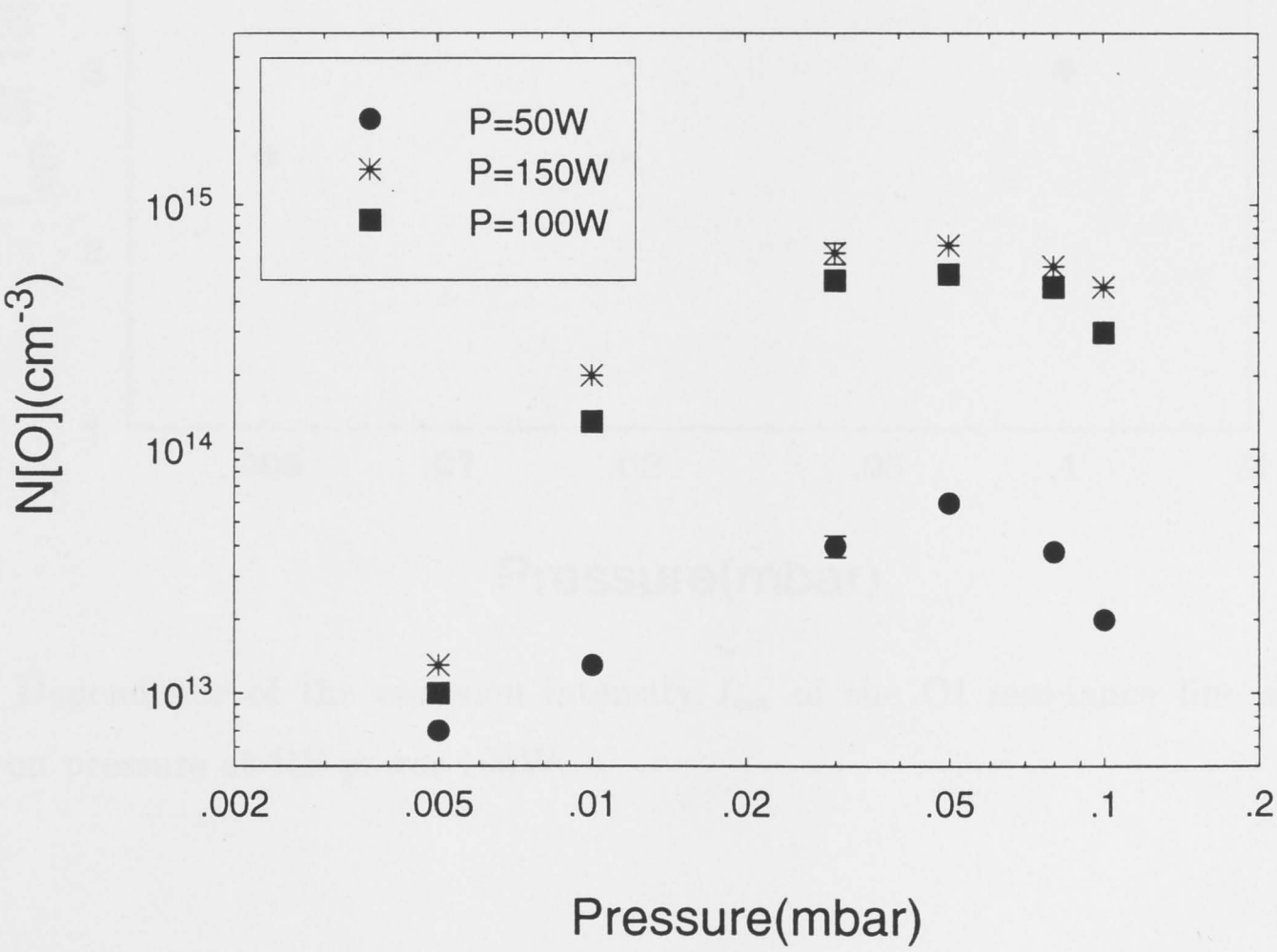

Fig.4.6 The dependence of the concentration of atomic oxygen on gas pressure in the chamber at three RF powers.

It is interesting to note that the three curves all peak at a pressure around 0.05mb. The curves show that the atomic concentration N[O] clearly increases from 50W to 100W at all presures but changes little between 100W and 150W.

Fig.4.7 shows the dependence of the emission intensity of the OI resonance line at 130nm on pressure at fixed RF power (100W). Notice that it has the same trend as the N[O] measured by absorption.

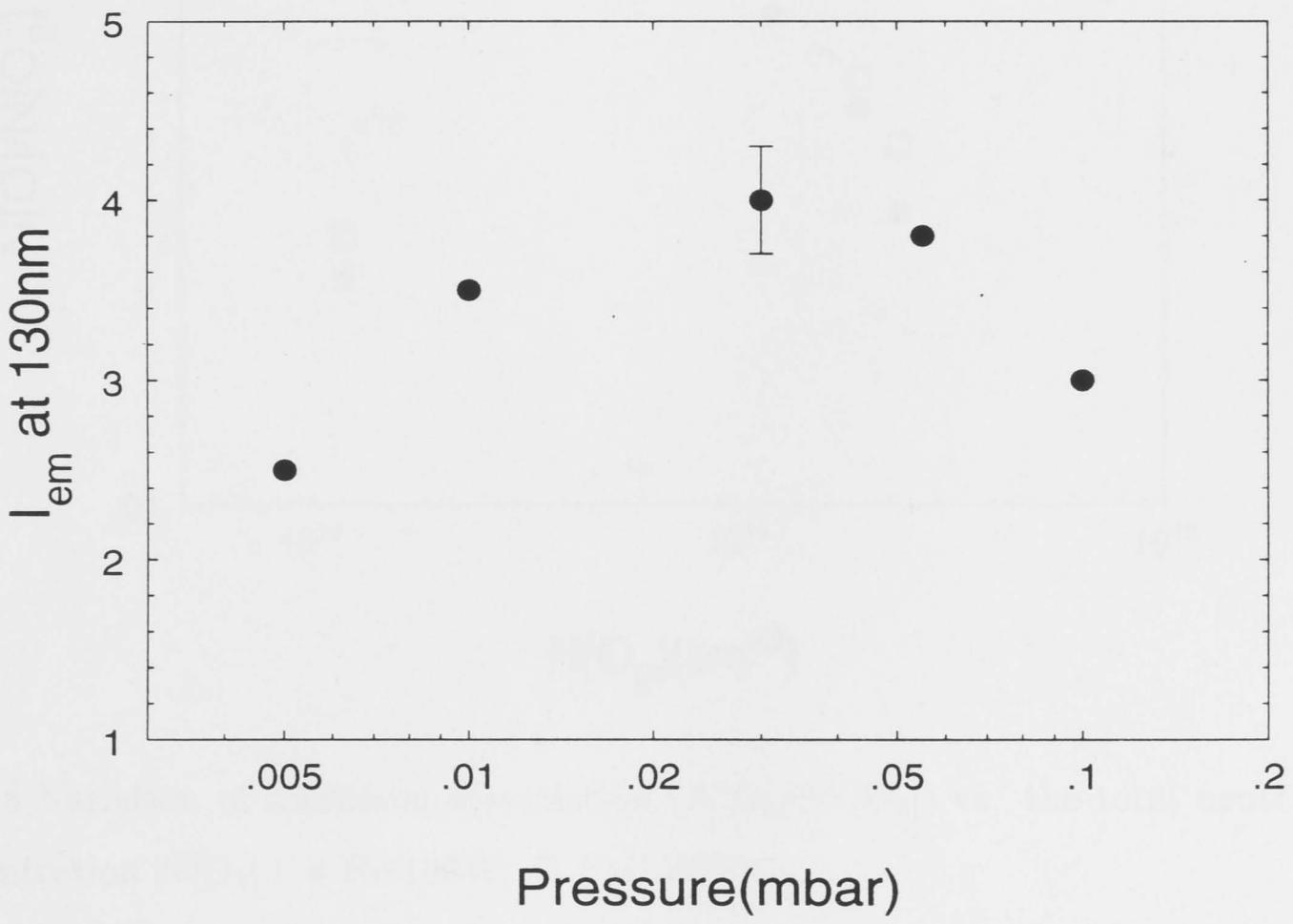

Fig.4.7 Dependence of the emission intensity I_{em} of the OI resonance line at 130nm on pressure at RF power 100W.

This trend of N[O] indicates that there is an optimum gas pressure for the production of O.

Fig.4.8 shows the variation of the fractional dissociation ($N[\mathrm{O}]/2N[\mathrm{O}_2]$) vs. the total neutral concentration $N[\mathrm{O}_2]$. The maximum dissociation of oxygen (about 40% of the initial gas filling) occurs at around p=0.03mbar.

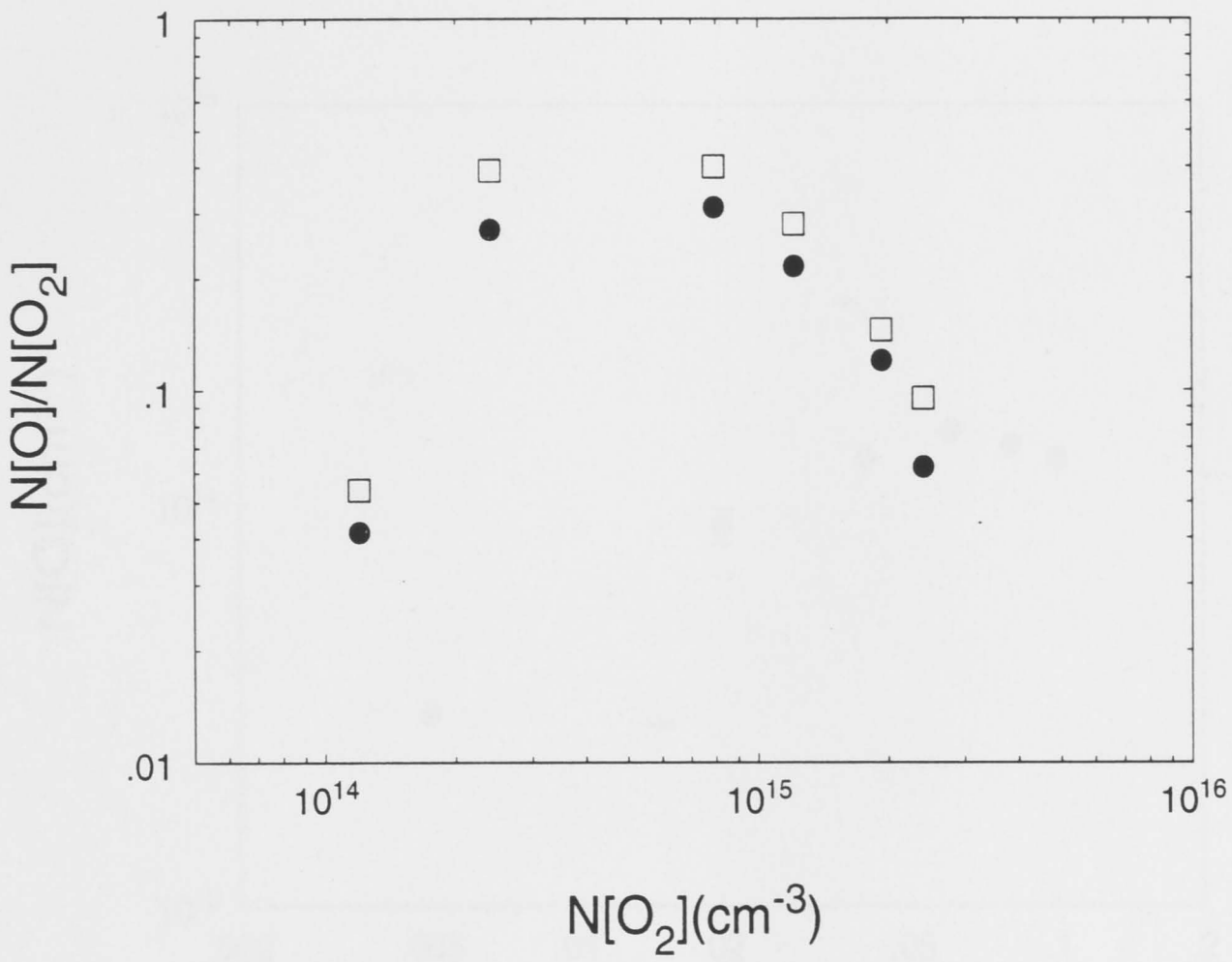

Fig.4.8 Variation of fractional dissociation ($N[\mathrm{O}]/2N[\mathrm{O}_2]$) vs. the total neutral concentration $N[\mathrm{O}_2]$ (• P=100W; □ P=150W).

Further evidence for an optimum pressure can be seen in discharges in dry air. Although there is only 20% oxygen constituent in air, the effect of pressure on the measured values of N[O] with air shows the same trend as that for the oxygen plasma (Fig.4.9).

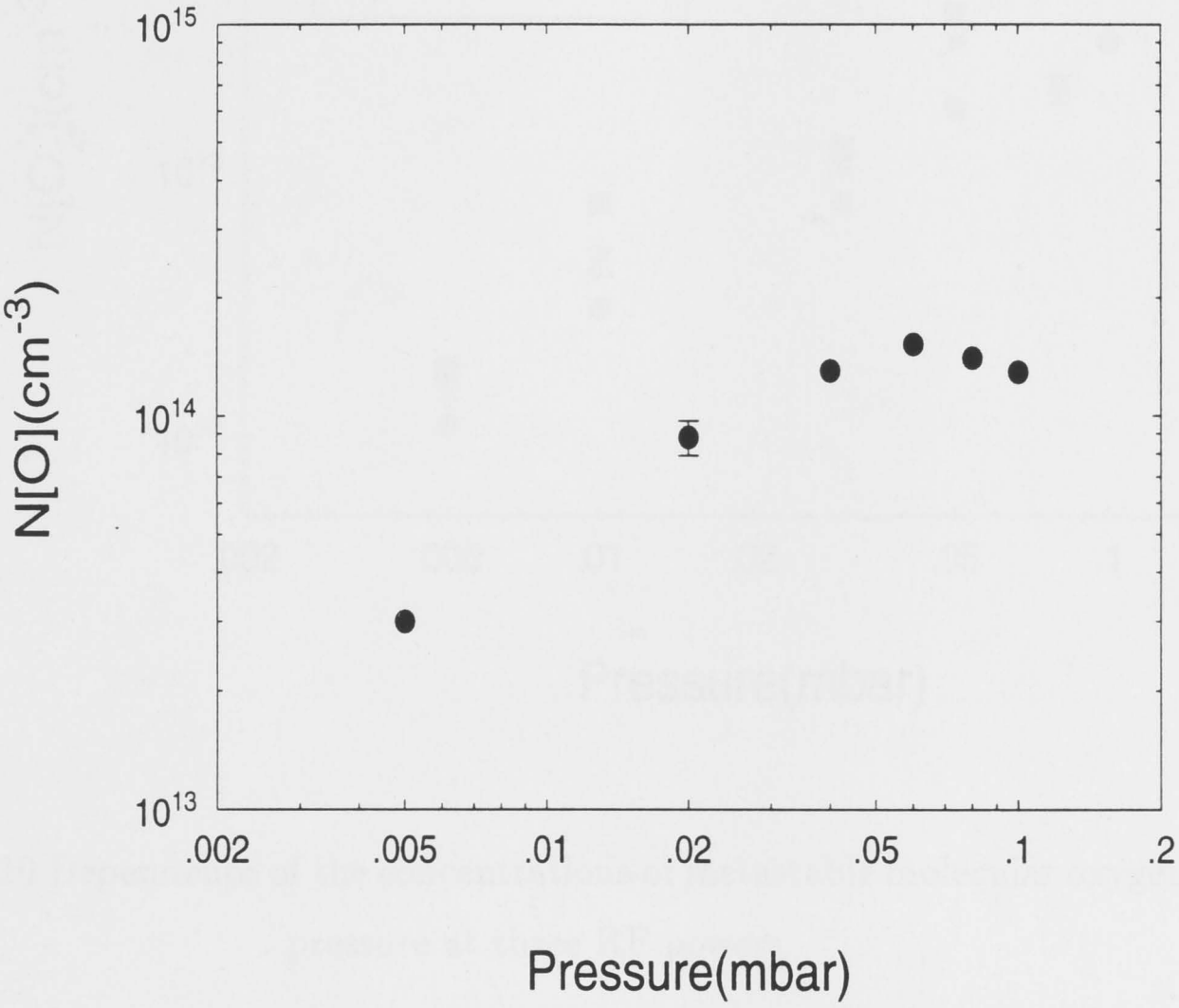

Fig.4.9 The dependence of the concentration of atomic oxygen in dry air on gas pressure in the chamber.

The dependence of the concentrations of metastable molecular oxygen on gas pressure at the three RF powers is shown in Fig.4.10. It should be noted that the concentration of O_2^* increases linearly with pressure.

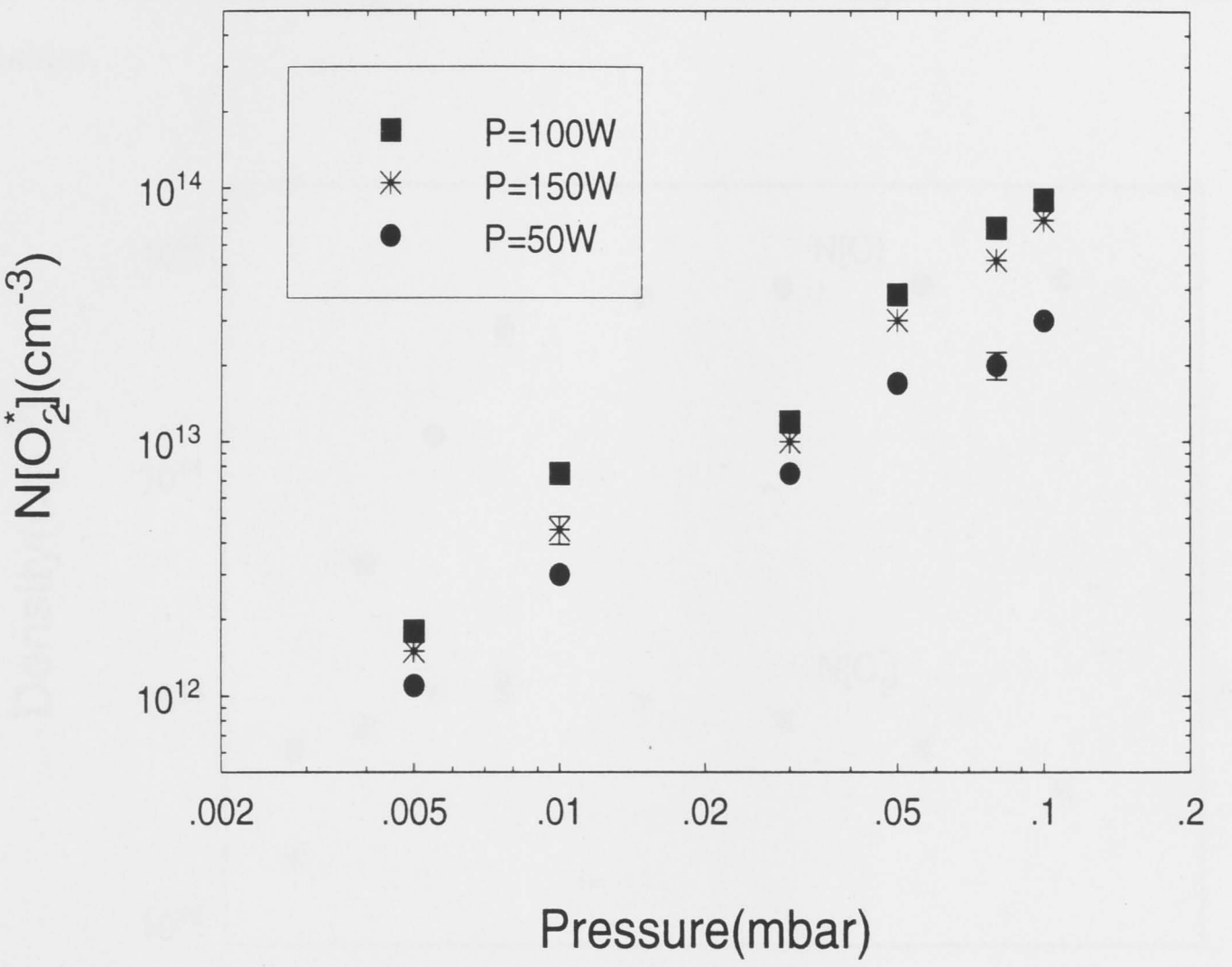

Fig.4.10 Dependence of the concentrations of metastable molecular oxygen on gas pressure at three RF powers.

4.3.2 Effects of RF Power

A typical result is shown in Fig.4.11, which shows how the densities of metastable oxygen molecules(O_2^*) and oxygen atoms(O) in the chamber vary with RF power at a fixed pressure 0.03mb, where the dissociation is most effective. The concentrations of both atomic and metastable molecular oxygen in the reaction chamber

increase with RF power up to about 100watts, higher powers producing little change. This is due to a full dissociation in the source (see Chapter 5). It can be seen that the atomic oxygen density is always much higher than that of the metastables.

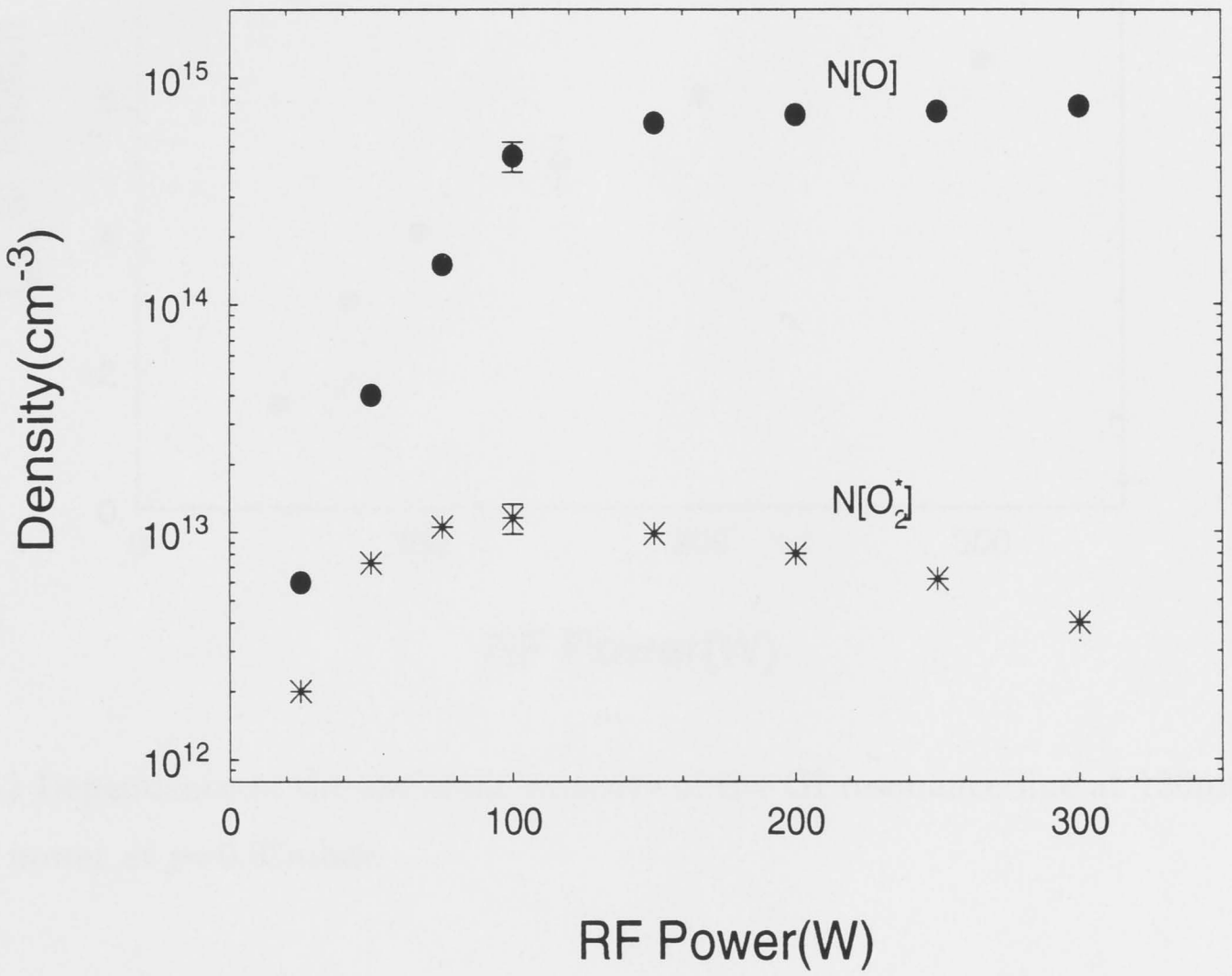

Fig.4.11 Concentrations of atomic oxygen and metastable molecular oxygen as functions of RF power at p=0.03mbar.

The variation of N[O] with RF power can also be seen from the measured emission intensity of the OI resonance line at 130nm. This is shown in Fig.4.12, which exhibits the same trend as that of N[O] measured by absorption.

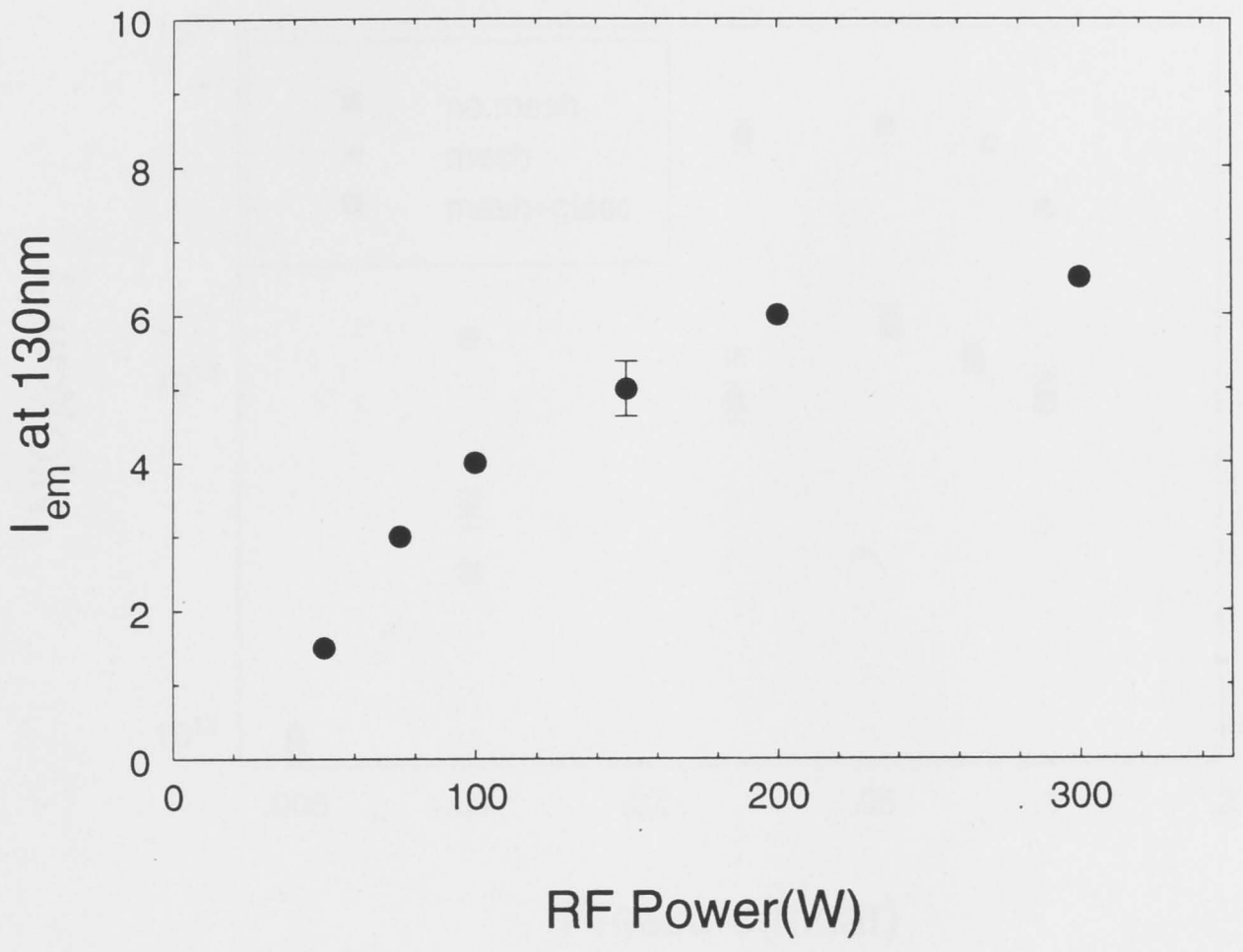

Fig.4.12 Dependence of the emission intensity of the OI resonance line at 130nm on RF power at p=0.03mbar.

4.3.3 Effects of Baffles

The baffles and their use have been described in Chapter 3. The concentrations of the two reactive neutral particles in the chamber were measured when the baffles were inserted between the plasma source and the reaction chamber.

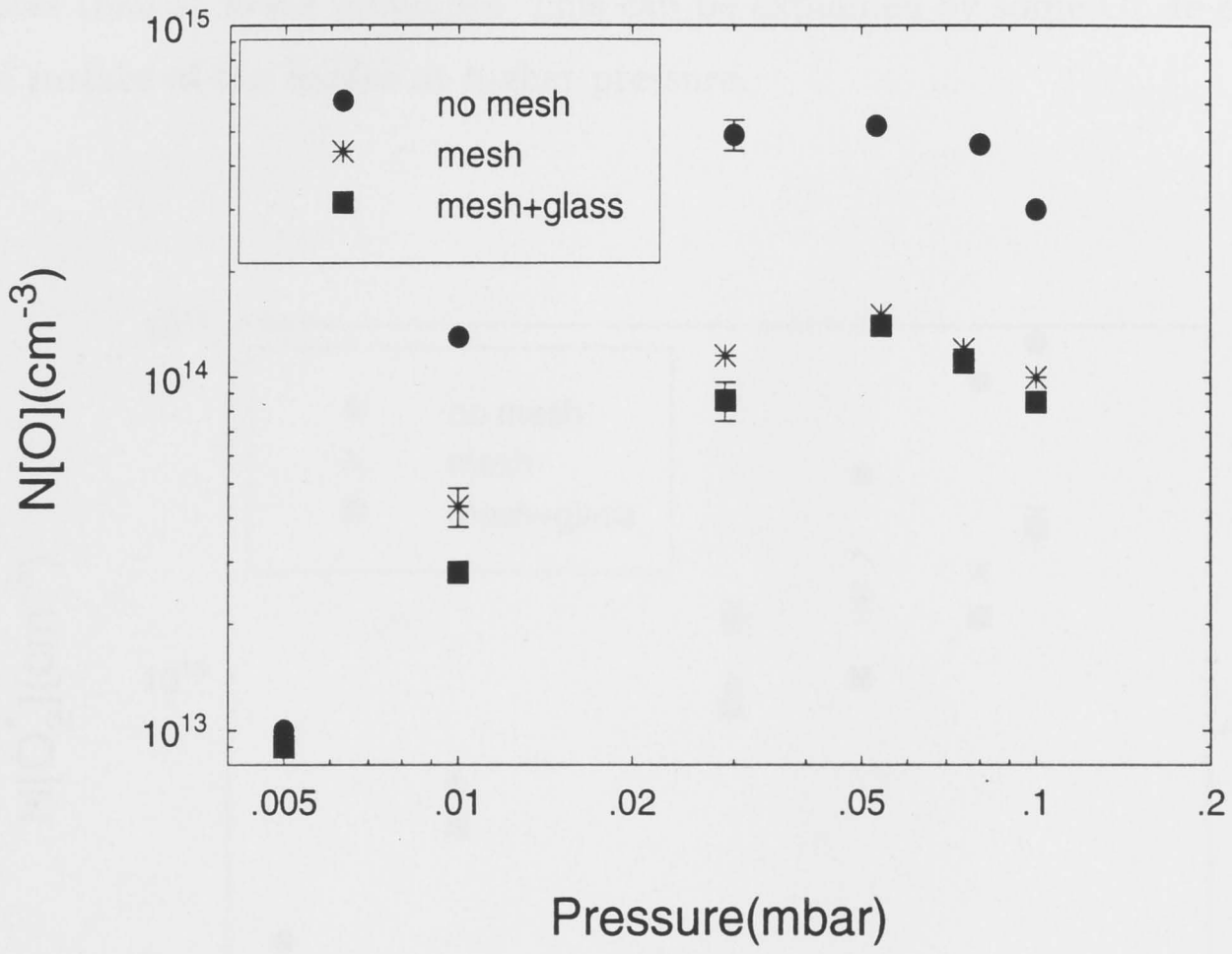

Fig.4.13 The effect of the baffles on N[O] for different pressures.

Fig.4.13 shows the effect of the baffles on N[O] for different pressures. It can be seen that the concentration of atomic oxygen N[O] is reduced by the presence of the baffles but by much less than their effect on the charged particles (N_i was reduced to a level too small to measure). This reduction is caused by the mesh which greatly reduces the flow of energetic electrons into the chamber so that little or no dissociation occurs there, and by some of O was lost on the mesh. With baffles in place all the atomic oxygen in the chamber must come from the plasma source. This is consistent with the model calculation (see Chapter 5).

The dependence of metastable molecular oxygen on gas pressure with and without baffles is shown in Fig.4.14. Density is reduced more by the baffles at higher pressures than at lower pressures. This can be explained by some O_2^* de-exciting on the surface of the baffles at higher pressure.

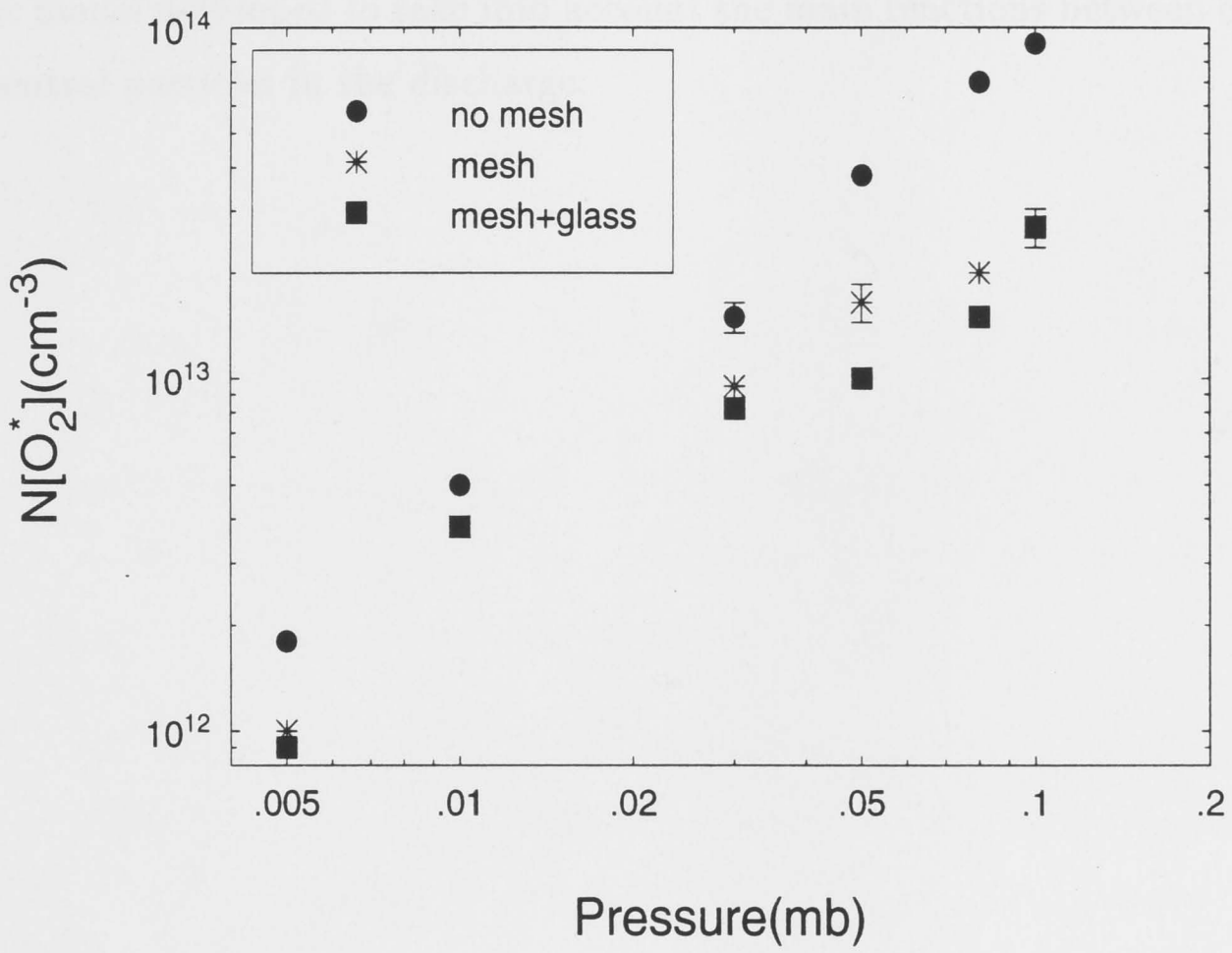

Fig.4.14 The effect of the baffles on $N[O_2^*]$ for different pressures.

4.4 SUMMARY

It has been shown that the vuv absorption technique is a powerful tool for investigating oxygen discharges allowing line-of-sight measurements of the concentration of the two main reactive species. It was also found that an RF excited radiation source seems to have practical advantages over a conventional microwave dis-

charge. The experimental results indicate that there is an optimum gas pressure for the production of O, while increasing RF power above 100W has only little effect on both $N[O]$ and $N[O_2^*]$. The results obtained using baffles indicate that while some of the main reactive particles in the chamber are produced locally by energetic electrons in the chamber, some of them come from the source. The experimental results presented here will be compared in the next chapter with a kinetic model developed to take into account the main reactions between charged and neutral particles in the discharge.

5

KINETIC MODEL

5.1 INTRODUCTION

In Chapters 3 and 4, the composition of the plasma derived from experiments has been described. This chapter attempts to explain the observed results in terms of several collision processes and the measured electron energy distributions. In order to understand the complicated physical and chemical processes occurring in the plasma, a theoretical model is developed.

As described in Chapter 3, most of the plasma is produced in the plasma source and then flows into the reaction chamber. Therefore, the theoretical model is set up for conditions inside the plasma source. A global model is assumed, i.e. the rate equations are spatially averaged throughout the plasma source and the neutral particles (O_2, O, O_2^*) temperatures are all taken to be 300K. Because of the limitations of the experimental equipment, the concentrations of the neutrals can only be measured in one region of the chamber. This undoubtedly results in some difficulty when we come to compare the model with the experimental results. However, as described in Chapter 3, the electron energy distribution is quite radially uniform in the source, and most of plasma in the chamber comes from the source. The concentration of the neutrals in the chamber should, therefore, follow the *trends* deduced from the modelling of the source. It is also reasonable for us to assume that the active neutrals in the chamber have a uniform distribution,

especially in the chamber central region of most interest ($-R_s < (x, y) < R_s$), since volume atomic recombination and molecular de-excitation can be neglected at the low pressures used, and recombination occurs at the walls with low probability [62, 63, 64].

In section 5.2, a set of the most important reaction equations is developed and the fundamental production and loss processes discussed. Reaction rate calculations are presented in section 5.3. In section 5.4, we calculate the concentration of the active species as a function of the experimental parameters from the reaction equations. Finally, the calculated values are compared with the experimental results.

5.2 PRINCIPAL SPECIES AND THEIR REACTION EQUATIONS

Any model for the kinetics of reactions occurring in the plasma must first take into account the major plasma components to be included. In principle, it should be possible to model the whole process of plasma production. While some attempts [63, 65, 66, 67] have been made along these lines, such an approach is far too ambitious and unnecessarily complicated for our purpose. Since this work is predominantly interested in explaining how the useful reactive species O and O_2^* are generated, the modelling has concentrated on the relevant dissociation, ionization, and excitation processes which control their formation and loss, starting from the known initial neutral gas filling and the experimentally measured parameters of charge density and electron energy distribution, and making use of their relationship to the applied RF power and pressure (described in Chapter 3). In this work, ten fundamental reaction equations are considered to describe

the production and loss processes of the main species which occur in our plasma. They are as follows:

$$O_2 + e \xrightarrow{K_i} O_2^+ + 2e \tag{5.1}$$

$$O_2 + e \xrightarrow{K_e} O_2^* + e \tag{5.2}$$

$$O_2 + e \xrightarrow{K_d} 2O + e \tag{5.3}$$

$$O_2 + e \xrightarrow{K_{da}} O + O^- \tag{5.4}$$

$$O_2^+ + e \xrightarrow{K_{r1}} 2O \tag{5.5}$$

$$O_2^* + e \xrightarrow{K_{r2}} 2O + e \tag{5.6}$$

$$O_2^* + e \xrightarrow{K_{r3}} O_2 + e \tag{5.7}$$

$$O + O^- \xrightarrow{K_{r4}} O_2 + e \tag{5.8}$$

$$O + O + \text{wall} \xrightarrow{K_{w1}} O_2 \tag{5.9}$$

$$O_2^+ + \text{wall} \xrightarrow{K_{w2}} O_2 \tag{5.10}$$

where $K_i, K_e, K_d, K_{da}, K_{r1}, K_{r2}, K_{r3}, K_{r4}, K_{w1}$ and K_{w2} are the corresponding reaction rate coefficients.

In the case of atomic oxygen, our experimental results *in the chamber* showed a high concentration with the fractional dissociation, $N[O]/2N[O_2]$, as high as 40% in the optimum pressure range (see Fig.4.8). Such a high concentration suggests that the atomic oxygen results not only from the direct electron collision dissociation process(5.3), but also from subsequent dissociation of O_2^+ and O_2^* both of which are in a higher energy state than O_2 and thus are more easily dissociated by electron collisions (5.5 and 5.6). The main loss mechanism for the atomic oxygen is assumed to be through recombination at the walls (5.9). The gas phase recombination can be neglected in the low pressure range investigated [68]. The loss of O by the detachment reaction (5.8) can also be neglected since

the reaction rate ($3.0\text{x}10^{-10}\text{cm}^3\text{s}^{-1}$) is much smaller than the wall recombination rate in the plasma (see Section 5.3).

Although the measured concentration of metastable excited molecular oxygen O_2^* is about one order lower than that of atomic oxygen O, it has been suggested that O_2^* might be a useful and selective reagent in the surface reaction [69]. The O_2^* is produced mainly by collisional excitation (5.2) and is lost principally through electron induced vibrational dissociation into atomic oxygen (5.6) and by super-elastic collisions with electrons to the ground-state (5.7).

We assume that the predominant positive ions are O_2^+ in the oxygen discharges in the pressure range of interest. The O_2^+ is mainly produced by direct ionization (5.1), and lost by electron collisional dissociation (5.5) and by neutralization at the walls (5.10). The values of the positive ion density used in the calculation of the kinetic equations are taken from the experimental data.

Because oxygen is electronegative, it can form negative ions either by direct attachment or by dissociative attachment [70], although experimentally we were unable to identify their presence in our plasma (see Chapter 3). The former process requires a three-body collision involving an electron and two oxygen molecules, which produces an O_2^- ion with the second molecule carrying away the attachment energy. However, the rate for the three-body process is very small [71] at our low pressures and the process can therefore be neglected. In contrast, dissociative attachment is a two-body process leading to the formation of an O^- ion and an oxygen atom. Charles *et al.* [72] using an energy selective mass spectrometer observed that the main negative ions in an RF oxygen discharge in a similar apparatus to ours are O^-. Therefore, dissociative attachment from the ground-state has been considered to be the main source of negative ions (5.4). The principal loss of the negative ions is by collision detachment with atoms (5.8).

5.3 CALCULATION OF REACTION RATES

Reaction rates for the electron collision processes(5.1-5.8) described above can, in principle, all be calculated through the following integration

$$K_j = \int_0^\infty \sqrt{(E/2m)}\sigma_j(E)f(E)dE \tag{5.11}$$

where E is the electron energy, $f(E)$ is the electron energy distribution function (EEDF), and $\sigma_j(E)$ is the appropriate cross-section. The EEDF in our plasma has been measured in detail using a Langmuir probe as described in Chapter 3. Therefore, provided the relevant cross-sections are known, the reaction rates can be evaluated through Eq.(5.11).

Only four cross-sections corresponding to ionization (5.1) [73], excitation (5.2) [74], dissociation (5.3) [75], and dissociative attachment (5.4) [76] are available from the literature, and are reproduced in Figure 5.1.

The electron energy thresholds of the processes are respectively 12.21, 0.97, 6.0, and 3.64eV. Notice that the cross-section for the dissociative attachment of O_2 is much smaller than those for its ionization and dissociation. In the electron energy range of interest, direct dissociation is the main process for producing O.

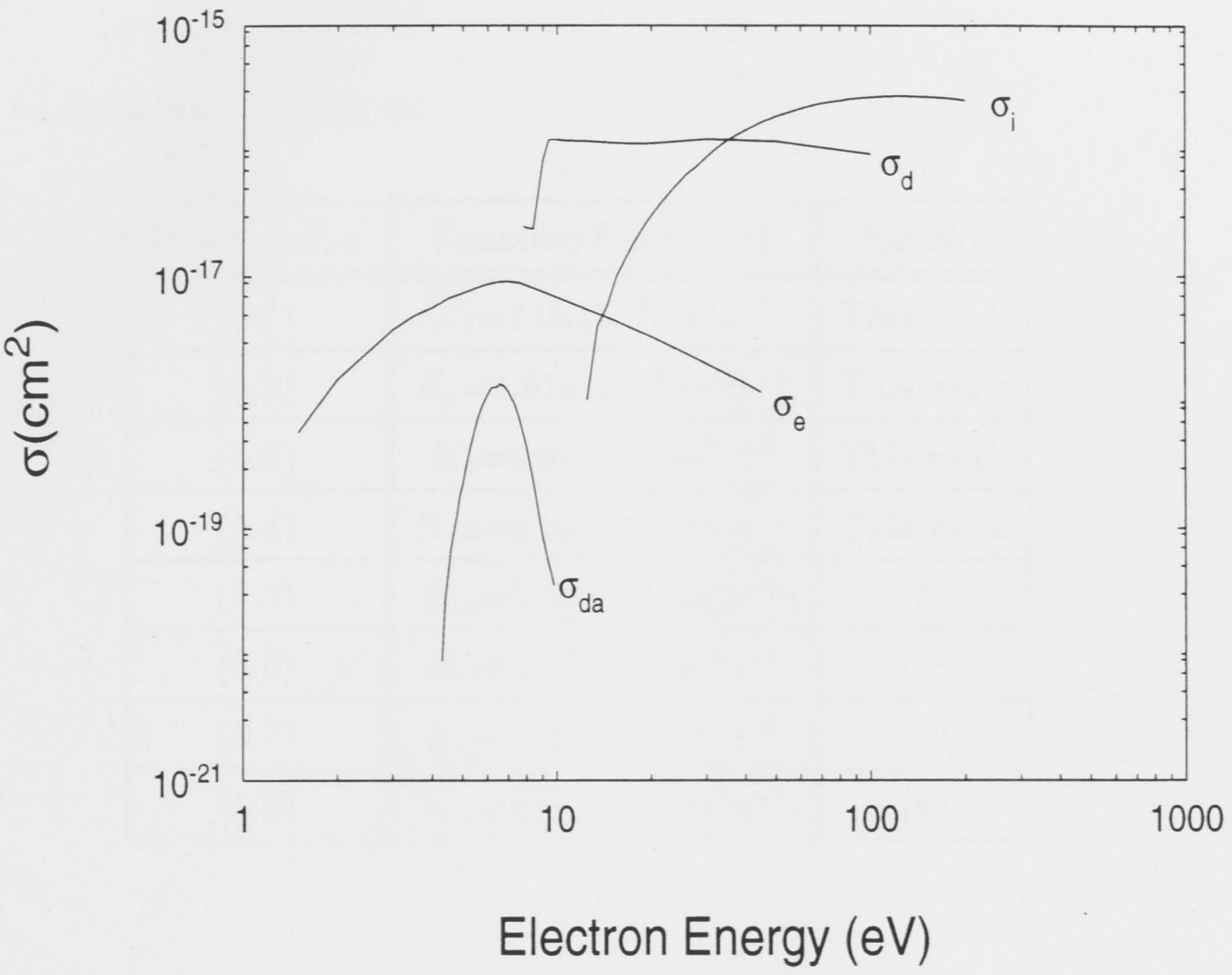

Fig.5.1 Four cross-sections corresponding to ionization, excitation, dissociation, and dissociative attachment.

If we now substitute the cross-sections and their energy dependence, and the measured EEDF in the plasma source into Eq.(5.11), we can obtain the reaction coefficients (K_i, K_e, K_d, K_{da}) by numerical integration. As we could not find the cross-sections corresponding to the equations (5.5–5.8) from the literature, the reaction coefficients $(K_{r1}, K_{r2}, K_{r3}, K_{r4})$ have been taken directly from the references shown, in which a Maxwellian distribution has been assumed. Table 5.1 lists the reaction coefficients used in this model.

Table 5.1 Reaction Coefficients

Reaction Eq.	Reaction Coefficient	Ref.No.
(5.1)	K_i=2.0x10$^{-9}cm^3s^{-1}$	This work
(5.2)	K_e=4.87x10$^{-10}cm^3s^{-1}$	This work
(5.3)	K_d=9.0x10$^{-9}cm^3s^{-1}$	This work
(5.4)	K_da=3.9x10$^{-11}cm^3s^{-1}$	This work
(5.5)	K_{r1}=2.0x10$^{-7}cm^3s^{-1}$	[77]
(5.6)	K_{r2}=1.5x10$^{-9}cm^3s^{-1}$	[78]
(5.7)	K_{r3}=1.4x10$^{-9}cm^3s^{-1}$	[79]
(5.8)	K_{r4}=3.0x10$^{-10}cm^3s^{-1}$	[80]

When the mean free path (λ) of O is smaller than R_s, K_{w1} is obtained by:

$$K_{w1} \propto \frac{1}{\tau_a} \tag{5.12}$$

where τ_a is the confinement time of the atomic oxygen, which can be derived from [81]

$$\begin{aligned} \tau_a &= \frac{\Lambda^2}{D} \\ &= \Lambda^2(\frac{M_a\nu_a}{k_BT_a}) \end{aligned} \tag{5.13}$$

where T_a is the temperature of the atoms of mass M_a (here assuming $T_a = T_g$=300K), ν_a=v_a/λ, v_a=$\sqrt{8kT_a/\pi M_a}$ is the mean thermal velocity of the oxygen atoms, and Λ is the diffusion length. For a cylindrical system, Λ is given by [82]

$$\frac{1}{\Lambda^2} = (\frac{2.405}{R_s})^2 + (\frac{\pi}{L})^2 \tag{5.14}$$

where L is the length of the source tube.

If $\lambda \geq R_s$, K_{w1} is calculated using the relation [83]:

$$K_{w1} = \frac{\gamma v_a}{2R_s} \tag{5.15}$$

where γ is the surface recombination coefficient of oxygen atoms at the source wall (Pyrex glass). The value of γ ($\simeq 5\text{x}10^{-3}$) is taken from experiments described in reference [63], which used the same material for the discharge tube as ours. From equation (5.15), $K_{w1}=24\text{s}^{-1}$.

Although λ is a little smaller than R_s in the pressure range of interest ($5\text{x}10^{-2}$-10^{-1}mbar), the value of K_{w1} changes little from the value obtained from the equation (5.15). In order to simplify the calculation of the rate equations, we take the value of $K_{w1}=24\text{s}^{-1}$.

The positive ion recombination rate coefficient at the wall K_{w2} is calculated from the relation [84]:

$$K_{w2} = \frac{2V_{B,O_2^+}(R_s^2 h_L + R_s L h_R)}{R_s^2 L} \tag{5.16}$$

where $V_{B,O_2^+}=\sqrt{kT_e/M_i}$ is the Bohm velocity, with M_i the mass of the O_2^+ ion, and L the length of the source tube. The coefficients h_L and h_R are respectively [85]:

$$h_L = N_{s,axial}/N_i = 0.86/\sqrt{3.0 + 2L/\lambda_i} \tag{5.17}$$

$$h_R = N_{s,radial}/N_i = 0.8/\sqrt{4.0 + R_s/\lambda_i} \tag{5.18}$$

where $N_{s,axial}$ and $N_{s,radial}$ are local values of sheath-edge ion densities in the axial and radial directions respectively, λ_i is the mean free path between the collisions of O_2^+ and O_2. The values of K_{w2} are between $5.8\text{x}10^4\text{s}^{-1}$ and $3.1\text{x}10^4\text{s}^{-1}$ for the pressure range 0.005 mbar to 0.1mbar.

5.4 RATE EQUATIONS, CALCULATION RESULTS AND COMPARISON WITH EXPERIMENTS

Having determined the main reaction processes as well as their reaction rates, we are now in the position to calculate the concentrations of the main species.

5.4.1 Rate Equations

The concentrations of the main species can be calculated by solving the rate equations. To complete the rate equations from the reactions (5.1—5.10), we must include the flow terms (one from the source to the chamber, the other from the chamber to the source) since one end of the plasma source is open to the reaction chamber in our experimental apparatus. In order to simplify the rate equations, the flow terms are only considered for the atomic oxygen because its measured concentration is much higher than other species. We consider two flow terms in this calculation, one from the source to the chamber, the other from the chamber to the source. A and B (Eq. 5.19) are taken as flow rate coefficients which are determined by the thermal velocity of the particle as well as by the geometry of the source and the chamber. At room temperature, the values of A and B in our conditions are $15.37s^{-1}$ and $36s^{-1}$ respectively. Under those assumptions described in the introduction, the rate equations for the main species in the plasma, from the expressions given earlier, can be written as:

$$\frac{\partial N_1}{\partial t} = 2K_d N_2 N_e + K_{da} N_2 N_e + 2K_{r1} N_i N_e + 2K_{r2} N_m N_e + B N_{1c} - K_{r4} N_1 N_n - K_{w1} N_1 - A N_1 \tag{5.19}$$

$$\frac{\partial N_2}{\partial t} = K_{r3} N_m N_e + K_{r4} N_1 N_n + \frac{1}{2} K_{w1} N_1 + K_{w2} N_i - (K_i + K_e + K_d + K_{da}) N_2 N_e \tag{5.20}$$

$$\frac{\partial N_m}{\partial t} = K_e N_2 N_e - K_{r2} N_m N_e - K_{r3} N_m N_e \tag{5.21}$$

$$\frac{\partial N_n}{\partial t} = K_{da} N_2 N_e - K_{r4} N_1 N_n \tag{5.22}$$

where AN_1 and BN_{1c} describe respectively the flow from the source to the chamber and vice versa. N_{1c} is the atomic oxygen concentration in the chamber taken from the experimental data. No equation for N_i is required since this is taken from experiments. The other symbols N's in the above equations designate the respective particle number densities as shown in Table 5.2.

Table 5.2: The symbols N's for the respective particle number densities.

species	subscripts
electron	e
O_2^+	i
O	1
O_2	2
O_2^*	m
O^-	n
total neutral density	0

In addition, two other conditions must be met, namely the conditions of neutrality and of mass conservation:

$$N_i = N_e + N_n \tag{5.23}$$

$$N_0 \simeq N_2 + N_m + \frac{1}{2} N_1 \tag{5.24}$$

where N_0 is the total number density of the particles and $N_0 = p/k_B T_g$, p is the filling gas pressure and T_g is room temperature. In Eq. (5.24), N_i and N_n are

neglected since their densities ($\sim 10^8 - 10^{10}$ cm^{-3}) are much much lower than the neutrals ($\sim 10^{14} - 10^{16}$ cm^{-3}).

In a steady-state $\partial/\partial t$=0, and the above rate equations reduce to:

$$2K_d N_2 N_e + K_{da} N_2 N_e + 2K_{r1} N_i N_e + 2K_{r2} N_m N_e + B N_{1c}$$

$$-K_{r4} N_1 N_n - K_{w1} N_1 - A N_1 = 0 \tag{5.25}$$

$$K_{r3} N_m N_e + K_{r4} N_1 N_n + \frac{1}{2} K_{w1} N_1 + K_{w2} N_i$$

$$-(K_i + K_e + K_d + K_{da}) N_2 N_e = 0 \tag{5.26}$$

$$K_e N_2 N_e - K_{r2} N_m N_e - K_{r3} N_m N_e = 0 \tag{5.27}$$

$$K_{da} N_2 N_e - K_{r4} N_1 N_n = 0 \tag{5.28}$$

The computer software 'Mathematica' is used to solve these above equations and calculate the concentrations of O, O_2^*, O_2, O^- and e.

5.4.2 Results and Comparison with Experiments

The effects of pressure on the concentrations of atomic oxygen in the source as derived from the model calculations are compared with the experimental data in the chamber, shown in Fig.5.2. They clearly show the same general trend. From the rate balance equations, it can be seen that O is produced by several reaction routes. The concentration of atomic oxygen depends not only on N_e and $N[O_2]$ but also on $N[O_2^+]$ and $N[O_2^*]$. As we know, within the pressure range used, N_e and $N[O_2^+]$ decrease while $N[O_2]$ and $N[O_2^*]$ increase as the pressure increases. It is this intricate situation that results in a peak value in $N[O]$ within the pressure

range investigated. It also provides a means to choose the optimum experimental parameters for wool treatment.

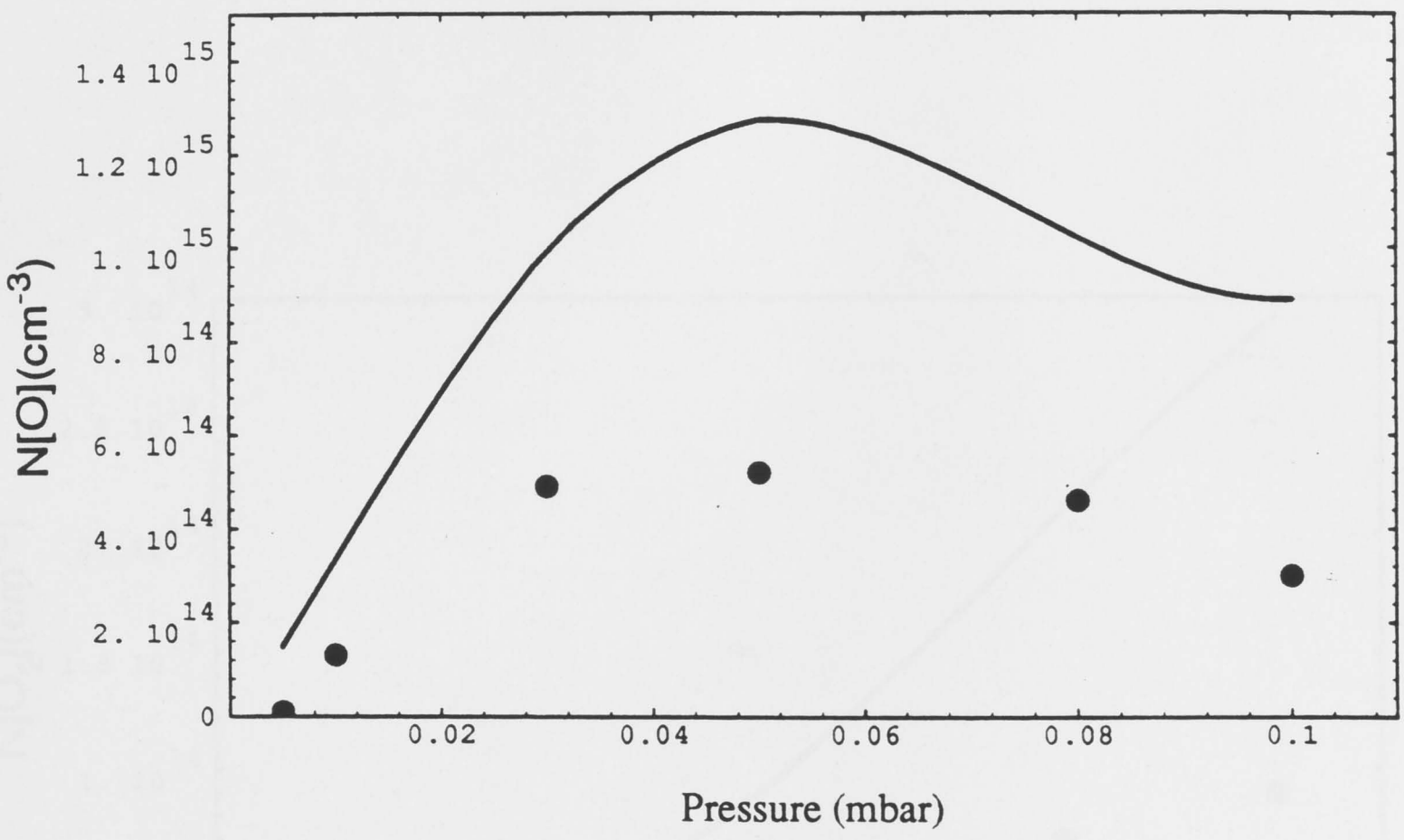

Fig.5.2 Comparison of the concentration of atomic oxygen in the source derived from the model calculation with the experimental data in the chamber as a function of pressure. (• the experimental data in the chamber ; —— the model calculation in the source).

A similar comparison for metastable molecular oxygen is shown in Fig.5.3. Both the model calculation and the experimental data show the same trend. As can be

seen, at low pressure (≤ 0.01mbar), the values from the model calculation and the experimental data agree. However, when the pressure increases, the values in the source and chamber diverge. This can be explained since, during flow from the source to the chamber in the higher pressure, more and more metastables are lost by vibrational dissociation to produce more atomic oxygen and by super-elastic collisions to the ground-state.

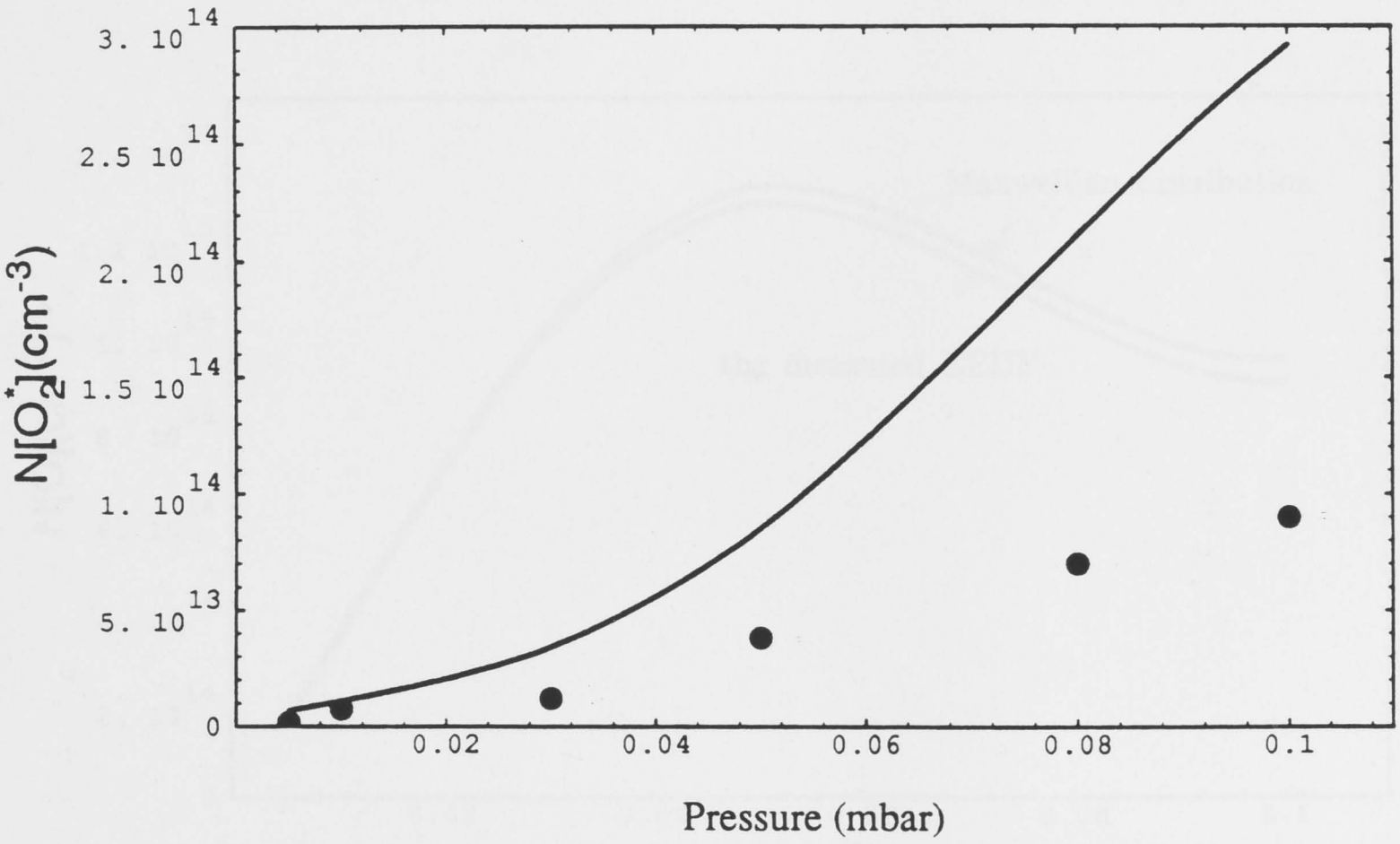

Fig.5.3 Comparison of the concentration of metastable molecular oxygen in the source derived from the model calculation with the experimental data in the chamber as a function of pressure.

It is interesting to compare the concentration of atomic oxygen as a function of pressure derived from the model calculations using our measured electron energy distribution function and those resulting from a Maxwellian distribution with the same mean energy. This is shown in Fig.5.4. There is only a small difference between them. It indicates that the different electron energy distribution leads to different reaction rates, resulting in somewhat different particle density. On the other hand, it shows that the results do not depend very sensitively on the details of the distribution functions because there is only a little difference between the Maxwellian distribution and ours.

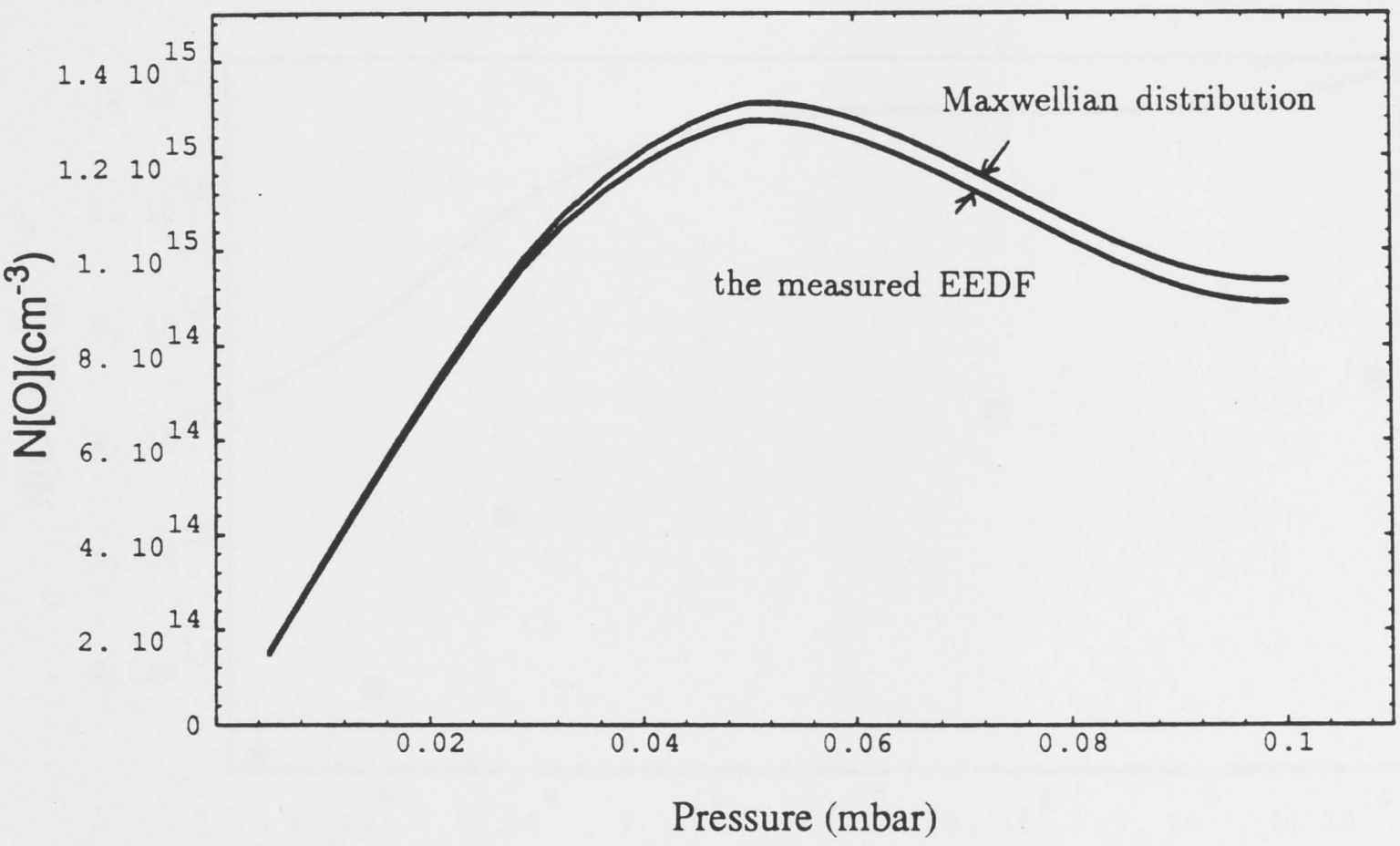

Fig.5.4 Comparison of N[O] as a function of pressure derived from the model calculation using our measured EEDF with those resulting from a Maxwellian distribution

Fig.5.5 shows the effects of the charged particle density on the concentration of atomic oxygen as calculated by the model compared with the experimental data. The trend is the same as the experimental measurements. N[O] increases for ion densities up to about $5\text{x}10^{9}\text{cm}^{-3}$ (corresponding to 100W RF power), while the higher ion densities produced by higher RF powers cause little change. The saturation can be explained by the ratio of $N[\text{O}]/2N[\text{O}_2]$, which indicates that about 80% of the oxygen *in the source* is dissociated at higher powers when p=0.03mbar. It means there is no more O_2 left to dissociate in this case. It also indicates that only low RF power is needed to produce a high concentration of atomic oxygen.

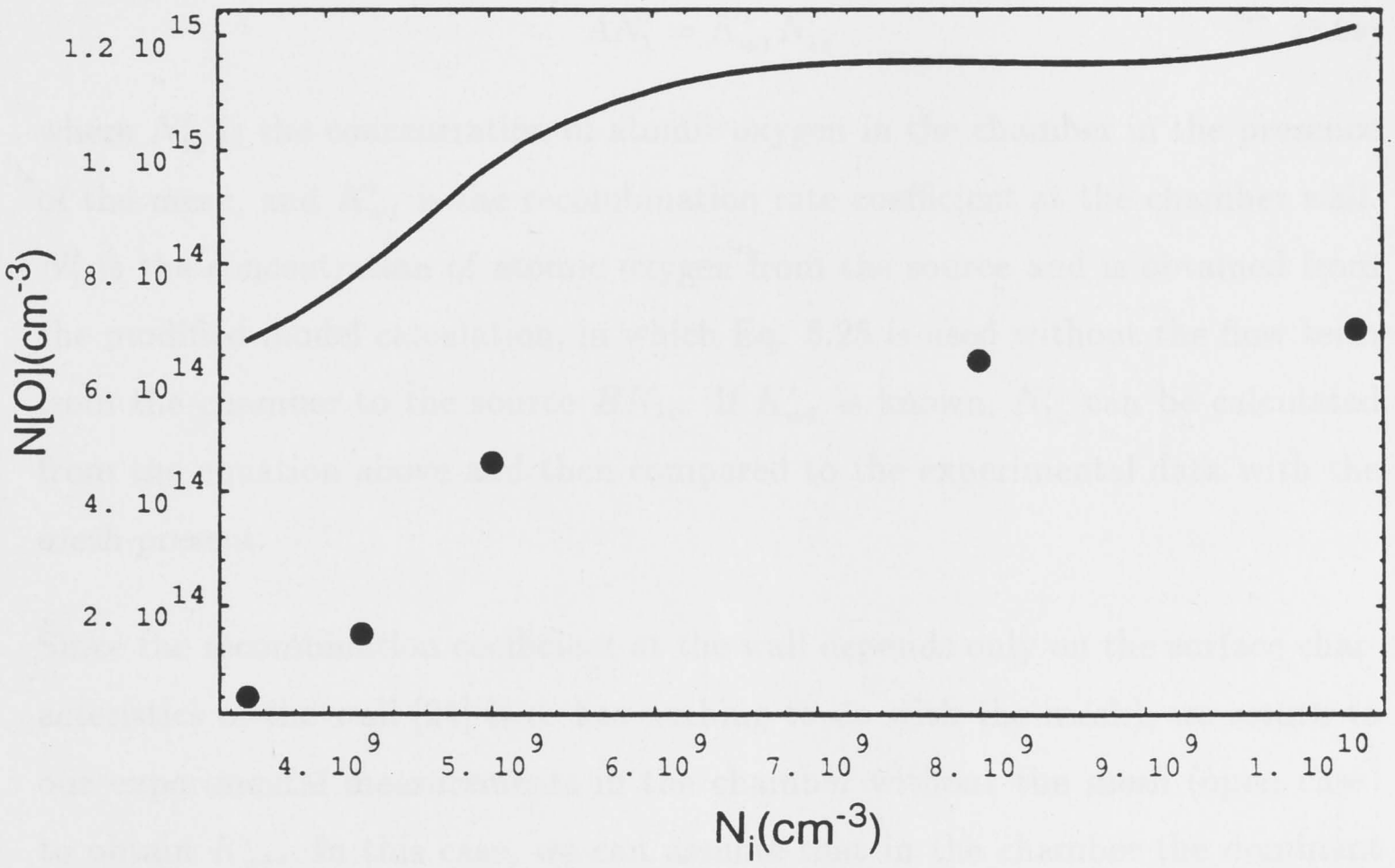

Fig.5.5 Comparison of the concentration of atomic oxygen in the source derived from the model calculation with the experimental data in the chamber as a function of the charged particle density.

As a further check on the reaction model, the experimental results with the mesh present can be compared with the calculation made by modifying the model. As discussed in Chapters 3 and 4, the presence of the mesh greatly reduces the flux of charged particles but still allows the neutral particles into the chamber. In this case, the measured concentration of atomic oxygen can only come from flow out of the plasma source since there are few charged particles in the chamber to produce atomic oxygen locally.

Assuming no plasma components are produced in the chamber, only flow (AN_1') from the source to the chamber need be considered for O input in the chamber. The O loss in the chamber is considered to be by recombination at the chamber wall. Therefore, the rate balance equation in this case is:

$$AN_1' = K_{w1}' N_{1c}' \tag{5.29}$$

where N_{1c}' is the concentration of atomic oxygen in the chamber in the presence of the mesh, and K_{w1}' is the recombination rate coefficient at the chamber wall. N_1' is the concentration of atomic oxygen from the source and is obtained from the modified model calculation, in which Eq. 5.25 is used without the flow term from the chamber to the source BN_{1c}. If K_{w1}' is known, N_{1c}' can be calculated from the equation above and then compared to the experimental data with the mesh present.

Since the recombination coefficient at the wall depends only on the surface characteristics of the wall [24] (i.e. has nothing to do with the mesh), we return to our experimental measurements in the chamber without the mesh (open case) to obtain K_{w1}'. In this case, we can assume that in the chamber the dominant production terms for the atomic oxygen are dissociation by local electron impact plus the flow from the source (AN_1), while the principal loss terms are the recombination at the chamber walls and flow back into the source (BN_{1c}). Thus

the balance equation becomes

$$2K'_d N_2 N_e + AN_1 = BN_{1c} + K'_{w1} N_1 \tag{5.30}$$

where K'_d=8.0x10^{-9}cm^{3}s^{-1} is the dissociation rate coefficient calculated from the measured EEDF in the chamber, N_2 and N_{1c} are experimental data. It can be assumed that $N_e \approx N_i$ as $N_n/N_e \ll 1$ in the pressure range interested from the model calculations. By substitution in Eq.(5.30), we obtain a value of K'_{w1} around 100 s^{-1}.

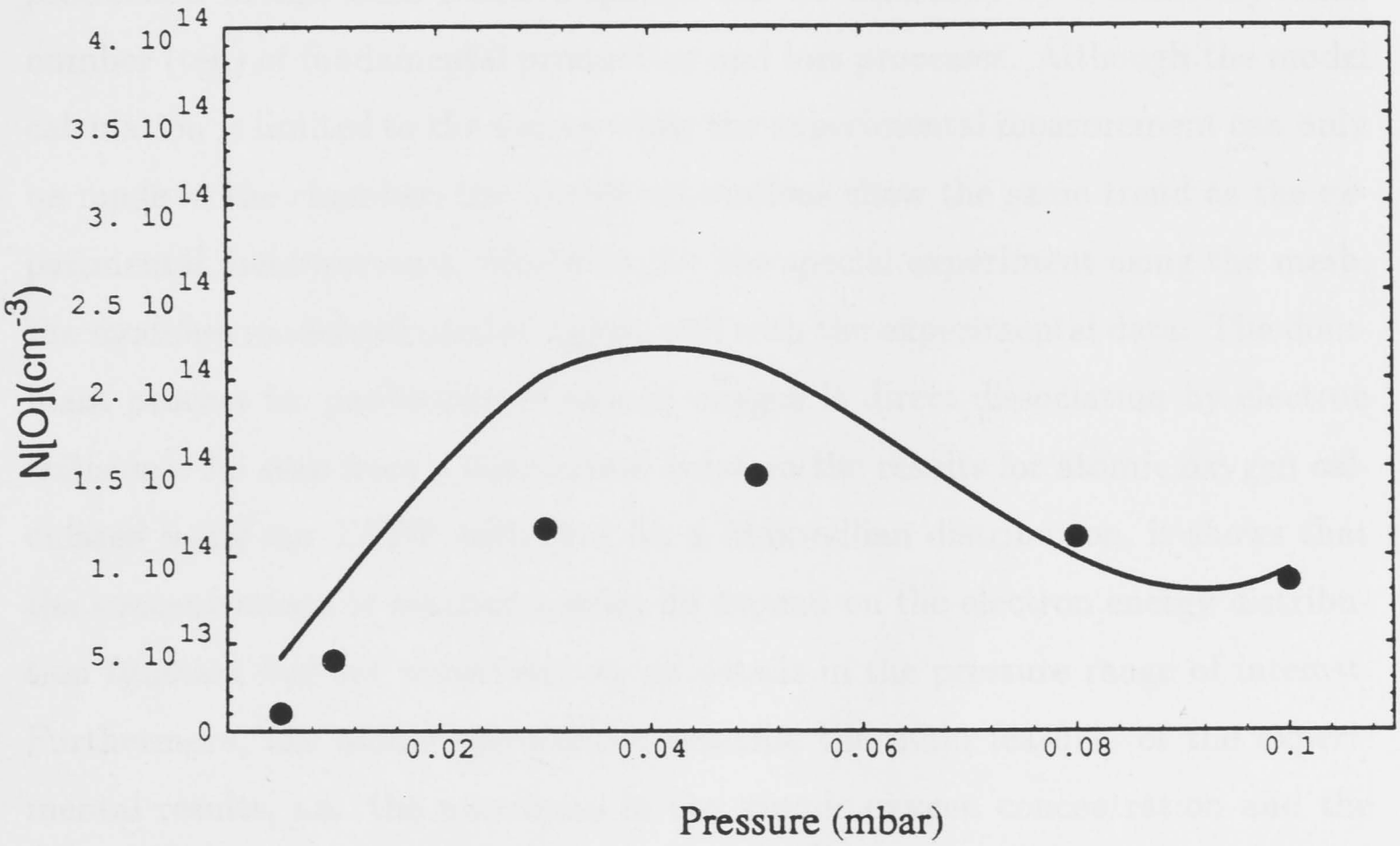

Fig.5.6 Comparison of the concentration of atomic oxygen flow from the source derived from the modified model calculation with the experimental data with the mesh present in the chamber as a function of pressure.

Fig.5.6 shows the comparison between the calculation of N'_{1c} from Eq.(5.29) and the data from experimental measurement with the mesh present. The agreement between them indicates the reaction model developed here successfully describes the kinetic processes in our plasma.

5.5 SUMMARY

A kinetic model of the chemical reactions occurring in an RF induced oxygen plasma has been successfully developed. It has shown that in our plasma the production of the main reactive species can be described by a relatively small number (ten) of fundamental production and loss processes. Although the model calculation is limited to the source while the experimental measurement can only be made in the chamber, the model calculations show the same trend as the experimental measurements. Moreover, for the special experiment using the mesh, the modified model calculation agrees well with the experimental data. The dominant process for production of atomic oxygen is direct dissociation by electron collisions. As seen from a comparison between the results for atomic oxygen calculated using our EEDF with that for a Maxwellian distribution, it shows that the concentrations of reactive species do depend on the electron energy distribution function but not sensitively on its details in the pressure range of interest. Furthermore, the model calculations describe the main features of the experimental results, i.e. the maximum in the atomic oxygen concentration and the linear relationship in concentration of metastable molecular oxygen as a function of gas pressure, as well as the saturation of the atomic oxygen concentration at the higher ion densities (or higher RF power). Also, the model provides a means to choose optimum experimental parameters for wool treatment.

6

SURFACE MODIFICATIONS AND UNDERLYING MECHANISMS

6.1 INTRODUCTION

As stated in Chapter 1, the interaction of plasma with wool is a very complicated process. In the first part of this work we studied experimentally the behaviour of the composition of this complex plasma mixture, and investigated the dominant process for the production of the main neutral reaction species in the plasma by developing a theoretical kinetic model. Now we turn our attention to the following essential matters: What are the key issues in the improvement of the wool surface properties? What are the main reactive species responsible for the surface modification? How do the reactive species react with the wool surface? Can a particular level of wool surface change be achieved by controlling of the experimental parameters?

An extensive study of the changes of the physical and chemical properties of the wool surface after oxygen plasma treatment has been carried out; the results are presented in section 6.2. In order to determine the dominant process responsible for the wool surface modification, a series of experiments (using different gases and different baffle configurations) have been used to help separate the contributions from the charged particles, the neutral particles, and the uv photons in the plasma. These experiments are described in section 6.3. In section 6.4, the

relationship between the surface properties of wool and the reactive species in plasma is presented and a reaction model for the process proposed.

6.2 MODIFICATIONS OF WOOL SURFACE PROPERTIES BY OXYGEN PLASMA TREATMENT

6.2.1 Changes in Surface Energy

As mentioned in Chapter 1, the hydrophobic character of the outer cuticle layer of the wool fibre corresponds to a low surface energy. This low surface energy of natural wool results in difficulties in spinning, printing, dyeing, shrink-proofing etc. Therefore, the enhancement of the surface energy has been identified as one of the key issues in this investigation.

In this study, the changes in surface energy of wool fibre have been measured for an extensive range of plasma conditions. The surface energy was measured using the Wilhelmy Plate inspired method with water as a liquid probe (see Chapter 2). The measurements show that the surface energy of clean natural wool is slightly negative (~ -4 mJ/m^2), but it can be increased to 60 mJ/m^2 after oxygen plasma treatment, a considerable enhancement. The surface energy increases and quickly reaches a saturation level as shown in Figures 6.1 and 6.2 in which the surface energy increase ($\triangle$W) is plotted as a function of RF power and treatment time, respectively. As can be seen in these figures that the saturation occurs roughly at an energy input to the plasma ('dose') of about 100 J (power x time), and that this value holds at all other pressures investigated. It should be noted that the trend is similar to the curve of atomic oxygen concentration as a function of RF power.

It is interesting that a peak in $\triangle$W is observed as a function of pressure when the dose is below the saturation level (e.g. at 50J, corresponding to half of the saturation dose), as shown in Fig.6.3, which is similar to the curve of N[O] as a function of pressure. A similar trend has been also found in samples treated with air plasma but for a different plasma dose. All the above show that only a small plasma dose is needed to achieve the saturation level of the surface energy, and that below the saturation level there is an optimum gas pressure corresponding to a maximum increase in surface energy.

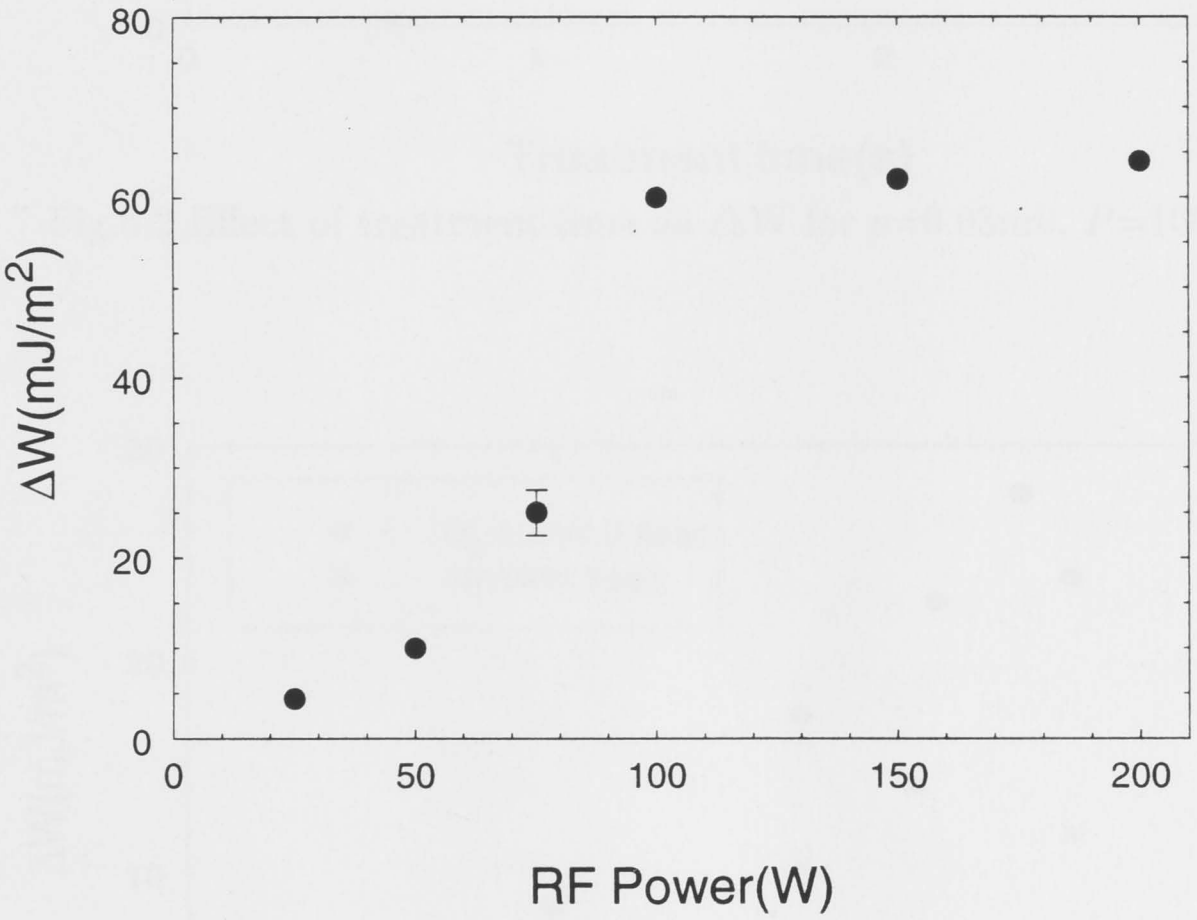

Fig.6.1 Dependence on RF power of change in surface energy of wool $\triangle$W, p=0.03mb, t=1sec.

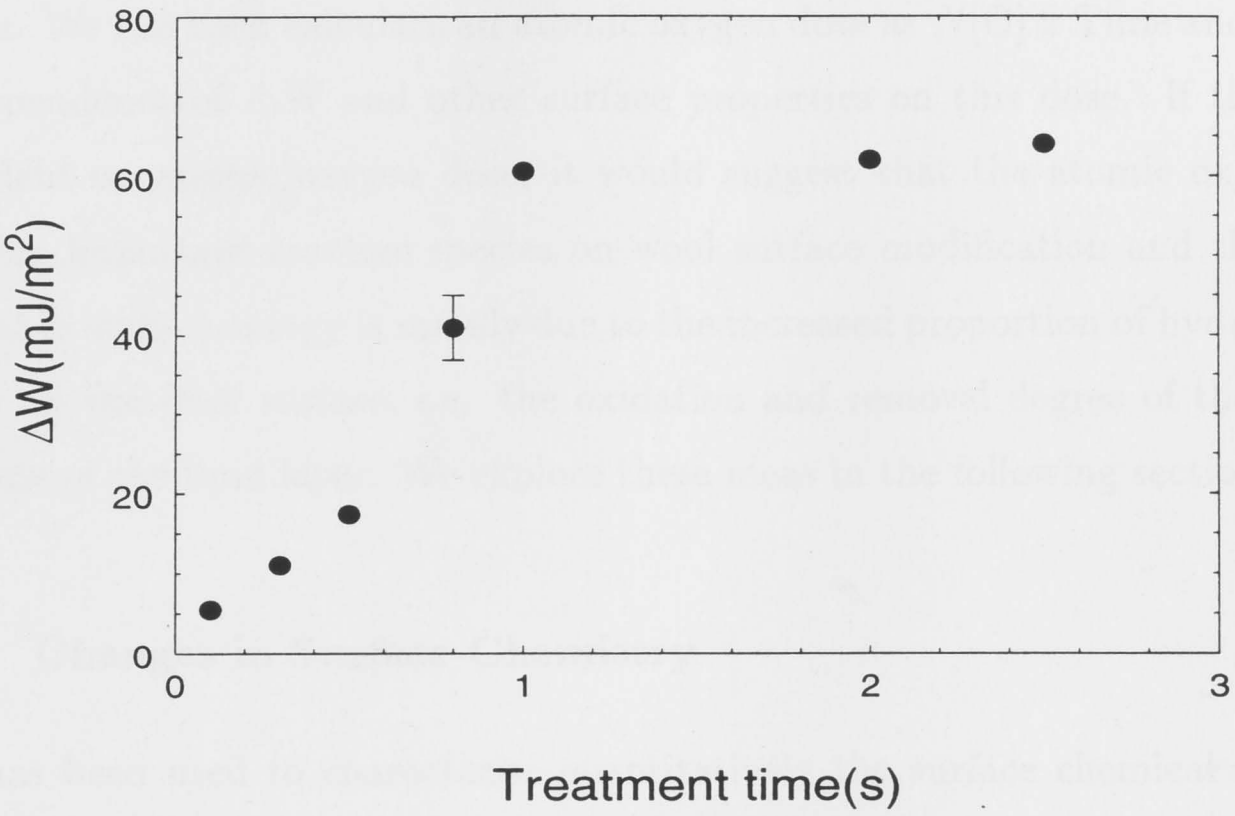

Fig.6.2 Effect of treatment time on $\triangle$W for p=0.03mb, P=100W.

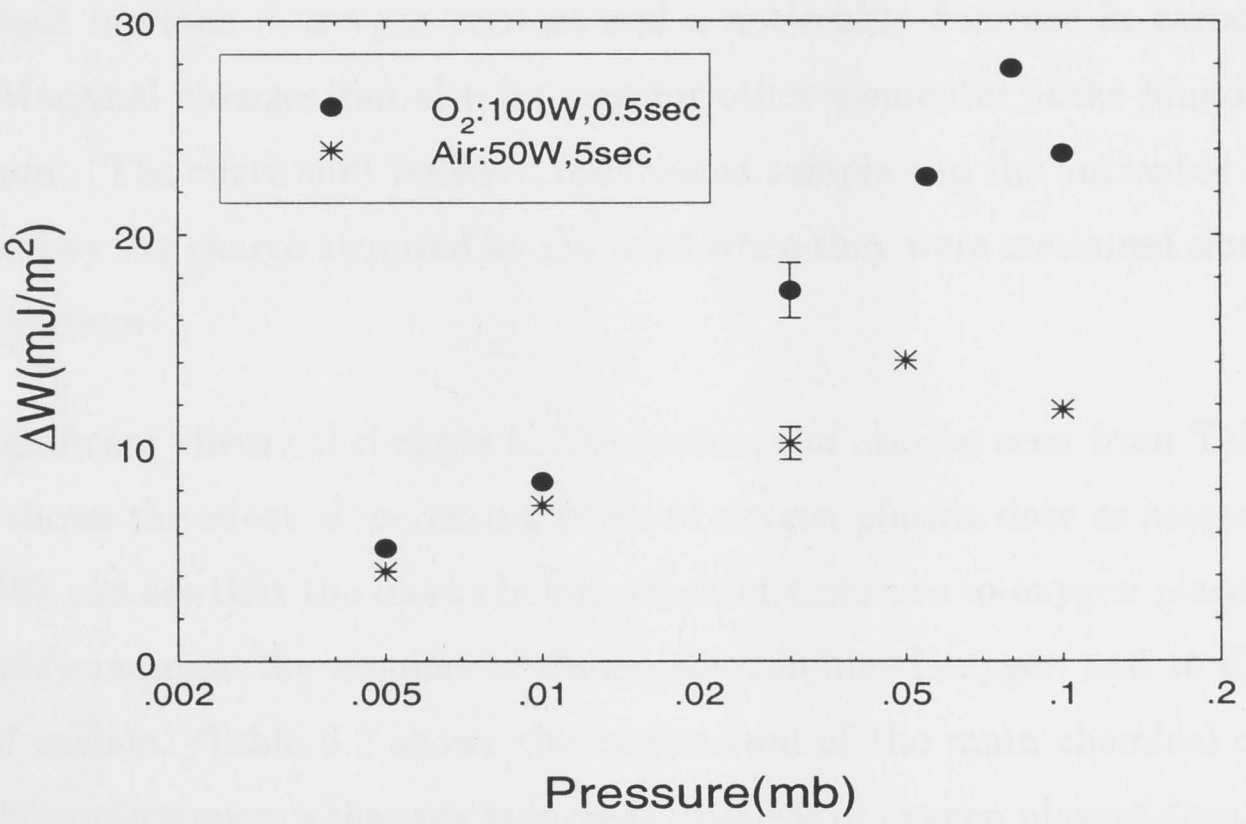

Fig.6.3 Dependence of $\triangle$W on pressure.

The fact that $\triangle$W changes with the experimental parameters in a similar way to N[O] suggests that $\triangle$W is related to the atomic oxygen concentration in the plasma. We can then calculate an atomic oxygen dose as N[O] x Time and study the dependence of $\triangle$W and other surface properties on this dose. If they are dependent on atomic oxygen dose, it would suggest that the atomic oxygen is the most important reactive species on wool surface modification and that the increase in surface energy is mainly due to the increased proportion of hydrophilic groups on the wool surface, i.e. the oxidation and removal degree of the outer segments of the lipid layer. We explore these ideas in the following sections.

6.2.2 Changes in Surface Chemistry

XPS has been used to characterise quantitatively the surface chemical composition for untreated and oxygen-plasma treated wool samples. In Figure 6.4 a representative XPS spectrum is shown for an untreated wool sample (solid line) and for a treated sample (broken line). Overall, the treated sample showed a significant increase in oxygen content and a noticeable decrease in carbon content. Marginal changes can also be seen for other elemental peaks found in the spectrum. (The curve shift between the treated sample and the untreated sample is caused by the charge acquired by the wool when they were measured since wool is an insulator).

The significant chemical changes in the surface can also be seen from Table 6.1, which shows the effect of increasing levels of oxygen plasma dose as measured by XPS. We can see that the most obvious effect of exposure to oxygen plasma is to noticeably increase the amount of chemically combined oxygen and to decrease that of carbon. Table 6.2 shows the comparison of the main chemical changes with the surface energy changes as increasing levels of oxygen plasma dose. It can

be seen there is a clear link between increasing level of oxidised species present and the increase in surface energy.

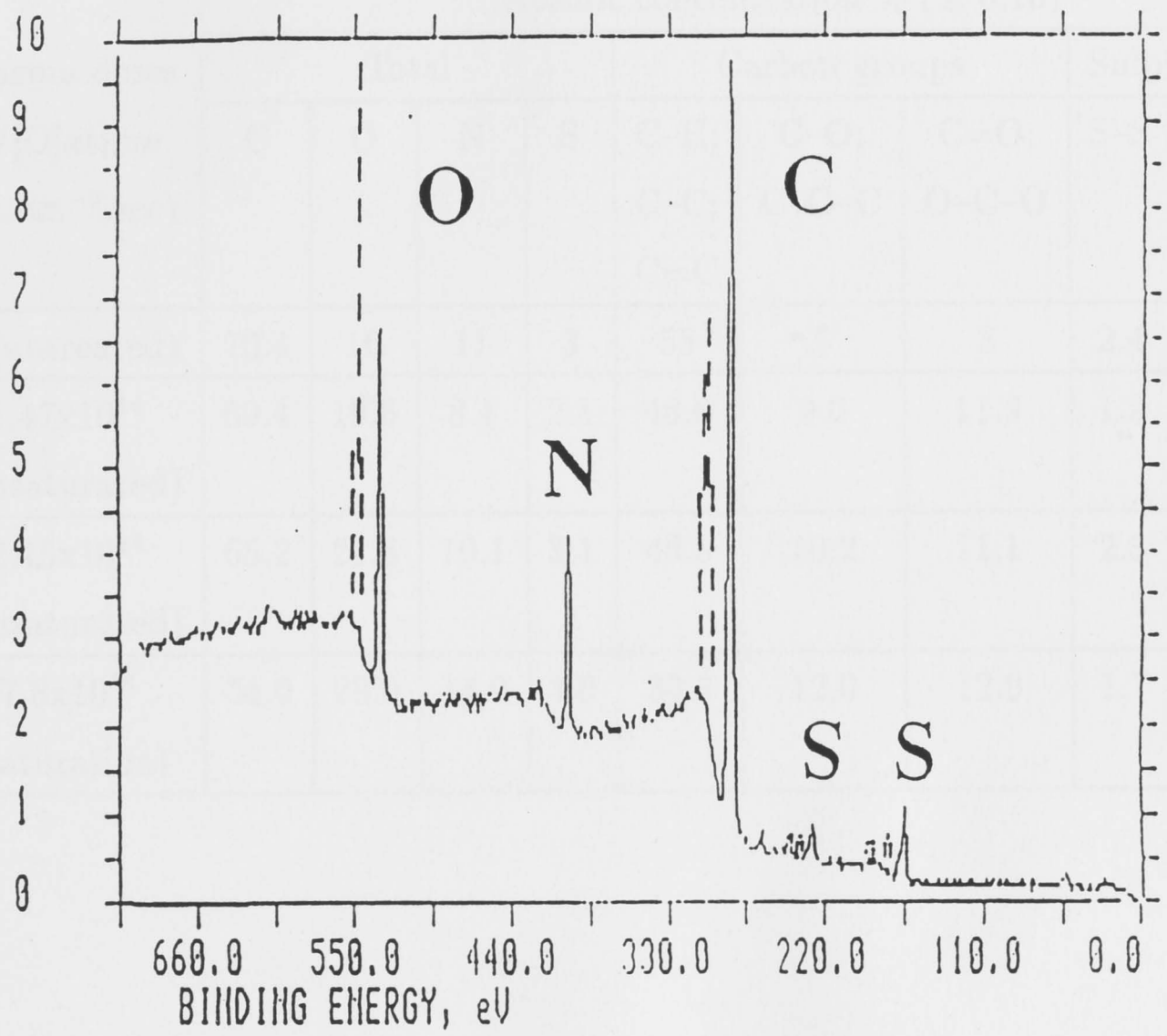

Fig.6.4 XPS for a sample treated by oxygen plasma (plasma dose 7.8×10^{14} at.cm^{-3}.sec, dotted line) and an untreated sample (solid line).

Table 6.1: Changes in atomic composition of wool surface with different plasma doses as measured by XPS.

Plasma doses N[O]xtime (at.cm^{-3}.sec)	Atomic concentration % (± 0.10)								
	Total				Carbon groups			Sulphur groups	
	C	O	N	S	C–H; C–C; C=C	C–O; C–O–C	C=O; O–C–O	S–S	SO_2; SO_3H
0 (untreated)	70.4	16	11	3	55	7	8	2.4	0.4
1.47×10^{14} (unsaturated)	69.4	19.6	8.4	2.1	48.6	9.0	11.9	1.9	0.2
2.45×10^{14} (unsaturated)	65.2	21.6	10.1	3.1	43.8	10.2	11.1	2.3	0.8
7.8×10^{14} (saturation)	54.0	28.0	14.0	3.0	30.0	12.0	12.0	1.7	0.9

Table 6.2: The main chemical changes in the wool surface (measured by XPS) by comparison of the surface energy changes as increasing levels of oxygen plasma dose.

Plasma doses N[O]xtime (at.cm^{-3}.sec)	$\triangle$W mJ.m^{-2}	Atomic concentration % ($\pm$ 0.10)				
		Total		Carbon groups		
		C	O	C–H; C–C; C=C	C–O; C–O–C	C=O; O–C–O
0 (untreated)	–4	70.4	16	55	7	8
1.47x10^{14} (unsaturated)	11	69.4	19.6	48.6	9.0	11.9
2.45x10^{14} (unsaturated)	17	65.2	21.6	43.8	10.2	11.1
7.8x10^{14} (saturation)	60	54.0	28.0	30.0	12.0	12.0

6.2.3 Changes in Surface Morphology

Images of the untreated and treated wool fibres extracted from fabrics have been recorded using a field emission SEM. No significant differences are observed for low plasma doses. This implies that only the outermost surface layers of the fibres are affected by these treatments.

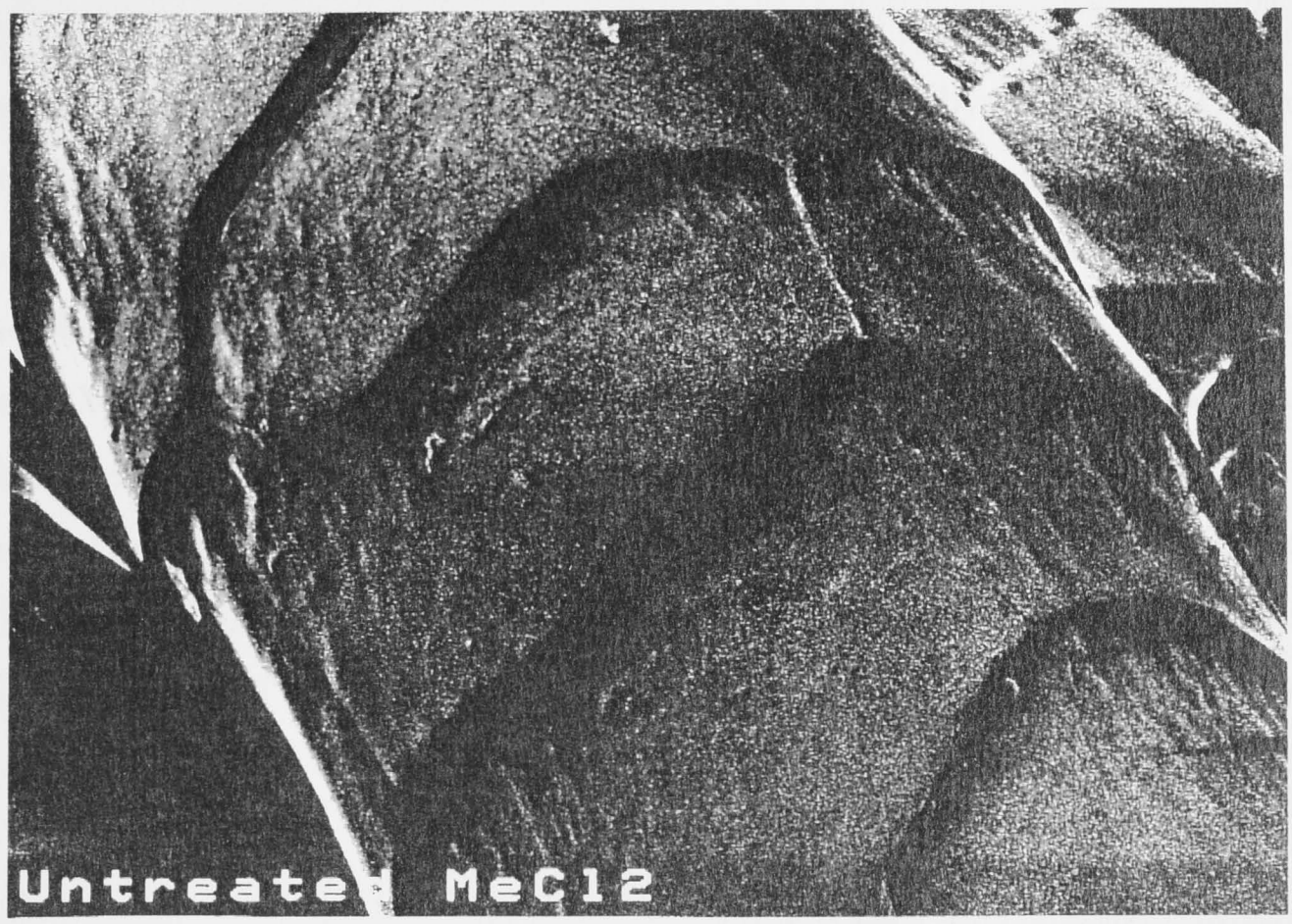

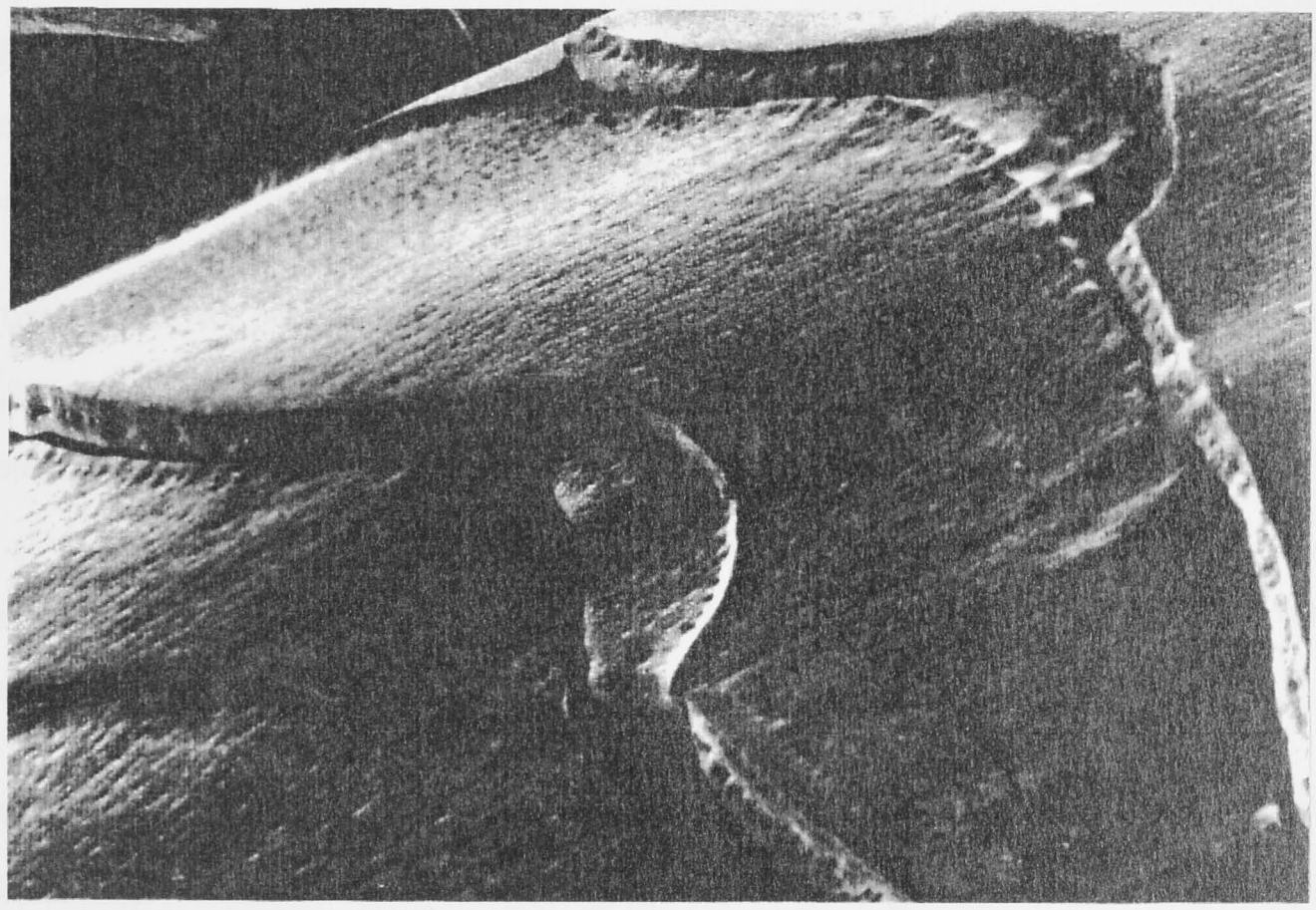

Fig.6.5 SEM for (a) untreated wool; (b) treated wool by oxygen plasma (N[O] x time = 4x10^{17} at.cm^{-3}.sec)

However, a comparison in wool surface appearance seen by electron microscopy is presented in Figure 6.5 between untreated wool (Fig.6.5(a)) and wool treated with a large oxygen plasma dose, $4x10^{17}$ at.cm^{-3}.sec (Fig. 6.5(b)). It can be seen that some observable physical changes do occur on the wool surface for high treatment doses. Oxygen plasma etches the fibre producing a longitudinally striated surface, with some preferential etching occurring along the centre of the scale edge. This observation suggests that there are chemically different types of material present in the scales of the wool fibre after oxygen plasma treatment. The more resistant layers are believed to correspond to highly cross-linked, disulphide rich areas of the wool fibre [22].

6.2.4 Technological Improvements to the Wool

In addition to the changes of wool surface energy, other quantitative improvements of the plasma-treated wool are related to its printing, dyeing and shrinkage resistance.

Figure 6.6 shows a quality improvement in printing and dyeing, with colour pastes of Lanasol Black (5055 2%) and with Lanasol Blue (8G–1%) respectively. It can be seen that both the colour yield (Kubella–Munk K/S) and the lightness values Δ L(=L_{dyed} - L_{undyed}) are increased. More quantitatively, an increase of 100 % or more was obtained in the colour yield while the lightness value increased between 30 to 50%.

It is known that natural wool has a high concentration of disulphide cross-linkage in the a-layer of the exocuticle (see Fig.1.2) which sets up a diffusion barrier for dyeing and printing. As mentioned above, the saturation of the surface energy corresponds to the oxidation and removal of the outer lipid layer, leaving the more complex, sulphur rich protein layer exposed. In this case, the plasma

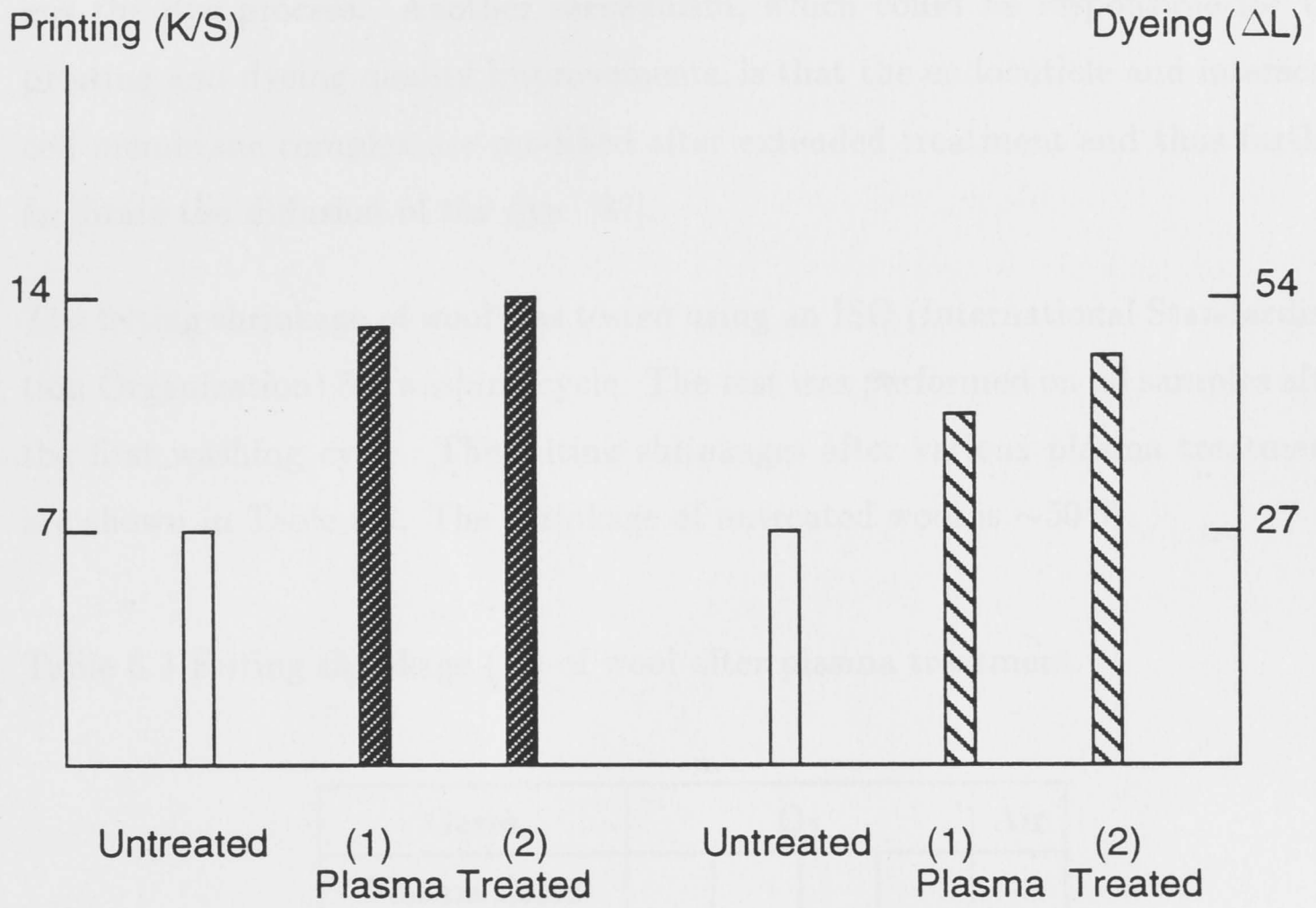

Fig.6.6 Improvement in printing after oxygen plasma treatment compared with the untreated. Plasma doses: (1) $7x10^{15}$ at.cm^{-3}.sec; (2)$1.4x10^{16}$ at.cm^{-3}.sec. Improvement in dyeing after oxygen plasma treatment compared with the untreated. Plasma doses: (1)$6x10^{15}$ at.cm^{-3}.sec; (2)$3x10^{16}$ at.cm^{-3}.sec.

treatment with large doses reduces the cystine sulphur content and consequently increases the oxidized sulphur content (see last column in Table 6.1). This process facilitates a transcellular diffusion, in addition to the usual intercellular dye diffusion [86], which accelerates the dye absorption by the fibre, and thus shortens the dye process. Another mechanism, which could be responsible for the printing and dyeing quality improvements, is that the endocuticle and interscale cell membrane complex are modified after extended treatment and thus further facilitate the diffusion of the dye [87].

The felting shrinkage of wool was tested using an ISO (International Standardisation Organization) 5A washing cycle. The test was performed on all samples after the first washing cycle. The felting shrinkages after various plasma treatments are shown in Table 6.3. The shrinkage of untreated wool is ~50 %.

Table 6.3 Felting shrinkage (%) of wool after plasma treatment.

Gases	O_2				Air
Plasma doses 10^{14} at.cm^{-3}.sec	4.9	6.5	60	140	48
Felting shrinkage %	32	10	9	8	7

It can be seen that the felting shrinkage has been greatly reduced by the plasma treatment. With treatment doses above saturation level, the felting shrinkage is reduced 5-fold, to 10% or less but nearly constant. Similar improvements in felting shrinkage have been found in samples treated with an air plasma. Felting shrinkage of wool results mainly from the differences in directional structure of the scale on the surface of the fibre (see section 1.2.1). Plasma treatment ~~could~~ seems to lead

to an increase in single-fibre surface friction [8] and thus reduces the differential friction effect.

6.3 STUDIES OF WOOL SURFACE PROPERTIES USING SELECTIVELY CONTROLLED PLASMAS

As shown above, an oxygen plasma has a great effect on the wool surface. In order to investigate the roles played by the various plasma constituents in this modification, some experiments have been performed using specially controlled conditions. One is to control the flow of the various plasma constituents from the plasma source to the reaction chamber using baffles. The other is by using other plasma gases, i.e. dry air, argon and hydrogen, which all produce plasma containing charged particles and uv radiation but have quite different chemical compositions.

6.3.1 Use of Baffles

In plasma processing, energy can be transferred from plasma to sample surface by neutral particle fluxes, optical radiation, and charged particle fluxes.

As described in Chapter 3, two baffles were used in order to distinguish the effects of charged particles (electrons and ions) and/or radiation (uv photons) from those of reactive neutrals (O, O_2^*) formed in the oxygen plasma. One is the mesh which does greatly reduce the charged particle fluxes from the plasma source into the reaction chamber (see Chapter 3); the other is the mesh plus a loose-fitting glass plate which blocks both the charged particles and uv radiation without greatly affecting the neutral particle fluxes from the source to the chamber (see Chapter 4).

The effects on the surface energy of the samples treated under these special arrangements are summarised in Table 6.4, compared with the experimental conditions without the baffles.

Table 6.4 The changes in surface energy with different baffles.

Plasma doses ($at.cm^{-3}.sec$)	Baffles	$\triangle W$ (mJ/m^2)
$5.5x10^{14}$ (saturation)	none	58.9 ± 1.6
	mesh	58.8 ± 1.8
	mesh+glass	57.1 ± 3.0
$1.12x10^{14}$ (unsaturated)	none	15.2 ± 1.0
	mesh	13.6 ± 0.6
	mesh+glass	7.7 ± 1.9

From the table, it can be seen that the wool surface energy increase $\triangle W$ was hardly changed either with the mesh or with the mesh and glass when the plasma dose exceeded the saturation level. However, when the plasma dose was at a level below that required for saturation, a significant reduction in $\triangle W$ was found with the mesh and glass present, but little change was observed with only the mesh.

From these experiments, it can be concluded that the reactive neutrals in oxygen plasma play the most important role in wool surface modifications when the plasma doses are greater than the saturation level. For plasma doses below this, the similar effects observed with and without the mesh further suggest the charged particles are not important in the surface modification process. However, with both the mesh and glass present the efficiency of surface modification was reduced,

indicating that the role of uv radiation cannot be ignored in cases of low plasma doses.

What role is played by uv radiation in the wool surface modification? To investigate this question, further experiments were carried out using Electron Paramagnetic Resonance (EPR) spectroscopy. EPR is a sensitive technique for detecting free radicals [88]. Direct evidence for the formation of free radicals on the wool surface caused by uv radiation in the oxygen plasma has been obtained by EPR. In order to separate the effects due to other plasma components on the wool surface, wool samples were placed inside EPR quartz tubes (4mm o.d.) and vacuum-sealed (10^{-6}mbar). Therefore, the wool was not in contact with the plasma when the tube with its sample was in the plasma, but was exposed to uv radiation at wavelengths where the quartz is transparent, i.e. $\lambda \geq$200nm (possible effects of visible and infrared radiation will be discussed in section 6.4). Vacuum-sealed samples provide a better environment for the detection of free radicals because in general they react with air. During EPR measurements, the microwave power was 20 mW and a 100 kHz modulation with a modulation amplitude of 0.2 mT was used.

Typical X-band ESR spectra are shown in Fig.6.7. There is no detectable signal for the untreated sample (see Fig.6.7(c)). Fig.6.7(a) is the ESR spectrum measured immediately after a 30 minute plasma exposure under discharge conditions, p=0.03mb and P=100W. As seen, there is an intense and broad ESR signal with some fine structure. The peak-to-peak linewidth exceeds 70mT. Such an intense and broad signal indicates that there are a large number of free radicals present on the wool surface. It is believed that the spin-spin interaction is mainly responsible for the broadening of the signal [89]. The free radicals were found to

be relatively stable in air. Sample tubes were cut allowing the wool sample to be exposed to air for a certain period of time and then its EPR spectrum measured

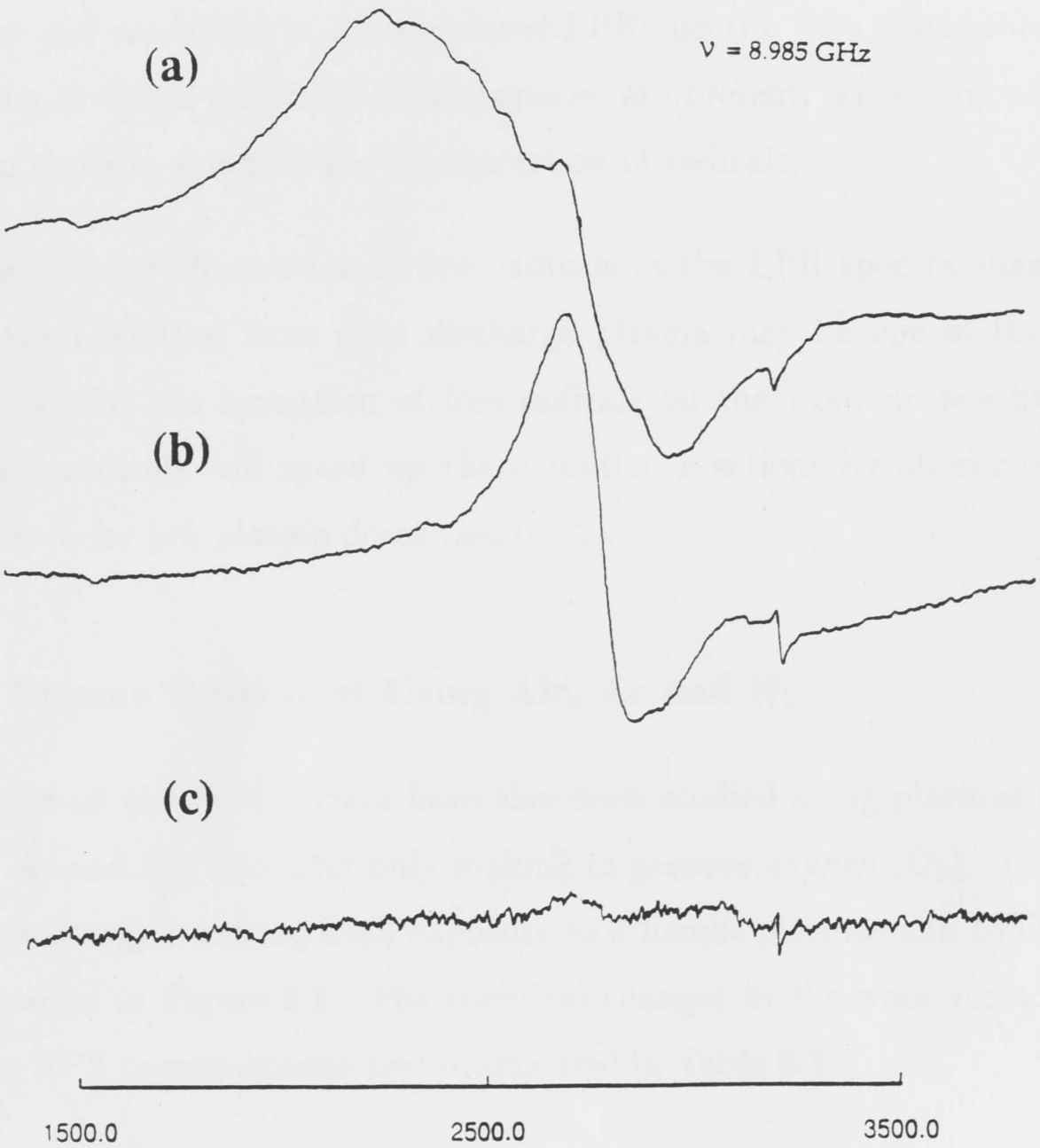

Fig.6.7 X-band EPR spectra for the sample exposed to an oxygen plasma 30min (p=0.03mbar; P=100W): (a) measured immediately after the plasma treatment; (b) the same sample but being exposed to air for one hour. (c) untreated sample. The spectra were recorded at the same conditions expect for a difference in the receiver gain ((a) 630; (b) 1000; (c) 2500 in arb.units).

again. The spectrum in Fig.6.7(b) was recorded on the same sample as used for Fig.6.7(a) but after it was exposed to air for one hour, showing that there were still a considerable amount of free radicals. Because of a lack of detailed fine structure and resolution in the measured EPR spectra, it is impossible to know how many or which particular radical species are present. Therefore, no attempt has been made to quantify the concentration of radicals.

Nevertheless, the observation of free radicals in the EPR spectra suggests that uv radiation emitted from glow discharge plasma may be one of the primary mechanisms for the formation of free radicals on the wool surface by plasma. These free radicals will speed up the oxidation reactions by atomic oxygen on wool surface for low plasma doses (see 6.4.2).

6.3.2 Plasma Treatment Using Air, Ar and H_2

The effects on the wool surface have also been studied using plasmas formed in dry air, Ar and H_2, also after only soaking in gaseous oxygen (O_2). The changes of surface energy resulting from exposure to different plasmas and to O_2 soaking are presented in Figure 6.8. The chemical changes in the wool surface derived from the XPS measurements are summarised in Table 6.5.

From Fig.6.8, it is clear that nothing happens to the wool surface when the sample was soaked in O_2 gas. From the figure and the table, it can be seen that exposure to H_2 plasma resulted in no measurable changes to the surface energy although there are both abundant charged particles and intense uv radiation emanating from the plasma. On the other hand, a significant effect is observed with air, although less than that with pure oxygen, consistent with the composition of air. The absorption spectrum for a discharge in air shows that its 20% oxygen constituent is about 29% dissociated at 0.1mb and 46% at 0.03mb, while the

metastable molecular oxygen concentration is too low to measure (see Chapter 4).

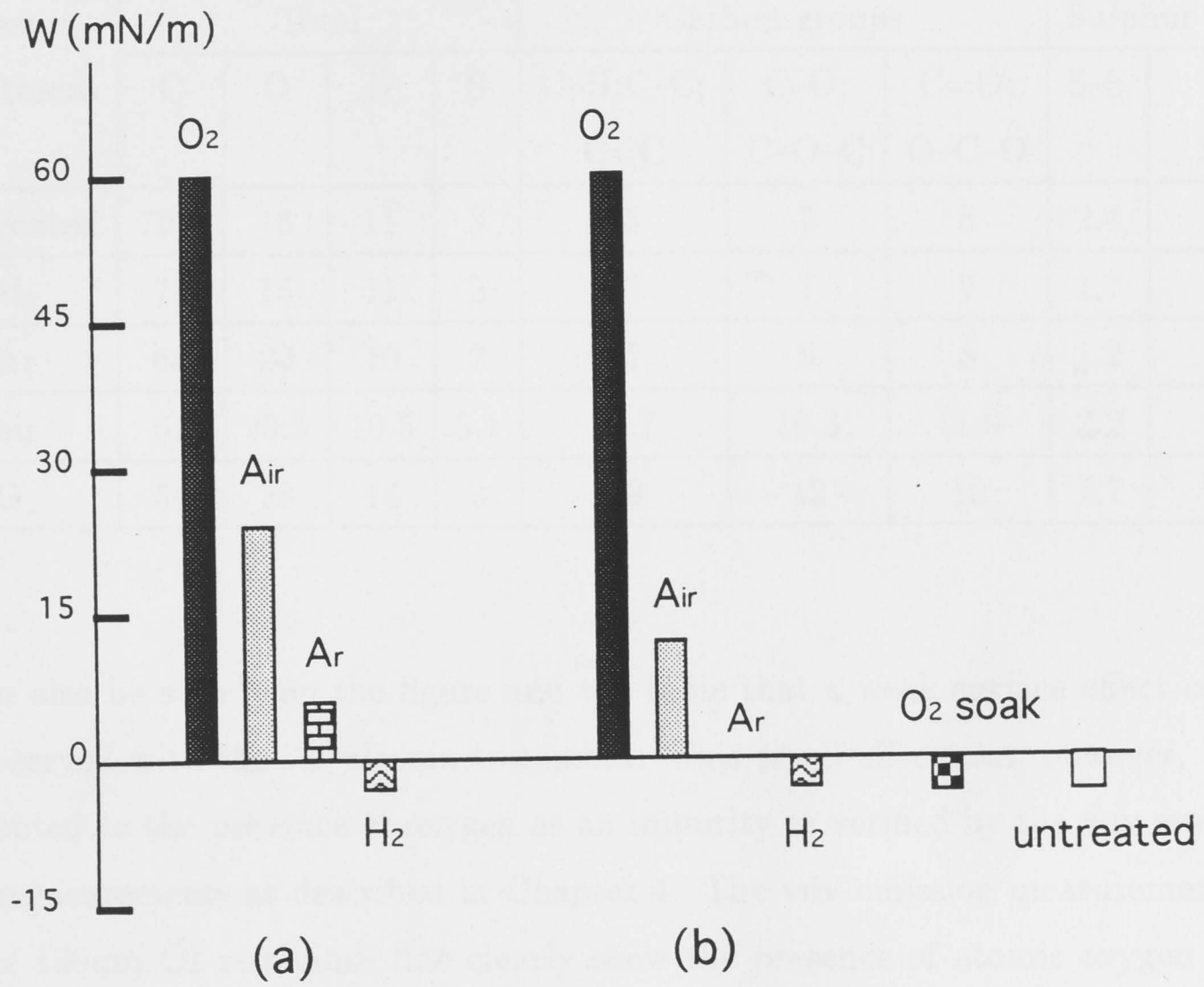

Fig.6.8 $\triangle$W with different plasma gases compared with the untreated wool, under plasma conditions: (a) 0.1mbar/100W/5sec; (b) 0.03mbar/100W/1sec.

Table 6.5 Changes in surface chemical composition measured by XPS for untreated sample and the samples treated with H_2, Ar, and O_2 gases under the discharge conditions (0.005mbar/200W/60s) and with dry air (0.1mbar/100W/5s).

Plasma treatment	Atomic concentration % (± 0.10)								
	Total				Carbon groups			Sulphur groups	
	C	O	N	S	C–H;C–C; C=C	C–O; C–O–C	C=O; O–C–O	S–S	SO_2; SO_3H
Untreated	70.4	16	11	3	55	7	8	2.4	0.4
H_2	71	15	11	2	57	7	7	1.7	0.4
Ar	68	20	10	2	51	9	8	1.2	0.3
air	61	25.5	10.5	3.1	38.7	10.3	11.9	2.2	0.9
O_2	54	28	14	3	30	12	12	1.7	0.9

It can also be seen from the figure and the table that a weak surface effect can be observed with the Ar plasma treatment. This small effect can, however, be attributed to the presence of oxygen as an impurity as verified by the vuv emission measurements as described in Chapter 4. The vuv emission measurements at the 130nm OI resonance line clearly show the presence of atomic oxygen in the argon plasma both with and without wool samples. When a 225 cm^2 wool sample was present in the chamber during an argon discharge (0.03mbar/200W), the intensity of OI in the chamber increased about three times above the value obtained in the absence of a sample. Fig.6.9 shows some physical changes which occur on the wool surface using argon with the same plasma treatment condition as used for Figure 6.5(b), displaying a much weaker etching than that observed with oxygen (see Fig.6.5(b)). Small differences can be seen with the scale edges becoming more clearly defined and some longitudinal striation showing faintly on

the surface. This weaker effect correlates well with the minute amount of atomic oxygen present in the argon plasma.

Fig.6.9 SEM for sample treated by Ar plasma (0.1mbar/300W/10min).

Although there also is some oxygen present as an impurity in the H_2 discharge, which came either from residual gas or the wool, the treatment by hydrogen plasma showed no observable chemical changes when compared with untreated samples. This is most likely due to the removal of O by the rapid formation of OH in the discharge through the gas phase reaction of H + O = OH.

These experiments further support the conclusion that it is the reactive neutrals in oxygen plasma which play the most important role in wool surface modifications since there is no surface effect with the hydrogen plasmas, and the surface effects are very weak for treatments by argon plasmas despite there being abundant charged particles and intense uv radiation emanating from these plasmas. The result from the air discharge also suggests that the metastable molecular oxygen seems to be insignificant in wool surface modification.

6.4 REACTION MECHANISMS

In this section, we first summarise the results obtained in the previous sections. Further discussion is made in order to form a more coherent picture about the wool processing in the oxygen plasmas. Finally, a reaction model is presented.

6.4.1 Summary and Discussion

First of all, the experiments carried out under the arrangements using baffles, and using other plasma gases have conclusively shown that the charged particles (ions and electrons) from the plasma have little direct effect on the wool surface. The support to this conclusion can be seen from Fig.6.10, which shows the change of surface energy as a function of the product of the ion density and exposed time. It is clear that there is no correlation between $\triangle$W and the ion dose (N_i x time). Therefore, any kinetic energy carried by the charged particles is most likely to be dissipated on the wool surface as heat and sputtering which do not involve any chemical reactions.

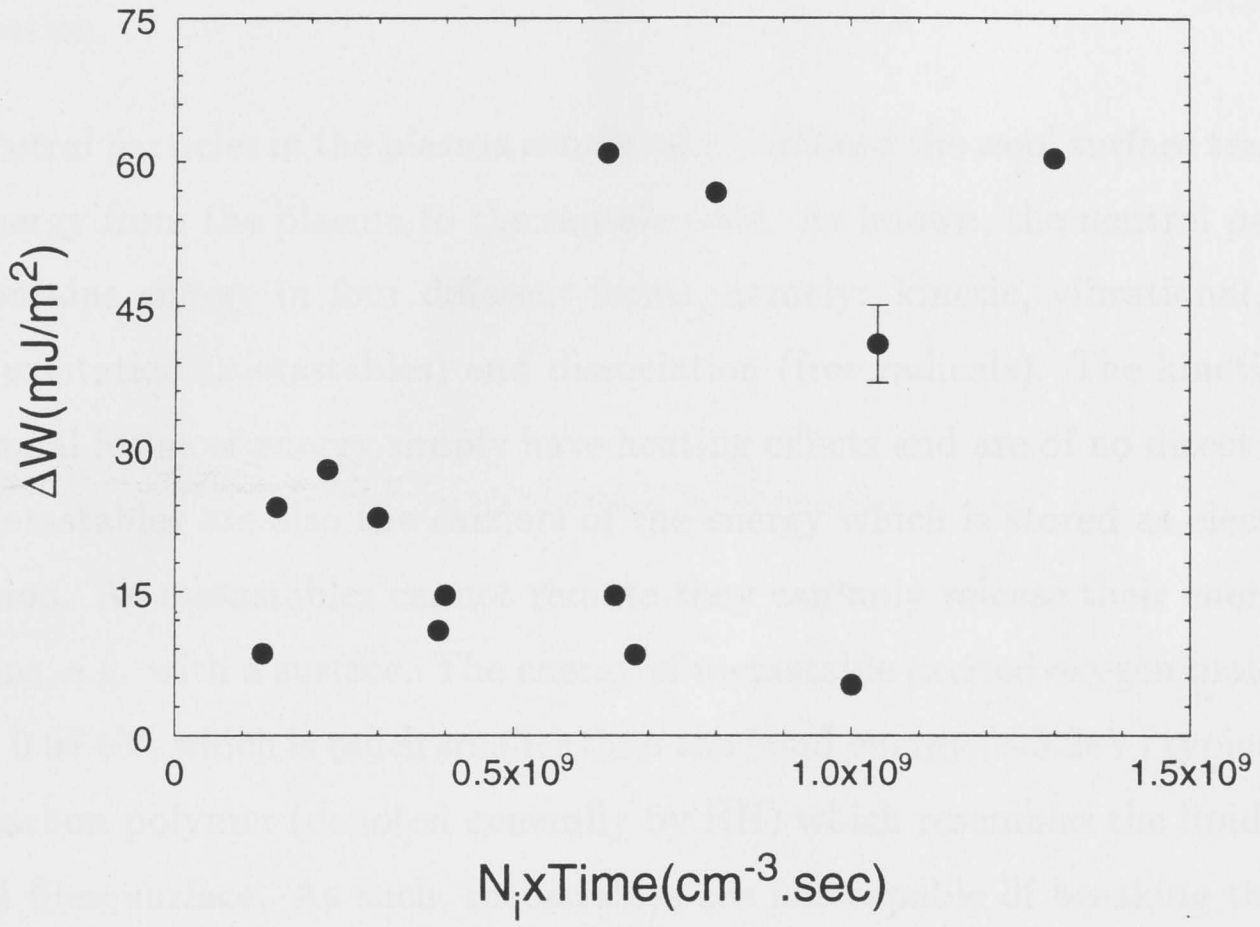

Fig.6.10 Dependence of $\triangle$W on the dose of ions.

The radiation emitted by plasma spans a wide spectral range extending from infrared, through visible to vacuum ultraviolet (vuv). For polymers, the radiation in the visible range is only weakly absorbed. The infrared can be strongly absorbed but is dissipated as heat [5]. Therefore, radiation in both infrared and visible ranges is likely to be unimportant in wool surface modification. However, some evidence has been obtained about the role played by uv radiation at low plasma doses, as shown in Table 6.4, by the significant difference in $\triangle$W between the samples treated with and without the mesh and glass plate (see 6.3.1). Electron Spin Resonance spectra have also shown intense signals arising from free radicals

on samples irradiated only by the uv plasma component (see 6.3.1) although the nature of these free radicals could not be identified due to the lack of spectral information.

The neutral particles in the plasma continually bombard the wool surface transferring energy from the plasma to the sample wool. As known, the neutral particle flux contains energy in four different forms, namely: kinetic, vibrational, electronic excitation (metastables) and dissociation (free radicals). The kinetic and vibrational forms of energy simply have heating effects and are of no direct interest. Metastables are also the carriers of the energy which is stored as electronic excitation. As metastables cannot radiate they can only release their energy by collisions, e.g. with a surface. The energy of metastable excited oxygen molecules (O_2^*) is 0.97 eV, which is much smaller than the bond energy ($\sim$3.2eV) typical of a hydrocarbon polymer (denoted generally by RH) which resembles the lipid layer of wool fibre surface. As such, metastables are not capable of breaking the RH bonds simply from the viewpoint of available energy. Thus, we should expect the role of O_2^* to be insignificant, as already deduced from experiments using air plasmas. Fig.6.11, which shows the relationship between the surface energy changes $\triangle$W and the dose of the metastable O_2^*, further supports this view. It can be seen that there is no clear correlation between $\triangle$W and the dose of $N[O_2^*]$ x time. This is further supported by the studies of felting shrinkage for samples treated with the oxygen plasma and dry air. Table 6.3 shows that for the same plasma condition, the oxygen plasma which contains a significant amount of metastable O_2^* produced a felting shrinkage improvement very similar to one observed with the dry air plasma, in which the metastable O_2^* content was negligible (see 6.3.2).

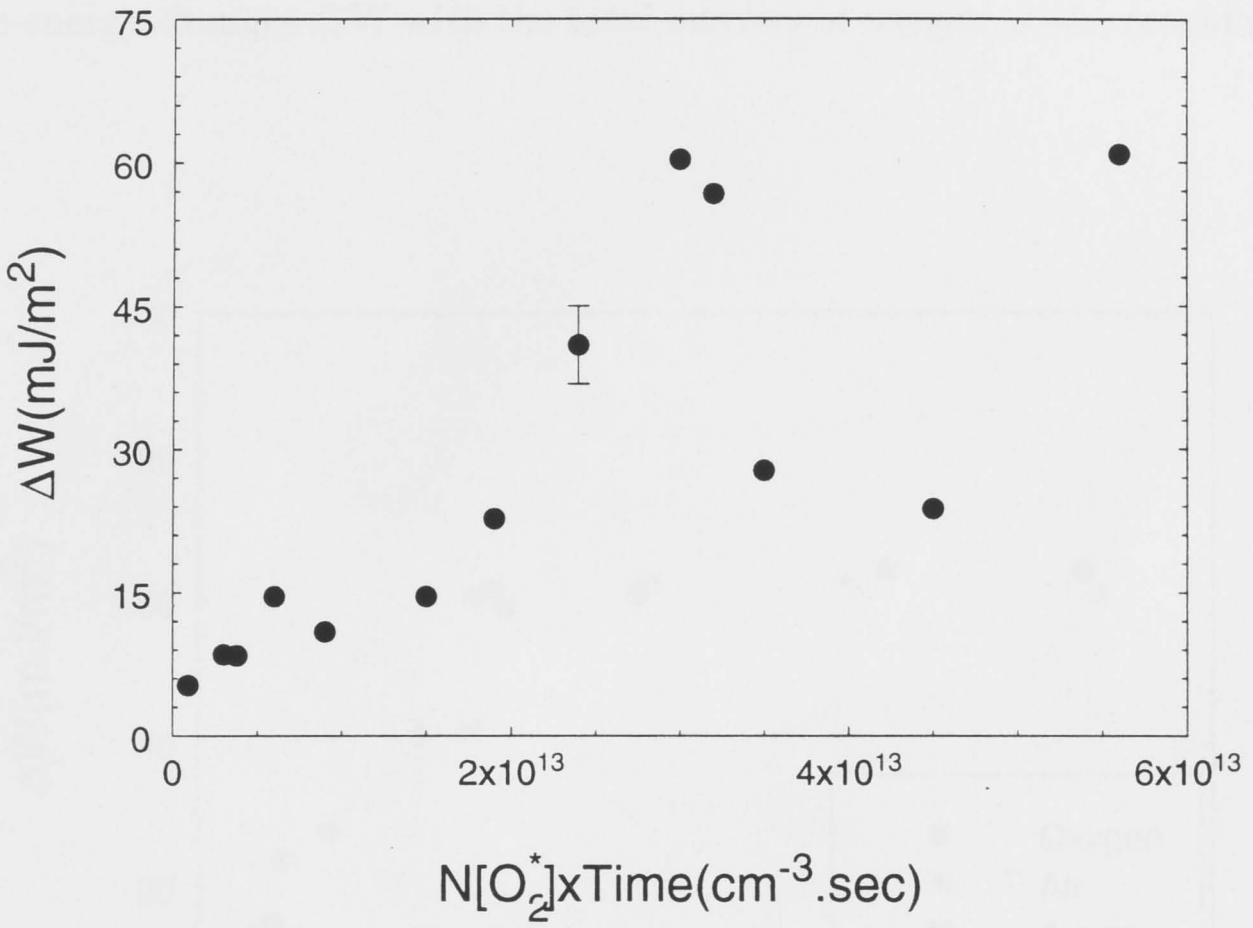

Fig.6.11 Dependence of $\triangle$W on the dose of the metastable O_2^*.

The dissociation energy of the atomic oxygen free radical (see Chapter 5, Eq.(5.4)) is believed to be the most important source of energy for chemical reactions which occur on the wool surface during oxygen plasma treatment. It can be lost through surface chemical reactions such as abstraction, addition, and oxidation as well as through heating caused by free-radical recombination on the surface of the wool. The atomic oxygen concentration has been described in detail in Chapter 4, and its dependence on RF power and the gas pressure shown in Figures 4.11 and 4.6. When compared, respectively, with Figures 6.1 and 6.3, a clear correlation is demonstrated between the atomic oxygen concentration and the increase in

surface energy. However, the most clear-cut relation, and thus one which points to the most likely cause of the observed changes, can be seen by comparing the surface energy changes $\triangle$W with the total number of oxygen atoms reaching unit

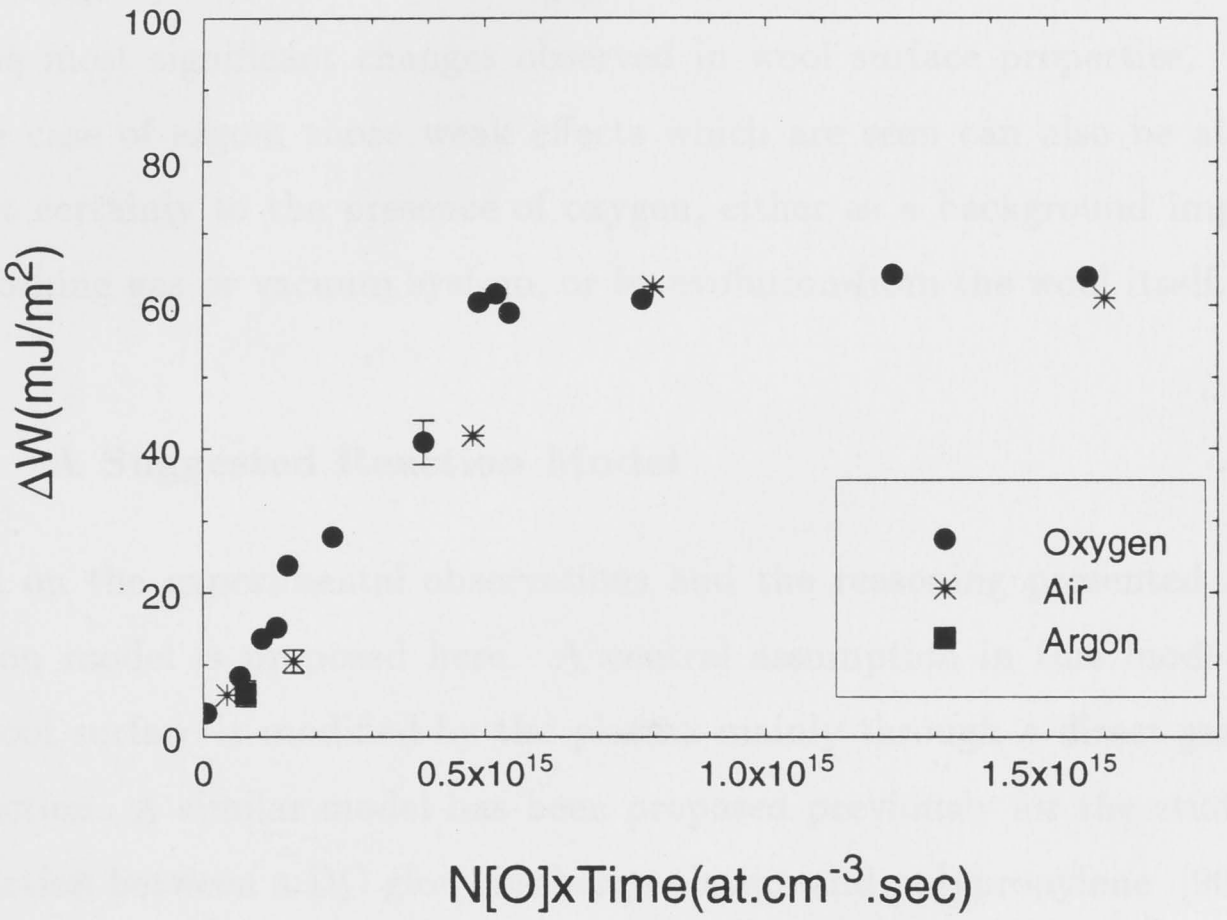

Fig.6.12 Dependence of $\triangle$W on the dose of atomic oxygen for all discharge conditions.

area of the surface which is proportional (assuming constant gas temperature) to the product of the atomic oxygen concentration N[O] and the exposure time t. We find that all the available data can be represented on the single plot shown in Fig.6.12, which includes results for the entire range of discharge conditions ($50 \leq P \leq 300$W, $0.005 \leq p \leq 0.1$mb, $0.1 \leq t \leq 600$sec) formed in oxygen, dry air,

as well as argon (the value of $N[O]$ for argon was estimated from the 130nm line emission). The progressive increase and saturation of the surface energy at an appropriate 'dose' show a clear correlation with the amount of atomic oxygen reaching the wool.

The results obtained and summarized above are consistent with a picture that in an oxygen plasma the atomic oxygen is the main reactive species responsible for the most significant changes observed in wool surface properties. Further, in the case of argon, those weak effects which are seen can also be attributed almost certainly to the presence of oxygen, either as a background impurity in the working gas or vacuum system, or by evolution from the wool itself.

6.4.2 A Suggested Reaction Model

Based on the experimental observations and the reasoning presented above, a reaction model is proposed here. A central assumption in this model is that the wool surface is modified by the plasma mainly through a direct gas-surface interaction. A similar model has been proposed previously for the study of the interaction between a DC glow-discharge plasma and polypropylene [90].

The gas-surface interaction may be considered as a three-stage process. The first stage involves the production of various plasma species and uv radiation in the discharge through electron collisions (for details, see Chapter 5). The second stage involves the interaction of reactive species which have been identified to be mainly the atomic oxygen and uv irradiation with the wool surface. This results in the formation of free radicals on the wool surface leading to the desorption of certain reaction products (e.g. H_2O, CO_2...) into the gas phase, accompanied by the reaction of the free radicals and the absorption of the reaction products into the wool surface. This is shown schematically in Fig.6.13.

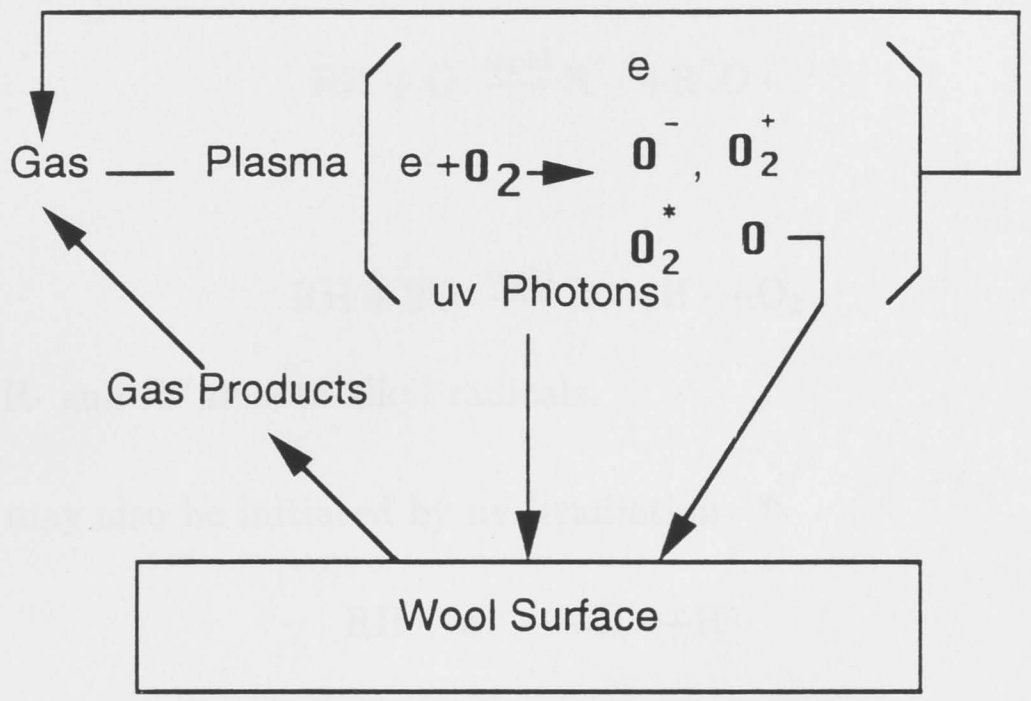

Fig.6.13 A schematic diagram for the gas-surface interaction process.

The dominant role of oxygen is seen in the most significant chemical changes shown by the XPS results, i.e. the increase of the O at the expense of C. It was shown from reaction rate calculations (Chapter 5) that under our discharge conditions the main process for producing the active oxygen free radical (O·) is by direct collisional dissociation by electrons,

$$O_2 + e \rightarrow O\cdot + O\cdot + e$$

The lipid surface layer of wool fibre is believed to be attacked mainly by the atomic oxygen free radicals (O·). Oxidation is initiated by O· through the following

reaction channels:

$$RH + O\cdot \xrightarrow{\text{rapid}} R\cdot + OH\cdot \tag{6.1}$$

$$RH + O\cdot \xrightarrow{\text{rapid}} R'\cdot + R''O\cdot \tag{6.2}$$

$$RH + 2O\cdot \xrightarrow{\text{rapid}} R\cdot + H\cdot + O_2 \tag{6.3}$$

where the R· and R·′ denote alkyl radicals.

Oxidation may also be initiated by uv irradiation

$$RH + uv \longrightarrow R\cdot + H\cdot \tag{6.4}$$

Reactions (6.1) and (6.2) are the oxygen-abstraction reaction. Reactions (6.3) and (6.4) are bond-dissociation reactions which are driven, respectively, by the absorption of the dissociation energy of O_2 (6eV), and the uv radiation (3-6eV). Both energy sources have ample energy to produce break down of the RH bonds which are typically about 3.2eV. It has been shown in this study that the reaction (6.4) is quite important for low plasma doses.

Once oxidation is initiated, the ensuing reactions are similar to those of thermal oxidation of hydrocarbon polymers. The dominant oxidation reactions for wool are as follows:

$$R\cdot + O\cdot \longrightarrow RO\cdot \tag{6.5}$$

$$R\cdot + 2O\cdot \longrightarrow ROO\cdot \tag{6.6}$$

$$ROO\cdot + R'H \longrightarrow R'\cdot + ROOH \tag{6.7}$$

$$2ROOH \longrightarrow R{=}O + H_2O + ROO\cdot \tag{6.8}$$

In this way some new chemical bonds, such as those of the oxygen-containing groups which have been detected by XPS, are formed on the wool surface, rendering the hydrophobic surface hydrophilic, thus increasing the wool surface energy and changing the properties of the wool surface.

7

CONCLUSION

From this study, the plasma processing has shown its special advantages for modification of wool surface. Exploratory experiments have clearly demonstrated a dramatic increase in wool surface energy and a great improvement in the surface properties of printing, dyeing, and shrink-proofing after oxygen plasma treatment, in which not only the degree of surface modification can be greater and achieved without deleterious effects when compared with the wet chemical treatment, but also does not affect the bulk properties of the wool. Furthermore, plasma processes can be easily controlled, with safer working conditions, through various independent parameters such as gas pressure, discharge power and exposure time. In fact, the discharge power needed is so low, and the treatment time so short that it is of potentially great economic benefit. This treatment also represents a solution to the environmental problems associated with wet chemical treatment. All of these imply a potential for a commercial process for the plasma treatment of wool.

From the thorough experimental investigation of the behaviour of various plasma components and their effects on wool surface properties, the following has been found:

- the modification effects are not caused by charged particles ;
- molecular oxygen itself has no effect on wool surface;

- the role of metastable excited molecular oxygen appears small;
- the remarkably rapid surface modifications are due to the effects of the chemically active species (atomic oxygen)
- and the ultraviolet radiation from the plasma speeds up the process, especially at low treatment doses.

Although electrons and ions have no direct effect on the wool surface modification, the plasma produces atomic oxygen by electron-neutral collisions. As the chemically active species are created by electron collisions with the neutral particles through ionization, excitation, and dissociation, it is important to design a suitable plasma source to obtain a suitable electron energy distribution for creating more atomic oxygen. This can also be seen from the theoretical model developed successfully for the kinetics of chemical reactions occurring in the plasma and the qualitative reaction model between wool and plasma. An oxygen glow discharge is used here in order to obtain more atomic oxygen by electron collisional dissociation. The separation of the reaction chamber from the plasma source is to allow a high concentration of reactive species without the presence of any high electromagnetic fields at the wool and allow isolation from excessive ultra-violet radiation and bombardment by charged particles if necessary, which can be significant for industrial application. Furthermore, this study has obtained a very efficient enhancement of the surface energy and achieved a specific level of surface change through the control of the experimental parameters which correspond to known plasma doses. All of these studies will undoubtedly provide a path to speed up the progress of further research and the development of an industrially viable process.

However, it might be better to say that it is a prologue of this research rather than an epilogue to my thesis. Although many studies on wool pre-treatment in both experiment and theory have been carried out during my three-year Ph.D study,

there is still much work to be done. Especially, in order to add value to woollen garments in industrial treatments, plasma polymerization as well as its reaction process would be the main focus of subsequent research efforts to further improve the shrinkage resistance, durable stain repellence and print uptake of wool fibre and fabric. Different suitable monomers can be selected to graft onto the wool surface in order to obtain the desired surface for enhancing colour life. It is to be hoped that an overall chemical dynamic reaction model could be developed soon to enable the first steps to be taken towards industrial application of plasmas to wool treatment.

REFERENCES

[1] Witold Rakowski, *Melliand Textiberichte*, **70**, 780(1989).

[2] R.W.Crompton, M.Hayashi *et al*, *Gaseous Electronics and its Applications*, KTK Scientific Publishers, 1991.

[3] G.S.Mathad and D.W.Hess, *Plasma Processing*, The Electrochemical Society, 1990.

[4] D.C.Schram, Th.H.J.Bisschops *et al*, *Plasma Physics and Controlled Fusion*, **29**(10A), 1353-1364(1987).

[5] J.R.Hollahan, A.T.Bell, *Techniques and Applications of Plasma Chemistry*, John Wiley & Sons, New York, 1974.

[6] A.W.Adamson, *Physical Chemistry of Surfaces*, Interscience, New York, 1960.

[7] R.J.Ward, H.A.Willis *et al*, *Textile Research Journal*, **63**(6), 362-368(1993).

[8] W.J.Thorsen and R.Y.Kodani, *Textile Research Journal*, 36, 651-659(July 1966).

[9] W.J.Thorsen, *Textile Research Journal*, 38, 644-650 (June 1968).

[10] W.J.Thorsen and R.C.Landwehr, *Textile Research Journal*, 40, 688-695 (August 1970).

[11] A.E.Pavlath and R.F.Slater, *Applied Polymer Symposium* **No.**18,1317-1324(1971).

[12] K.S.Lee and A.E.Pavlath, *Journal of Polymer Science: Polymer Chemistry Edition*, *Vol.***12**, 2087-2090(1974).

[13] T.Klausen, Private communication(1993).

[14] R.C.Marshall, J.M.Gillespie *et al*, *Proceedings of the 7th International Wool Textile Research Conference*, Tokyo **2**, 36-38(1985).

[15] L.Wagner, M.Giesen and H.Zahn, *Colloid Polym.Sci.*, **261**, 365-369(1983).

[16] K.R.Makinson, *Shrinkproofing of Wool, 1st ed.*, Marcel Dekker,Inc,New York,1979.

[17] J.H.Bradbury, *Adv. Protein Chem.*,**27**,111-211(1973) .

[18] J.A.M◡Laren and B.Milligan, *Wool Science. The Chemical Reactivity of the Wool Fibre* Science Press, Marrickville, 1981.

[19] H.A.W.S.John, *Ph.D Thesis*, The University of Queensland(199 3).

[20] J.D.Leeder and J.A.Rippon, *J.Soc.Dyers Colour*, **10(1)**, 11-16(1985).

[21] J.H.Brooks and M.S.Rahman, *Text.Res.J.*, **56(3)**, (1986), 164-171

[22] A.R.Bean, Private communication(1995)

[23] A.J.Perry, D.Vender, and R.W.Boswell, *J.Vac.Sci.Technol.* **B 9(2)**,310-317(1991).

[24] R.W.Boswell, A.J.Perry, and M.Emami, *J.Vac.Sci.Technol.* **A 7(6)**,3345-3350(1989).

[25] R.W.Boswell and R.K.Porteous, *Appl.Phys.Lett.* **50(1 7)**,1130-1132(1987).

[26] B.Eliasson, and U.Kogelschatz, *IEEE Transactions on Plasma Science, Vol.***19(6)**, 1063-1077(1991).

[27] P.M.Chung, L.Talbot, K.J.Touryan, *Electric Probes in Stationary and Flowing Plasmas: Theory and Application*, Springer-Verlag Berlin, 1975.

[28] James A.R.Samson, *Techniques of Vacuum Ultraviolet Spectroscopy*, John Wiley & Sons,Inc., New York.London.Sydney, 1967.

[29] IWTO Specification of Test Methods, *Test IWTO-10-66(E)*, Internation Wool Textile Organisation, 1966.

[30] Y-L.Hsieh, B.Yu, *Textile Research Journal*, **62(11)**, 677-685(1992).

[31] A.Granier, S.Pasquiers, C.Boisse-Laporte *et al*, *J. Phys.D: Appl.Phys.* **22**, 1487-1496(1989).

[32] B.R.Soller and R.F.Shuman, *J.Electrochem.Soc.*, 131(6), 1353-1356 (1984).

[33] A.von Engel, *Ionized Gases*, Clarendon press,Oxford, 1965.

[34] B.M.Smirnov, *Physics of Weakly Ionized Gases*, Mir Publishers Moscow, 1981.

[35] C.Charles, Private communication(1994).

[36] C.Charles, *J.Vac.Sci.Technol.*, **A 10(2)**,398-403(1992).

[37] C.Charles, R.W.Boswell *et al*, *J.Vac.Sci.Technol.*, **A 9(3)**, 661-663 (1991).

[38] Francis F.Chen, *Introduction to Plasma Physics and Controlled Fusion, 2nd Ed*, Plenum Press, New York and London, 1974.

[39] M.J.Druyvesteyn, *Z.Phys.*,**64**,781(1930).

[40] H.W.Rundle, D.R.Clark, and J.M.Deckers, *Can.J.Phys.*, **51**,144(1973).

[41] R.N.Franklin,*Plasma Phenomena in Gas Discharges*, Clarendon Press, Oxford, 1976.

[42] J.M.Cook and Brent W.Benson, *J.Electrochem.Soc.*, **130(12)**, 2459(1983).

[43] F.Kaufman, *Progress in Reaction Kinetics*, Pergamon,New York, *Vol 1*, 1961

[44] M.Brake, J.Hinkle, J.Asmussen, M.Hawley and R.Kerber, *Plasma Chem. Plasma Process.*,**3**,63(1983).

[45] P.Kocain, *Phys. Lett.* **73**,17(1979).

[46] L.F.Di Mauro, Richard A. Gottscho and Terry A. Miller, *J.Appl.Phys.*,**56(7)**, 2007(1984).

[47] W.Bischel, B.Perry and C.Crosley, *Chem.Phys.Lett.*, **82**, 85(1981).

[48] J.W.Coburn and M.Chen, *J.Appl.Phys.*,**51**,3134(1980).

[49] J.P.Booth, O.Joubert, and J.Pelletier, *J.Appl.Phys.* **69(2)**, 618(1991).

[50] J.L.Dumas and B.Garnier, *J.Chem.Phys.*, **72**,(1975),44

[51] A.N.Vassilieva, I.A.Grishna, K.S.Klopovskii, A.S.Kovalev, A.P.Osipov, A.T.Rakhimov, and T.V.Rakkhimova, *Sov.J.Plasma Phys.* **11**, 130(1985).

[52] Allan C.G.Mitchell, and Mark W.Zemansky, *Resonance Radiation and Excited Atoms*, Cambridge University Press, 1971.

[53] G.Gousset, P.Panafieu, M.Touzeau and M.Vialle, *Plasma Chem. Plasma Process.*, **7**, 409(1987).

[54] T.Cox, V.Deshmukh, D.Hope, A.Hydes, N.Braithwaite and N.Benjamin, *J.Phys.D*, **20**, 820(1987).

[55] J.Mckillop, J.C.Forster and W.M.Holber, *J.Vac.Sci. Technol.*,**A7**, 908(1989).

[56] R.E.Walkup, K.L.Saenger and G.S.Selwyn, *J.Chem.Phys.* **84(5)**, 2668-2674(1986).

[57] E.J.H.Collart, J.A.G.Baggerman, and R.J.Visser, *J.Appl. Phys.*,**70(10)**, 5278(1991).

[58] S.M.Hamberger, *Ph.D Thesis*, University of London, (1966).

[59] A.P.Thorne, *Spectrophysics*, London,Chapman and Hall, 1988 .

[60] P.C.Hill, *Ph.D Thesis*, Australian National University, (1991).

[61] P.G.Wilkinson and E.T.Byram, *Applied Optics*, **4**, 581(1965).

[62] H.Sabadil and S.Pfau, *Plasma Chem.Plasma Proc.* **5**, 67(1985).

[63] G.Gousset, M.Touzeau, M.Vialle, and C.M.Ferreira, *Plasma Chem. Plasma Proc., vol.9, No.***2**, 189-206(1989).

[64] I.J.Donnelly and E.K.Rose,*Aust.J.Phys.*,**43**, 45(1990).

[65] Yukimi Ichikawa and Richard L.C.Wu, Teruo Kaneda, *J. Appl.Phys.* **67(1)**, 108(1989).

[66] L.Laska, K.Masek, and T.Ruzicka, *Czech.J.Phys.*, **B 29** , 498(1979).

[67] K.Masek and L.Laska, *Czech.J.Phys.* **B 30**,805(1980).

[68] G.Glockler and S.C.Lind, *The Electrochemistry of Gases and other Dielectrics*, John Wiley, New York, 1939.

[69] S.N.Foner and R.L.Hudson, *J.Chem.Phys.*, **25**, 601(1956).

[70] H.Dreicer, *Phys.Rev.*, **117**, 343(1960).

[71] P.Pace and M.Lacombe, *IEEE J.Quant.El.*,**QE-14(4)**, 263-274(1978).

[72] C.Charles and R.W.Boswell, to be published in *J.Vac.Sci. Technol.A*, (Jul/Aug 1995).

[73] D.Rapp and P.Englander-Golden, *J.Chem.Phys.*,**43(5)**, 1464-1479(1965).

[74] P.E.Luft, *JILA Information Center Report No 14*, University of Colorado, Boulder, Colorado,1975.

[75] A.Konishi, K.Wakiya, M.Yamamoto, and H.Suzuki, *J. Phys. Soc.Japan*, **29**, 526(1970).

[76] D.Rapp and D.D.Briglia, *J.Chem.Phys.*, **43(5)**, 1480-1489(1965).

[77] C.Wills, A.Boyd, M.young, and D.Armstrong, *Can.J.Chem.*, **48**, 1505-1514(1970).

[78] G.Fournier, *Reactive dans les Plasmas*, Paris, pp297-372, 1983.

[79] K.Masek, L.Laska and T. Ruzicka, *Czech.J.Phys* **B28**, 1321-1334(1978).

[80] F.C.Fehsenfeld, E.E.Ferguson, and A.L.Schmeltekopf, *J.Chem.Phys.*, **45**, 1844(1966).

[81] J.L.Delcroix, *Plasma Physics Vol.***2**, John Wiley & Sons, New York, 1968.

[82] S.C.Brown, *Introduction to Electrical Discharges in Gases*, John Wiley & Sons, New York, 1966.

[83] A.A.Frimer, *Singlet Oxygen, vol.***I**, CRC Press, Boca Raton, Fla., 1985.

[84] C.Lee,V.Vahedi, and M.A.Lieberman, 1993 Gaseas Electronic Conferrence, Montreal Canada.

[85] M.A.Lieberman and A.J.Lichtenberg, *Principles of Plasma Discharges and Materials Processing*, John Wiley & Sons, Inc., New York, 1994.

[86] J.D.Leeder, L.A.Holt, J.A.Rippon, I.W.Stapleton, *Proc. 7th Int. Wool Text. Res. Conf.*, Tokyo, **IV**, 227-238(1985).

[87] M.Lee, J.Ryu, T.Wakida, Y.Sato, *Chem. Express* **7**, 241-244(1992).

[88] J.A.Weil, J.R.Bolton and J.E.Wertz, *Electron Paramagnetic Resonance: elementary theory and practical applications*, Wiley, New York, 1994.

[89] P.B.Ayscough, *Electron Spin Resonance in Chemistry*, Methuen & Co Ltd, London, 1967.

[90] X.J.Dai, Master Thesis, The Chinese Science and Technology University, (1987).